

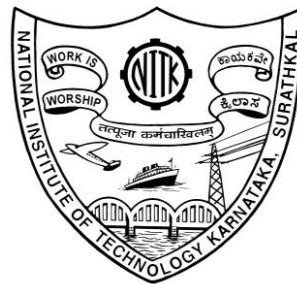
**HYDROELASTIC ANALYSIS OF VERY LARGE FLOATING  
STRUCTURE (VLFS) USING BOUNDARY ELEMENT  
APPROACH**

**Thesis**

**Submitted in partial fulfilment of the requirement for degree of  
DOCTOR OF PHILOSOPHY**

**By**

**ANOOP. I. SHIRKOL**



**DEPARTMENT OF APPLIED MECHANICS AND HYDRAULICS  
NATIONAL INSTITUTE OF TECHNOLOGY KARNATAKA  
SURATHKAL-575 025**

**APRIL – 2019**

**HYDROELASTIC ANALYSIS OF VERY LARGE FLOATING  
STRUCTURE (VLFS) USING BOUNDARY ELEMENT  
APPROACH**

**Thesis**

**Submitted in partial fulfilment of the requirement for degree of  
DOCTOR OF PHILOSOPHY**

**By**

**ANOOP. I. SHIRKOL**

**AM15F02**

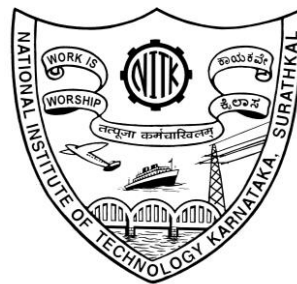
Under the guidance of

**Dr. T. NASAR**

Assistant Professor

Dept. of Applied Mechanics & Hydraulics

NITK Surathkal



**DEPARTMENT OF APPLIED MECHANICS AND HYDRAULICS  
NATIONAL INSTITUTE OF TECHNOLOGY KARNATAKA  
SURATHKAL-575 025**

**APRIL – 2019**

## **D E C L A R A T I O N**

*By the Ph.D. Research Scholar*

I hereby *declare* that the Research Thesis entitled **Hydroelastic Analysis of of Very Large Floating Structure (VLFS) using Boundary Element Approach**, which is being submitted to the **National Institute of Technology Karnataka, Surathkal** in partial fulfilment of the requirements for the award of the Degree of **Doctor of Philosophy in Applied Mechanics and Hydraulics Department** is a *bonafide report of the research work* carried out by me. The material contained in this Research Thesis has not been submitted to any University or Institution for the award of any degree.

155011AM15F02, ANOOP. I. SHIRKOL

(Register Number, Name & Signature of the Research Scholar)

Department of Applied Mechanics and Hydraulics

Place: NITK-Surathkal

Date:

## C E R T I F I C A T E

This is to *certify* that the Research Thesis entitled **Hydroelastic Analysis of of Very Large Floating Structure (VLFS) using Boundary Element Approach** submitted by ANOOP. I. SHIRKOL (Register Number: 155011AM15F02) as the record of the research work carried out by him, is *accepted as the Research Thesis submission* in partial fulfilment of the requirements for the award of degree of **Doctor of Philosophy**.

Dr. T. Nasar  
Assistant Professor  
Research Guide  
(Name and Signature with Date and Seal)

Chairman - DRPC  
(Signature with Date and Seal)

## Acknowledgements

First and foremost, I would like to thank the almighty God for giving such a beautiful life.

*“Don’t treat me like a stranger. Regard me as Thy man alone. Consider me as none but Thy son. O Lord, kudala Sangama.”*

I would like to express my sincere gratitude to my advisor **Dr. T. Nasar** for the continuous support of my Ph.D. study and related research, for his patience, motivation, and immense knowledge. His guidance helped me in all the time of research and writing of this thesis. I could not have imagined having a better advisor and mentor for my Ph.D. study.

Besides my advisor, I would like to thank the rest of my thesis committee: **Prof. Subba Rao** and **Dr. Chandhini G**, for their insightful comments and encouragement, but also for the hard question which incited me to widen my research from various perspectives.

I take this opportunity to thank **Prof. G.S. Dwarkish** and **Prof. A. Mahesha** the former Head and the present Head of Department of Applied Mechanics & Hydraulics for their kindness and continuous support. I would like to express sincere thanks to **Prof. Lakshman Nandagiri** for his help and suggestion in keeping myself motivated. I sincerely thank **Dr. B. M. Dodamani** for motivating me throughout my research. I also thank **Dr. Raviraj. H. M** for his continuous support and making me believe in myself. I would like to extend my deepest gratitude towards all the other faculty members of the department for their never-ending support, encouragement and help.

I would like to express my gratitude to the former Director of NITK, Surathkal, Prof. Swapan Bhattacharya, the former Director In-charge **Prof. K. N. Lokesh** and present Director **Prof. Karanam Uma Maheshwar Rao** for granting me the permission to use the institutional infrastructure facilities.

I sincerely acknowledge the help and support rendered by the faculty, staff and research scholars of the Department of Applied Mechanics and Hydraulics. I take this opportunity to thank **Mr. Jagadish** and **Mr. Seetharam**, and their supporting staff.

**Mr. Ananda Devadiga, Mr. Gopalakrishna, Mr. Harisha, Mr. Anil Kumar, Mr. Padmanaba, Mr. Niranjana** and **Ms. Ashwini**, for their help in conducting the lab duties. I also thank **Mr. Balakrishna** for his help in solving the computer snags during my research.

I thank all my fellow research scholars and M. Tech students for their cooperation. My thanks also go out to all my friends who have rendered their help at different times which made my stay in this institute a memorable period of my life. Special thanks to **Mr. Sumanth Morab** B. Tech student from Mechanical Department for his support in coding.

I owe thanks to **Prof. Udaykumar. R. Y** for his help and encouragement during this period of research. Last but not the least, I would like to thank my family: my parents and my sister for supporting me spiritually throughout writing this thesis and my life in general.

*- Anoop. I. Shirkol*

## Dedication

I dedicate this thesis to my beloved aunt *Late Ms. Annapurna. T. Shirkol*, a person who envisioned me a passion to learn and walk in a rightful way, and *Late Ganesh. V. Desai*, who always stay in my heart...

## ABSTRACT

Hydroelasticity is a subject of interest in marine science and technology involving the mutual interaction of water waves and elastic bodies. It is a branch which deals with the elastic deformation of bodies which is in contact with liquids. Interdisciplinary subjects like this require the knowledge of structural mechanics, fluid mechanics, concepts of water wave propagation and boundary conditions. In this thesis, a numerical procedure has been proposed to analyze the equation of motion of the elastic plate which is having a shallow draft,  $L/d \leq 1/20$  (small thickness) with arbitrary geometry subjected to monochromatic gravity waves. The numerical model is capable of investigating the Very Large Floating Structure (VFLS) at finite ( $0.05 \leq h/\lambda \leq 0.5$ ) and infinite ( $h/\lambda \leq 0.5$ ) water depths. Herein, VLFS is considered to behave as thin elastic plate due to its dimensions. VLFS of rectangular, triangular and trapezoidal geometries are considered and elastic motion or vertical deflections of these shapes have been studied. A hybrid numerical model which combines Boundary Element Method (BEM) and Finite Element Method (FEM) is developed and used to solve fluid structure interaction between the elastic thin plate and water wave. A Higher Order Boundary Element Method (HOBEM) has been adopted in order to maintain the same order basis function and contains the same nodes between BEM and FEM. Two equations have been derived to develop the relationship between the displacement of the plate and the velocity potential under the plate. The first equation is derived from the equation of motion for the plate and is solved by Finite Element Method (FEM) to extract the displacement of the floating structure. The second equation is from water wave theory which is based on Boundary Integral Equation (BIE) that relates the displacement of the floating plate and velocity potential using free-surface Green's function. A modified Green's function which differs from the bygone Green's function has been developed by using Bessel's, Hankel and Struve functions of order zero. Both the equations are solved simultaneously to get the displacement of floating elastic plate and velocity potential. The results obtained are validated with Wang and Meylan (2004). The performance of the developed model is examined by checking the convergence rate and simulation time. It is learnt that the model gives its better performance in finite depth, whereas, its performance in infinite

depth lags by an average of 20% in simulation time than the results obtained by Wang and Meylan (2004). It is concluded that the model works better in finite water depth for rectangular and trapezoidal plates.

## TABLE OF CONTENTS

| SI No. |  | Page No. |
|--------|--|----------|
|        | <b>CHAPTER 1 INTRODUCTION</b>                              |          |
| 1.0    | GENERAL  | 01       |
| 1.1    | VERY LARGE FLOATING STRUCTURES (VLFSs)                     | 03       |
| 1.1.1  | Advantages of VLFS   | 05       |
| 1.1.2  | Application of existing and proposed VLFSs                 | 07       |
| 1.1.3  | VLFS system  | 13       |
| 1.2    | <b>NUMERICAL METHODS</b>                                   | 16       |
| 1.2.1  | Boundary Element Method                                    | 18       |
| 1.2.2  | Finite Element Method                                      | 19       |
|        | <b>CHAPTER 2 LITERATURE SURVEY</b>                         |          |
| 2.0    | GENERAL  | 21       |
| 2.1    | BASIC ASSUMPTIONS IN THE ANALYSIS OF VLFS                  | 22       |
| 2.2    | DIFFERENT APPROACHES TO ANALYSE<br>HYDROELASTICITY PROBLEM | 23       |
| 2.3    | MODELS IN DIFFERENT WATER DEPTHS                           | 27       |
| 2.4    | APPLICATIONS AND PROBLEMS RELATED TO VLFS                  | 28       |
| 2.5    | DIFFERENT SHAPES AND MODELS OF VLFS                        | 30       |
| 2.6    | BREAKWATERS AND MOORING SYSTEMS                            | 31       |
| 2.7    | SUMMARY OF LITERATURE REVIEW                               | 35       |
| 2.8    | NECESSITY AND RELEVANCE OF THE PRESENT<br>STUDY            | 36       |
| 2.9    | OBJECTIVES OF THE STUDY                                    | 36       |
|        | <b>CHAPTER 3 MATHEMATICAL FORMULATION</b>                  |          |
| 3.1    | GENERAL THEORY AND PROPOSED SOLUTION                       | 38       |
| 3.2    | MATHEMATICAL FORMULATION                                   | 39       |
| 3.2.1  | Reduction to single frequency problem                      | 42       |
| 3.2.2  | Equation of motion for water wave                          | 42       |
| 3.2.3  | Boundary Element Method for solving fluid motion           | 43       |

|  |  |     |
|--|--|-----|
| 3.2.4  | Discrete versions of the plate using Finite Element Method | 49  |
| 3.2.5  | Higher Order Boundary Element Method [HOBEM]               | 52  |
| <b>CHAPTER 4 RESULTS AND DISCUSSION</b>      |  |     |
| 4.0  | GENERAL  | 56  |
| 4.1  | HYDROELASTIC BEHAVIOR OF RECTANGULAR PLATE                 | 58  |
| 4.2  | HYDROELASTIC BEHAVIOR OF TRIANGULAR PLATE                  | 81  |
| 4.3  | HYDROELASTIC BEHAVIOR OF TRAPEZOIDAL PLATE                 | 96  |
| <b>CHAPTER 5 CONCLUSIONS AND FUTURE WORK</b> |  |     |
| 5.0  | GENERAL  | 107 |
| 5.1  | RECTANGULAR PLATE  | 107 |
| 5.2  | TRIANGULAR PLATE   | 108 |
| 5.3  | TRAPEZOIDAL PLATE  | 109 |
| 5.4  | LIMITATIONS OF THE STUDY                                   | 109 |
| 5.5  | SCOPE FOR FUTURE WORK                                      | 110 |
| <b>REFERENCES</b>                            |  | 111 |
| <b>PUBLICATIONS</b>                          |  |     |
| <b>RESUME</b>                                |  |     |

## LIST OF FIGURES

|           |   |    |
|-----------|---|----|
| Fig. 1.1  | The Mega-Float, Tokyo Bay, Japan  | 05 |
| Fig. 1.2  | Kamigoto Floating Oil Storage Base, Nagasaki Prefecture,<br>Japan   | 07 |
| Fig. 1.3  | Bronnoysund Bridge and Nordhordland Bridge in Norway  | 08 |
| Fig. 1.4  | Lake Washington Hood Canal Bridge in Washington   | 09 |
| Fig. 1.5  | Yumemai floating bridge, Japan  | 10 |
| Fig. 1.6  | Central Japan International Airport, Nagoya   | 12 |
| Fig. 1.7  | Components of VLFS system   | 13 |
| Fig. 1.8  | (a) Titicaca Lake and (b) Chong Khneas village  | 14 |
| Fig. 1.9  | (a) Floating villages in Vietnam and (b) The spiral island  | 14 |
| Fig. 1.10 | (a) Transportable Information Centre Amsterdam and, (b) A<br>complex of three hemispheres Rotterdam   | 15 |
| Fig. 1.11 | Engineering solution of physical problem  | 17 |
| Fig. 2.1  | Existing breakwater in Latsi harbour  | 33 |
| Fig. 3.1  | Schematic diagram of floating structure. (a) Sectional View<br>and (b) Plan view  | 40 |
| Fig. 3.2  | Discrete version of BEM   | 44 |
| Fig. 3.3  | Decomposition of a 3-D fluid domain   | 45 |
| Fig. 3.4  | Schematic diagram of coupled plate–water problem  | 47 |
| Fig. 3.5  | Decomposition of 2-D surface $S_\infty$ into $S_\infty \cup S_\varepsilon$ (a) plan view<br>(b) side view. In case $\partial/\partial n = -\partial/\partial s$ | 48 |
| Fig. 3.6  | FEM panel showing three degree of freedom system  | 50 |
| Fig. 4.1  | Different shapes of the floating plate (a) Rectangular, (b)<br>Triangular and, (c) Trapezoidal  | 57 |
| Fig. 4.2  | Deflection of rectangular plate for different number of<br>panels and wave angle of $\theta = 0$ : (a) 625, (b) 400, (c) 225<br>and, (d) 100 panels             | 60 |
| Fig. 4.3  | Deflection of rectangular plate for different wave angle<br>attack (a) $\theta = 0$ , (b) $\theta = \pi/6$ , (c) $\theta = \pi/4$ and (d) $\theta = \pi/2$      | 62 |

|           |   |    |
|-----------|---|----|
| Fig. 4.4  | Deflection of rectangular plate for different wave angles of attack: (a) $\theta = 0$ , (b) $\theta = \pi/6$ , (c) $\theta = \pi/4$ and, (d) $\theta = \pi/2$   | 66 |
| Fig. 4.5  | Deflection of rectangular plate for different wave angles of attack: (a) $\theta = 0$ , (b) $\theta = \pi/6$ , (c) $\theta = \pi/4$ and, (d) $\theta = \pi/2$ for $N, M = 2$                            | 69 |
| Fig. 4.6  | Deflection of rectangular plate in infinite water depth for different wave angles of attack: (a) $\theta = 0$ , (b) $\theta = \pi/6$ , (c) $\theta = \pi/4$ and, (d) $\theta = \pi/2$ for $N, M = 4$    | 73 |
| Fig. 4.7  | Deflection of rectangular plate for integration points $N, M = 4$ and $\theta = 0^\circ$ (a) = 225, (b) = 400, (c) = 625 and, (d) = 900 panels  | 76 |
| Fig. 4.8  | Deflection of rectangular plate in infinite water depth for different wave angles of attack (a) $\theta = 0$ , (b) $\theta = \pi/6$ , (c) $\theta = \pi/4$ (d) $\theta = \pi/2$ for $N = 4$ and $M = 8$ | 79 |
| Fig. 4.9  | : Deflection of triangular plate for different number of panels and wave angle of $\theta = 0$ : (a) 77, (b) 152, (c) 252, (d) 377 and (e) 577 panels   | 82 |
| Fig. 4.10 | Deflection of triangular plate for different wave angles of attack: (a) $\theta = 0$ , (b) $\theta = \pi/6$ , (c) $\theta = \pi/4$ for $N, M = 2$   | 85 |
| Fig. 4.11 | Deflection of triangular plate for different wave angles of attack: (a) $\theta = 0$ , (b) $\theta = \pi/6$ , (c) $\theta = \pi/4$ for $N, M = 4$   | 88 |
| Fig. 4.12 | Deflection of triangular plate for different wave angles of attack in infinite water depth: (a) $\theta = 0$ , (b) $\theta = \pi/6$ and (c) $\theta = \pi/4$ for $N, M = 2$                             | 91 |
| Fig. 4.13 | Deflection of triangular plate for different wave angles of attack in infinite water depth: (a) $\theta = 0$ , (b) $\theta = \pi/6$ and (c) $\theta = \pi/4$ for $N, M = 4$                             | 93 |
| Fig. 4.14 | Deflection of trapezoidal plate for different wave angles of attack: (a) $\theta = 0$ , (b) $\theta = \pi/4$ , (c) $\theta = \pi/6$ for $N, M = 2$  | 96 |
| Fig. 4.15 | Deflection of trapezoidal plate for different wave angles of attack: (a) $\theta = 0$ , (b) $\theta = \pi/6$ , (c) $\theta = \pi/4$ for $N, M = 4$  | 99 |

- Fig. 4.16 Deflection of trapezoidal plate for different wave angles of attack: (a)  $\theta = 0$ , (b)  $\theta = \pi/6$ , (c)  $\theta = \pi/4$  for  $N, M = 2$  102
- Fig. 4.17 Deflection of trapezoidal plate for different wave angles of attack: (a)  $\theta = 0$ , (b)  $\theta = \pi/4$ , (c)  $\theta = \pi/6$  for  $N, M = 4$  104

## LIST OF TABLES

|            |  |    |
|------------|--|----|
| Table 4.1  | Plate Parameters used in the model   | 57 |
| Table 4.2  | Time and error as the function of panels with wave angle $\theta = 0$  | 58 |
| Table 4.3  | Time and error as the function of panels for integration points $N, M = 4$ and wave angle $\theta = 0$                         | 63 |
| Table 4.4  | Time and error as the function of panels for integration points $N, M = 4$ and wave angle $\theta = \pi/6$                     | 63 |
| Table 4.5  | Time and error as the function of panels for integration points $N, M = 4$ and wave angle $\theta = \pi/4$                     | 63 |
| Table 4.6  | Time and error as the function of panels for integration points $N, M = 4$ and wave angle $\theta = \pi/2$                     | 64 |
| Table 4.7  | Time and error as the function of panels for integration points $N, M = 2$ and wave angle $\theta = 0$                         | 67 |
| Table 4.8  | Time and error as the function of panels for integration points $N, M = 2$ and wave angle $\theta = \pi/6$                     | 67 |
| Table 4.9  | Time and error as the function of panels for integration points $N, M = 2$ and wave angle $\theta = \pi/4$                     | 67 |
| Table 4.10 | Time and error as the function of panels for integration points $N, M = 2$ and wave angle $\theta = \pi/2$                     | 68 |
| Table 4.11 | Time and error as the function of panels for integration points $N, M = 2$ and wave angle $\theta = 0$                         | 70 |
| Table 4.12 | Time and error as the function of panels for integration points $N, M = 2$ and wave angle $\theta = \pi/6$                     | 71 |
| Table 4.13 | Time and error as the function of panels for integration points $N, M = 2$ and wave angle $\theta = \pi/4$                     | 71 |
| Table 4.14 | Time and error as the function of panels for integration points $N, M = 2$ and wave angle $\theta = \pi/2$                     | 72 |
| Table 4.15 | Time and error as the function of panels for integration points $N, M = 4$ in infinite water depth and wave angle $\theta = 0$ | 74 |

|            |   |    |
|------------|---|----|
| Table 4.16 | Time and error as the function of panels for integration points $N, M = 4$ in infinite water depth and wave angle $\theta = \pi/6$          | 74 |
| Table 4.17 | Time and error as the function of panels for integration points $N, M = 4$ in infinite water depth and wave angle $\theta = \pi/4$          | 75 |
| Table 4.18 | Time and error as the function of panels for integration points $N, M = 4$ in infinite water depth and wave angle $\theta = \pi/2$          | 75 |
| Table 4.19 | Time and error as the function of panels for integration points $N = 4$ and $M = 8$ in infinite water depth and $\theta = 0$                | 79 |
| Table 4.20 | Time and error as the function of panels for integration points $N = 4$ and $M = 8$ in infinite water depth and wave angle $\theta = \pi/6$ | 79 |
| Table 4.21 | Time and error as the function of panels for integration points $N = 4$ and $M = 8$ in infinite water depth and wave angle $\theta = \pi/4$ | 79 |
| Table 4.22 | Time and error as the function of panels for integration points $N = 4$ and $M = 8$ in infinite water depth and wave angle $\theta = \pi/2$ | 80 |
| Table 4.23 | Time and error as the function of panels for integration points $N, M = 2$ and wave angle $\theta = 0$                                      | 83 |
| Table 4.24 | Time and error as the function of panels for integration points $N, M = 2$ and wave angle $\theta = \pi/6$                                  | 83 |
| Table 4.25 | Time and error as the function of panels for integration points $N, M = 2$ and wave angle $\theta = \pi/4$                                  | 84 |
| Table 4.26 | Time and error as the function of panels for integration points $N, M = 2$ and wave angle $\theta = 0$                                      | 85 |
| Table 4.27 | Time and error as the function of panels for integration points $N, M = 2$ and wave angle $\theta = \pi/6$                                  | 86 |
| Table 4.28 | Time and error as the function of panels for integration  | 86 |

|            |  |     |
|------------|--|-----|
|            | points $N, M = 2$ and wave angle $\theta = \pi/4$  |     |
| Table 4.29 | Time and error as the function of panels for integration points $N, M = 4$ and wave angle $\theta = 0$     | 88  |
| Table 4.30 | Time and error as the function of panels for integration points $N, M = 4$ and wave angle $\theta = \pi/6$ | 89  |
| Table 4.31 | Time and error as the function of panels for integration points $N, M = 4$ and wave angle $\theta = \pi/4$ | 89  |
| Table 4.32 | Time and error as the function of panels for integration points $N, M = 2$ and wave angle $\theta = 0$     | 91  |
| Table 4.33 | Time and error as the function of panels for integration points $N, M = 2$ and wave angle $\theta = \pi/6$ | 92  |
| Table 4.34 | Time and error as the function of panels for integration points $N, M = 2$ and wave angle $\theta = \pi/4$ | 92  |
| Table 4.35 | Time and error as the function of panels for integration points $N, M = 4$ and wave angle $\theta = 0$     | 94  |
| Table 4.36 | Time and error as the function of panels for integration points $N, M = 4$ and wave angle $\theta = \pi/6$ | 95  |
| Table 4.37 | Time and error as the function of panels for integration points $N, M = 4$ and wave angle $\theta = \pi/4$ | 95  |
| Table 4.38 | Time and error as the function of panels for integration points $N, M = 2$ and wave angle $\theta = 0$     | 97  |
| Table 4.39 | Time and error as the function of panels for integration points $N, M = 2$ and wave angle $\theta = \pi/6$ | 97  |
| Table 4.40 | Time and error as the function of panels for integration points $N, M = 2$ and wave angle $\theta = \pi/4$ | 98  |
| Table 4.41 | Time and error as the function of panels for integration points $N, M = 4$ and wave angle $\theta = 0$     | 100 |
| Table 4.42 | Time and error as the function of panels for integration points $N, M = 4$ and wave angle $\theta = \pi/6$ | 100 |
| Table 4.43 | Time and error as the function of panels for integration points $N, M = 4$ and wave angle $\theta = \pi/4$ | 101 |

|            |  |     |
|------------|--|-----|
| Table 4.44 | Time and error as the function of panels for integration points $N, M = 2$ and wave angle $\theta = 0$     | 102 |
| Table 4.45 | Time and error as the function of panels for integration points $N, M = 2$ and wave angle $\theta = \pi/6$ | 103 |
| Table 4.46 | Time and error as the function of panels for integration points $N, M = 2$ and wave angle $\theta = \pi/4$ | 103 |
| Table 4.47 | Time and error as the function of panels for integration points $N, M = 4$ and wave angle $\theta = 0$     | 105 |
| Table 4.48 | Time and error as the function of panels for integration points $N, M = 4$ and wave angle $\theta = \pi/6$ | 105 |
| Table 4.49 | Time and error as the function of panels for integration points $N, M = 4$ and wave angle $\theta = \pi/4$ | 106 |

## LIST OF ABBREVIATIONS, SYMBOLS AND NOTATIONS

---

| <b>Abbreviations</b> | <b>Description</b>                             |
|----------------------|--|
| BEM                  | Boundary Element Method                        |
| BIE                  | Boundary Integral Equation                     |
| BM                   | Bending Moment                                 |
| BVP                  | Boundary Value Problem                         |
| EEMM                 | Eigen function Expansion - Matching Method     |
| FDM                  | Finite Difference Method                       |
| FEM                  | Finite Element Method                          |
| FVM                  | Finite Volume Method                           |
| HDC                  | Hydroelastic Design Contour                    |
| HOBEM                | Higher Order Boundary Element Method           |
| HRC                  | Hydroelastic Response Contour                  |
| MIZ                  | Marginal Ice Zone                              |
| MOB                  | Mobile Offshore Base                           |
| MSL                  | Mean Sea Level                                 |
| OWC                  | Oscillating Water Column                       |
| TLSPH                | Total Lagrangian Smooth Particle Hydrodynamics |
| VLFS                 | Very Large Floating Structure                  |
| VLFP                 | Very Large Floating Platform                   |

|       |   |
|-------|---|
| VLMOS | Very Large Mobile Offshore Structures             |
| WCSPH | Weakly Compressible Smooth Particle Hydrodynamics |
| 2-D   | 2 - Dimensional                                   |
| 3-D   | 3 - Dimensional                                   |

### LIST OF SYMBOLS

---

| Greek Symbol                  | Description                                   |
|-------------------------------|---|
| $\phi$                        | velocity potential                            |
| $\phi_d$                      | velocity potential for a panel in vector form |
| $\phi_e$                      | velocity potential for an element             |
| $\nabla$                      | solution domain                               |
| $\nabla_d$                    | single panel domain                           |
| $S_\varepsilon$               | small sphere                                  |
| $X_p \check{\xi}_p$           | distance from source point to free surface    |
| $X_Q \check{\xi}_Q$           | distance from field point to free surface     |
| $\alpha$                      | angle measured from x-axis to $\check{\xi}$   |
| $\Delta_d$                    | field elements                                |
| $\Delta_d(x, y)$              | field element in FEM domain                   |
| $\Delta_e$                    | source element                                |
| $\Delta_e(\check{\xi}, \eta)$ | source element in FEM domain                  |

|                |   |
|----------------|---|
| $\Delta_r$     | parametric element                        |
| $\varepsilon$  | radius of the sphere                      |
| $\theta$       | incident wave angle                       |
| $\lambda$      | wavelength                                |
| $\nu$          | Poisson's ratio                           |
| $\xi$          | source point in x direction               |
| $\phi_I$       | incident wave potential                   |
| $\phi_R$       | radiation wave potential                  |
| $\phi_s$       | scattered wave potential                  |
| $\omega$       | wave angular frequency                    |
| $\rho_w$       | fluid density                             |
| $\rho_t$       | density of the floating platform          |
| $\zeta$        | coordinate of source point in z direction |
| $\eta$         | coordinate source point in y direction    |
| $\theta_x$     | rotation along x direction                |
| $\theta_y$     | rotation along y direction                |
| $\phi_{(x)}$   | velocity potential along x axis           |
| $\phi_{(x)}^n$ | incident velocity potential along x axis  |

## LIST OF NOTATIONS

| Notation   | Description   |
|------------|---|
| $N_d^T$    | finite element basis function   |
| $[G]_{de}$ | Green's matrix  |
| $[k]_d$    | stiffness matrix  |
| $[K_w]_d$  | stiffness matrix for a single panel                                       |
| $[m]_d$    | mass matrix   |
| $[N_M]$    | finite element matrix for $M$ integration points ( $M = 1, 2, 3, \dots$ ) |
| $[N_N]$    | finite element matrix for $N$ integration points ( $N = 1, 2, 3, \dots$ ) |
| $B$        | breadth of the floating plate   |
| $C_s$      | strength of potential   |
| $D$        | flexural rigidity   |
| $d$        | thickness of the floating plate   |
| $g$        | gravitational acceleration  |
| $G$        | Green's function  |
| $G^{(ij)}$ | Green's matrix along source and field points ( $i, j = 1, 2, 3, \dots$ )  |
| $G_{NM}$   | Green's matrix for integration points ( $N, M = 1, 2, 3, \dots$ )         |
| $h$        | water depth   |

|                               |   |
|-------------------------------|---|
| $H_0$                         | Struve function of order zero                         |
| $H_0^{(1)}$                   | Hankel function of first kind                         |
| $i$                           | imaginary number                                      |
| $J_0$                         | Bessel function of second kind                        |
| $k$                           | wave number   |
| $K_0$                         | Bessel's function of the second kind second order     |
| $k_m$                         | imaginary number with positive part                   |
| $L$                           | length of the floating plate                          |
| $N, M$                        | integration points                                    |
| $n, s$                        | normal and tangential vector                          |
| $N_d$                         | basis vector  |
| $N_{j1}, N_{j2},$<br>$N_{j3}$ | finite element basis vectors ( $j = 1, 2, 3, \dots$ ) |
| $p$                           | number of elements                                    |
| $P$                           | Pressure at water surface                             |
| $R$                           | distance between field point and source point         |
| $r, q$                        | natural coordinates for integration                   |
| $S$                           | boundary surface                                      |
| $S_\infty$                    | free surface towards infinity                         |
| $S_B$                         | plate bottom  |

|                 |   |
|-----------------|---|
| $S_d$           | surface domain for FEM  |
| $S_F$           | open free surface   |
| $S_G$           | sea bottom  |
| $S_\varepsilon$ | hemisphere boundary surface                                     |
| $T$             | draft of the plate  |
| $w$             | total Displacement  |
| $W(x,y,z,t)$    | plate displacement  |
| $w_d$           | constant vector   |
| $w_i^{(d)}$     | displacement along x direction for a panel ( $j = 1,2,3\dots$ ) |
| $w_j^{(d)}$     | displacement along y direction for a panel ( $j = 1,2,3\dots$ ) |
| $X$             | field point   |
| $Y_o$           | Bessel function of first kind                                   |

### LIST OF NORMALISED PARAMETERS

| Notation  | Description                |
|-----------|----------------------------|
| $\bar{x}$ | non-dimensional length     |
| $\bar{y}$ | non-dimensional breadth    |
| $\bar{z}$ | non-dimensional depth      |
| $\bar{w}$ | non-dimensional deflection |

|              |   |
|--------------|---|
| $\bar{W}$    | non-dimensional plate deflection              |
| $\bar{d}$    | non-dimensional thickness                     |
| $\bar{\phi}$ | non-dimensional velocity potential            |
| $\beta$      | non-dimensional stiffness                     |
| $\gamma$     | non-dimensional mass of the floating platform |

## CHAPTER 1

### INTRODUCTION

#### 1.0. GENERAL

This thesis examines fluid structure interaction, more predominantly the interaction between water waves and Very Large Floating Structure (VLFS). A numerical scheme is derived to solve the hydroelastic motion of a very large floating structure.

Earth is also called as “Blue” planet due to the rich source of water on its surface. If seen from space, it looks like a blue colored planet. The major part of the Earth’s surface is covered by oceans, seas, lakes, rivers, etc. The entire surface of the Earth measures 510,083,000 square kilometers, in which, the land surface measures 148,300,000 square kilometers. Thus, seventy percent of the earth’s total surface area is occupied by water. Only one third of the entire earth’s surface is available to live on.

A new problem was faced by entire humanity in the early twentieth century such as lack of land and increase in population. With rapid growth in earth’s population, urban agglomeration and evolution of industrial development, there is a need of land reclamation. The countries like Japan, China, India, Pakistan, USA and Indonesia are thickly populated and facing the problem of shortage of land to live on. Many countries from Asia and Europe are expected to add to the list in a very short time. In the year 2011, the population of the world was about seven billions and it is estimated to reach 9.3 billions and 10 billions by 2050 and 2100, respectively. As the population increases, the available space decreases, which leads to land reclamation from sea.

Few of the developed countries which have a long coastline and islands, and are in need of more land for development have taken successful measures to reclaim land from sea. Through land reclamation work, countries like Singapore, Japan, the Netherlands and etc. have expanded their areas significantly. The land reclamation works are, however, subject to certain restrictions such as negative impact on the coastline of the country. Huge cost is required in reclaiming land from deep waters, especially when the sand for reclamation has to be bought from other countries

(Watanabe et al., 2004a). The land reclamation solution is viable or suitable at shallow water depth or in general, water depth less than twenty meters. Many researchers and engineers have proposed interesting and attractive solutions to tackle the problems associated with reclamation works. The construction of Very Large Floating Structure (VLFS) is one of the suitable solutions to address the above said problem. VLFSs can be located far in the sea (deep ocean) as well as near the shore (shallow water). Due to its larger dimensions in plan view and comparing with thickness, it is assumed that the VLFSs behave as thin elastic plate. An elastic deformation is anticipated when it responds to wave load. Hence, it is necessary to study the hydroelastic behavior to analyze the VLFS. Hydroelasticity plays an important role in geophysics, where floating ice is modeled as elastic plate. In the case of offshore structures with larger surface area, the structural deformations are important rather than rigid body motions as they alter the surrounding pressure field.

Ice is the solid shape of water and it is the simplest and most common floating structure as it can be found all around the world. The Marginal Ice Zone (MIZ) is an interfacial region that forms the boundary between open and frozen ocean. MIZ consists of patchwork of ice flow and open water which can be divided into bands with floe size increasing with penetration depth. An extensive amount of literature exists to support the modelling of an ice-sheet as a floating elastic plate. Greenhill (1887) was the first to propose modeling a floating ice sheet by a thin elastic beam on a fluid foundation, suggested a dispersion relation based on the Euler-Bernoulli beam theory. Further, Squire et al. (1988) provided the most conclusive proof of the model by measuring the moving loads on ice. Wadhams et al. (1986, 1988), Kohout et al. (2014) and Kohout et al. (2014) conducted the experimental investigations on wave propagation in the MIZ. The researchers concluded that there is a strong attenuation of energy, which decreases as the wave period increases.

Container ships are cargo ships that carry their entire load in truck-size intermodal containers, in a technique called containerization. They are the common means of commercial intermodal freight transport, and have been carrying most seagoing non-bulk cargo. Today, about 90% of non-bulk cargo worldwide is transported by container, and modern container ships can carry over 19000 TEU. As container ships

have grown in size so has the problem of ship flexure and this is one of the most active areas of research in the domain of hydroelasticity. There have been several disasters at sea in which the flexural response has lead to ship failure. The study of the flexural response of a container ship to waves can be found in Huang and Riggs (2000), Hinrdaris et al. (2003) and Senjanovic et al. (2008, 2009). The responses wereanalyzed using the Finite Element Method for the elastic structure and the Boundary Element Method for the fluid.

### **1.1 VERY LARGE FLOATING STRUCTURES (VLFSs)**

Very Large Floating Structures (VLFSs) are referred as Very Large Floating Platform (VLFP) in few of the literatures. VLFS can be constructed as floating breakwater, bridges, airports, piers and docks, wind and solar power plants, storage facility, military and emergency bases, entertainment facility, parks, spare for industries and also for habitation. Very few VLFSs have been constructed and are presently in operation. The construction or use of VLFS for habitation could become reality in near future. Already several researchers have proposed different design aspects for floating cities or huge living complex. VLFS are classified broadly into two categories (Watanabe et al., 2004a), namely Pontoon type and semi-submersible type. The pontoon type VLFS have the characteristics of high stability, easy maintenance and repair and low manufacturing cost. The semi-submersibles are used in the open sea where the wave heights are relatively large. Semi-submersibles maintain the constant buoyant force and hence they are used in open sea or deep sea to minimize the effect of wave. Semi-submersible VLFSs are suited for oil and gas exploration in deep seas.

Floating structures offer several advantages over permanent structures which might extend from the shore into open water. They do not damage the marine eco-system, neither cause silt deposition in deep harbors nor do they disrupt the ocean currents. They are easy to construct, since most of the structural components are completed onshore, towed to the proposed offshore location and the installation is rapid. In VLFS, entire top surface is used as significant usable area, in contrast to the internal hold areas as used in water craft. The motion of the floating structure due to wind or

wave action must be substantially reduced to ensure the safety of people and facilities on a VLFS and to allow useful activities. Hence, VLFS must be securely moored to the ocean bed.

The large structure with small thickness floating on a sea is called as pontoon type VLFS. The said type is more flexible when compared with other kind of offshore structures due to its dimensions and elastic nature. In these type of structures, elastic motions are considered to be more important than the rigid body motions. Thus, hydroelastic analysis takes centre stage in the analysis of the pontoon type VLFSs. The study consists of elastic motion of a floating structure in response to water waves and their impact on the entire fluid domain. In literature, Pontoon type VLFSs are referred as mat-like VLFSs due to their small thickness or draft in relation to the length, i.e. the third dimension (thickness) of floating structure is very small when compared with other two dimensions (length and breadth). The usual dimensions of these types of structures may vary from five hundred to five thousand meters in length and hundred to one thousand meters in width, whereas, the thickness can be about two to ten meters. The largest prototype Mega-Float with five thousand meters long and four hundred meters wide is constructed in Tokyo Bay, Japan which can be seen in Fig. 1.1. Because of large dimensions, it is difficult to understand the behavior of VLFSs. It is not possible to model as a rigid structure and the allowance for the Bending Moment (BM) must be considered. Also, because of the large size, the problem is often extremely computationally demanding, especially at high frequencies. The simplest model for a VLFS is a floating elastic plate and a great deal of research on floating plates has been motivated by the application to VLFSs.



Fig. 1.1: The Mega-Float, Tokyo Bay, Japan (Watanabe et al., 2004a).

To be an efficient VLFS, it should always provide a very large surface, because the VLFS is used as ground for specific activities. VLFS can be formed by joining the necessary number of units, which can be of any arbitrary shape. The factor of safety and requirement of strength must be checked in the design of the structure. The materials used to construct the VLFS are either composite or non-composite materials. Usually, steel, concrete, pre-stressed and steel-concrete composite materials are used to build the floating structure.

### 1.1.1 Advantages of VLFS

Advantages of very large floating system over traditional land reclamation are as follows:

- Time required to construct the VLFS is less.
- Ease in construction.
- The components can be constructed at shipyards and later can be transported to site.

- Expansion, removal and relocation of VLFS can easily be done.
- As the depth of the water increases, construction cost of VLFS decreases and vice-versa.
- Depth of the sea bed or sea bed profile is not affected by the construction of VLFS.
- VLFSs don't damage the marine ecological system or disrupt ocean/sea currents. Hence, VLFSs are environment friendly.
- The structure will be safe in the deep water as the seismic energy will be dissipated by the sea.

Although, pontoon type VLFSs are best suitable for use in calm waters, naturally sheltered waters, lakes or areas near to the shoreline, breakwaters are usually constructed near the VLFSs to avoid the impact of waves on it. Further, to stabilize the behaviour of VLFS, researchers/engineers have used special anti-motion devices and mooring systems. Due to its large dimension many cycles of wave crests and wave troughs are covered under it, hence, VLFS are not affected by the waves under it. Local deflection with small amplitude can be observed in these type of structures. This phenomenon is called as elastic response. The present thesis mainly deals with the oscillatory propagation of local deflection, which is caused by waves travelling from one end of the floating structure to the other end. The elastic response must be investigated to ensure the stability and factor of safety of the structure.

According to Shuku et al. (2001), multi-stage reliability principle must be obeyed by VLFS. In addition, Shuku et al. (2001) and Watanabe et al. (2004a) describe that joining of floating units, safety regulations, environmental assessment technology and floating execution must also satisfy the reliability principle. The authors have also provided the required measures to be taken during airplane accidents, extreme marine and meteorological conditions. The expected lifespan of the floating structure is about one hundred years. With proper maintenance, the floating structure can further be used for the increased life span. Squire et al. (1988) and Watanabe et al. (2004a, 2004b) have studied the effect of VLFSs on marine ecological system. It is concluded that the installation of VLFSs has minimal effect on the natural ecosystem. The

following subsection 1.1.2 describes the overview of VLFSs constructed/proposed around the world and their applications.

### **1.1.2 Application of existing and proposed VLFSs**

Countries like Japan, Norway, UK, USA, Canada, Brazil and Saudi Arabia are already using Very Large Floating Structures for various purposes. Countries like China, the Netherlands, Singapore, Germany, Korea and Israel are planning to adopt very large floating structures in near future. In constructing the VLFS, Japan leads the entire world and has constructed the first Mega-Float (Isobe, 1999; Shuku et al., 2001; National Maritime Research Institute, Japan). They also constructed airstrips and VLFS test model for floating airport terminals in Tokyo Bay.



Fig. 1.2: Kamigoto Floating Oil Storage Base, Nagasaki Prefecture, Japan (Photo courtesy of Shirashima Oil Storage Co Ltd).

Further, the following structures have been constructed recently in Japan, such as Yumemai floating Swing Bridge in Osaka (Watanabe et al., 2000), floating emerging rescue base in Yokohama, the floating oil storage system in Kamigoto (Fig. 1.2), amusement and entertainment facilities, parks and spare for floating bridges. For storing fuel, many countries have already adopted the VLFSs. Flat-boxed tankers must be constructed initially and are connected to each other to serve as an offshore oil storage facility (Fig.1.2). Two floating oil storages are situated in Kamigoto (first storage base) and Shirashima, Japan having a capacity of 4.4 and 5.6 million kiloliters, respectively. Yoneyama et al. (2004) provides details regarding design, mooring and experimental aspect of the oil storage bases. A single barge has a capacity of 880,000 kiloliters, wherein, totally five huge barrels are connected to form a large floating structure. The floating harbor facility constructed by different countries around the world can be seen in Watanabe et al. (2004b).

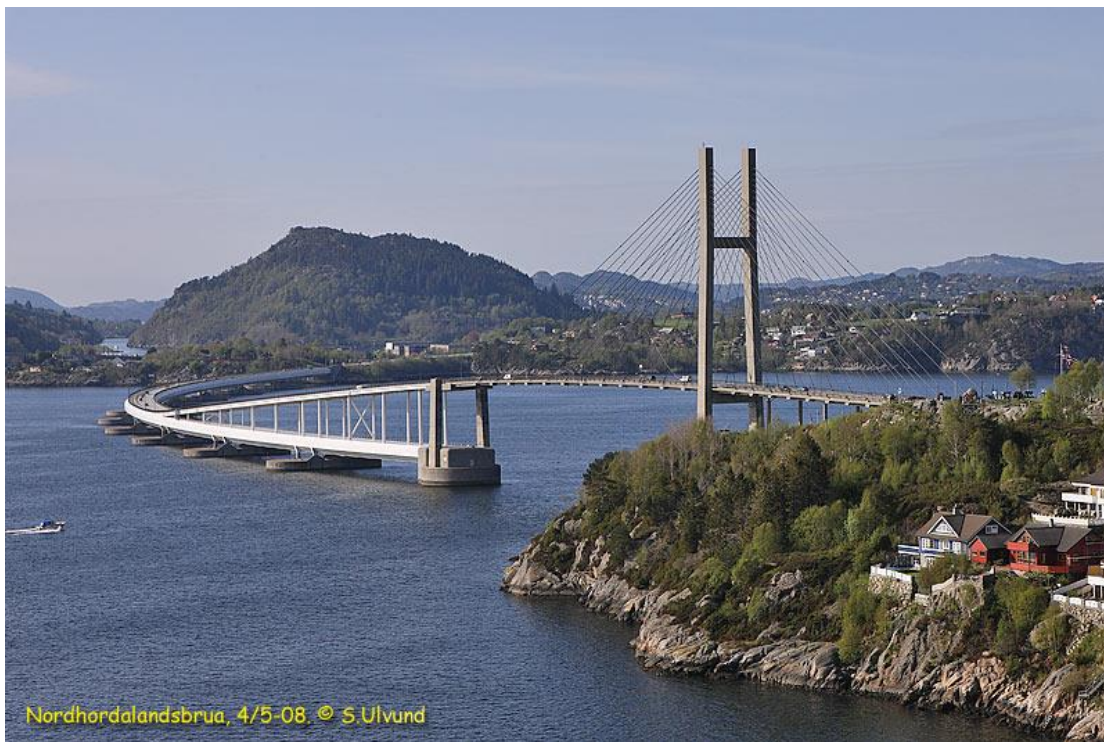


Fig. 1.3: Bronnoysund Bridge and Nordhordland Bridge in Norway, (Watanabe 2003).

Bergsoyund and Nordhorland floating bridges are built in Norway (Fig. 1.3) and Kelowna floating bridge is built in Canada. Washington State has a floating bridge

called Evergreen Point Floating Bridge. Countries like Saudi-Arabia, Brazil and UK also use floating structures as bridges. The worldwide development and the history of floating bridges have been described by Watanabe (2003). Pontoon type floating bridge and its earliest applications has been narrated by Watanabe et al. (2004b). The Galata floating bridge in Istanbul is the first floating structure to be constructed, followed by the Lake Washington Hood Canal Bridge in Washington (Fig. 1.4). The above mentioned floating structures have been constructed between 1910-1950.



Fig. 1.4: Lake Washington Hood Canal Bridge in Washington, (Watanabe et al., 2004b).

In early 1990s, construction of VLFSs gained its momentum and popularity for various applications. West India Qeray Foot Bridge in Docklands, New Swinging arch bridge in Germany, Admiral Clarey Bridge in USA, Dongjin Bridge in China etc. are few of the floating bridges present in the world. Countries like India, France and Austria are also developing floating bridge Structures. International Database and Gallery of Structures (<https://structurae.net/>), provide a complete detail of the pontoon bridges still in use.



Fig. 1.5: Yumemai floating bridge, Japan (Photo courtesy, kansai design).

Figure 1.5 shows the photographic view of a Yumemai Bridge in Osaka, Japan. It was built to connect the reclaimed islands Yumeshima and Maishima. The bridge consists of two floating pontoons and a movable floating arch bridge. Its dimensions are about nine hundred forty meters in length and forty meters in width. Container terminals, floating docks and piers are the additional applications of Very Large Floating Offshore Structures. A floating pier which has the capacity of fifty thousand tons of container ship has been designed in Valdez, Alaska. Countries like Japan, Vancouver and Canada have constructed many floating piers. The main advantage of a floating pier is that it always remains in a constant position with respect to the water line. Thus, smooth loading and unloading of cargo can be seen in floating piers. Countries like USA and Israel have floating docks and are used to repair ships.

Floating emergency bases can be conveniently moved from one place to another place and can be protected from seismic shocks. Japan has three Disaster Prevention Bases, which are located near Yokohama, Asaka and Nagoya. All the bases consist of facilities such as hell pool, track crane, mooring and interior storage for cargo. Floating rescue base specifications can be obtained or found in Yoneyama et al. (2004) and Watanabe et al. (2004b).

Floating plant is another potential application of VLFS. Researchers have proposed the extraction of power in the form of wind and solar power plants (Takagi and Yano, 2003; Takagi and Noguchi, 2005). A clean power plant concept was designed and proposed by the Association of Japan. Countries like Brazil, Saudi Arabia, Jamaica, Argentina and Japan are already using floating power plants in order to extract clean energy. For the purpose of amusement and entertainment, VLFSs are also used as floating entertainment facilities. Different shapes of VLFSs can be used for the construction of hotels, exhibition centres, shopping centres, recreation parks and fishing piers. The aesthetic and attractive panoramic views are the advantages of floating entertainment facilities can offer. Floating hotels can be seen in Australia, North Korea, Japan, Russia and Ukraine.

Floating airports are one of the most important and attractive application of VLFS. In recent times, many researchers and engineers are studying the possibility of constructing a floating airport in coastal waters. There is a need for airports as there is a considerable increase in the number of cities and air traffic as well. In Asia, great progress is being made in constructing airports and airport facilities in the sea. The world's first floating airport is Kansai International Airport, Osaka, Japan, however, it is built in an artificial island. The airports situated on reclaimed lands and their details are as follows. Central Japan International Airport (Fig. 1.6), Nagoya has been constructed on an artificial island in Ice Bay, 35kilometers South of Nagoya. In the year 2015, 10.2 millions of people used the airport and it is ranked as eighth busiest airports in the nation. Changi airport, Singapore built on the reclaimed land acts as a primary airport for the civilians. In South East, it is considered as one of the largest transportation hubs. "Skytrax" rated this airport as the world's best airport for the sixth time since 2013. It is one of the busiest airports in terms of international passengers. The airport is located approximately 17.24 kilometers from Marina Bay. Incheon International airport or Seoul-Incheon International airport is the largest airport in South Korea. Starting from the year 2005 and till now, it has been rated as the best airport worldwide by "Airport Council International". It is located on an artificially created island. There are two islands namely Yeongiong and Yongyu islands which are separated by a shallow sea. The area between these two islands was

reclaimed for the construction of airport. Hong Kong International Airport is located on the island of Chek Lap Kok, which is a reclaimed land for the construction of airport. The airport located at Chek Lap Kok which replaces Kai Taka airport and started its commercial operations since 1998 and is one of the world's busiest passenger and cargo gateway airport. Further, there are many small and large floating airports in countries like USA and Japan can be seen. Research has been going on towards the direction for the analysis of floating connected pontoons and can be used as airports for military purpose.



Fig. 1.6: Central Japan International Airport, Nagoya (Yoneyama, 2004).

The next generation of VLFS is Very Large Mobile Offshore Structures (VLMOS) or Mobile Offshore Base (MOB). Mobility is the main advantage when compared with other offshore structures. Researchers in Japan have proposed to use VLMOS, for disaster prevention bases (Yoneyama, 2004). Also, it can be used for the extraction of different kind of energies by providing space for wind and solar power plants (Takagi and Yano, 2003; Takagi and Noguchi, 2005) as well. Further, USA initiated the study to provide support for military operations when fixed bases are not available and the descriptions are given in Zilman and Miloh (2000) and Watanabe et al. (2004b). Floating cities are dreams of all engineers and researchers. In the twenty first century, these floating cities will become a reality in Japan as proposed by Japanese Society of Steel Construction (Watanabe et al., 2004b) in Japan. Thus, for various purposes, lots of VLFSs are being used, but in the near future, even more applications would have been proposed.

### 1.1.3 VLFS system

Fig. 1.7 shows the general concept and components of VLFS system. The system consists of

- 1) Mat-like (very large) floating structure.
- 2) A means of entry in the form of floating road or access bridge to connect floating structure from the shore.
- 3) Breakwaters for providing sheltered area.
- 4) Mooring facility to keep the platform in a specific place.
- 5) Super structures, amenities and communication facilities on VLFS.

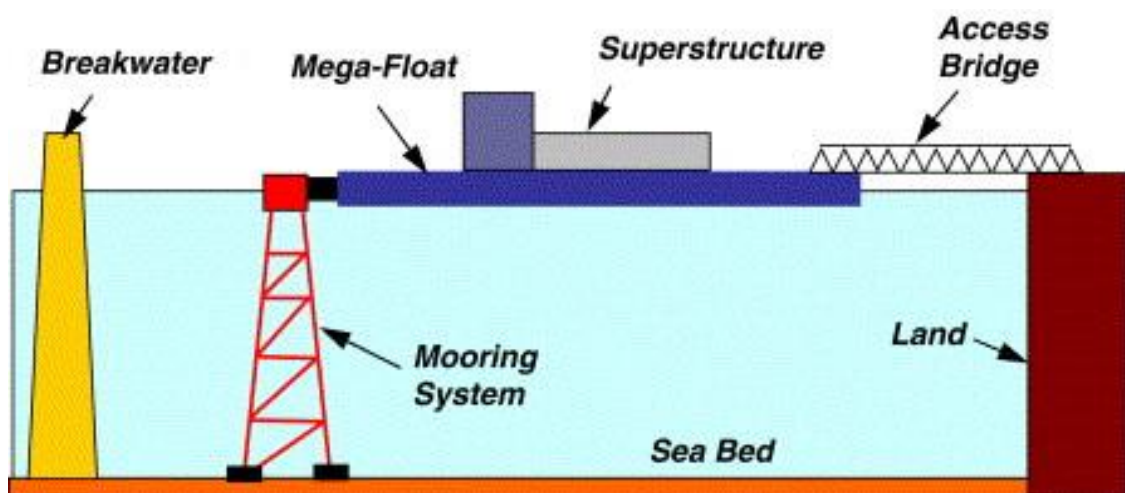


Fig. 1.7: Components of VLFS system (Andrianov, A. I., and Hermans, A. J. 2003).

The present thesis mainly concentrates on the determination of vertical deflection of the floating platform with arbitrary shapes which are having many applications/operations related to human beings on floating islands or floating platforms. Following are some of the examples of floating platform with arbitrary shapes either formed naturally or man-made. The highest navigable lake in the world is called as Titicaca Lake, which is located 3.812 meters above Mean Sea Level (MSL). Uros-Indians are the inhabitants of this lake. The islands are made of Titora

reeds stacked together and it needs proper maintenance. The reeds which are in contact with water result in rotting, so new reeds are added constantly at an intervals of thirty years. These types of structures may be of any shape. Figure 1.8 (a) shows an island floating on the surface of the water in Titicaca Lake. Titicaca Lake Island is a natural island and it requires regular maintenance.



(a)



(b)

Fig. 1.8: (a) Titicaca Lake and (b) Chong Khneas village (Kashiwagi, M. 1999).

Siem Reap in Cambodia is one of the floating islands in Asia. The Chong Khneas village always be floating as shown in Figure 1.8 (b), except when there are really dry periods. Most of these small villages keep on changing their location, so that they can always stay floating.



(a)



(b)

Fig. 1.9: (a) Floating villages in Vietnam and (b) The spiral island (Kashiwagi, M. 1999).

Villages on water can also be found in Vietnam as in Figure 1.9 (a), SouthEast Asia. The floating villages in Vietnam are made of small houses built on top of rafts. The lower end of the rafts is attached with wooden planks, which are connected to empty

barrels. Spiral islands in Mexico are the islands which consist of two-storey houses as shown in Figure 1.9 (b). The spiral island-I are constructed from filling the nets with discarded plastic bottles which support a structure of plywood and bamboo. Spiral island-II consists of three beaches and has been constructed by using similar method followed for Spiral island-I.

In the year 2000, a transportable information centre was constructed in Amsterdam. The building is designed by Attika Architects to meet ultimate flexibility. Figure 1.10 (a) provides three separate platforms which were initially constructed and then connected together to form a rigid floating structure. Initially, three platforms were launched into water separately and then they were pretensioned to form a rigid structure. A complex consisting of three hemispheres is situated in the centre of Rotterdam shown in Figure 1.10 (b). Three interconnected floating domes are used to build this floating hemisphere. The building is durable and it is constructed of used materials. The structure is flexible and it can move on the surface of water as a floating platform.

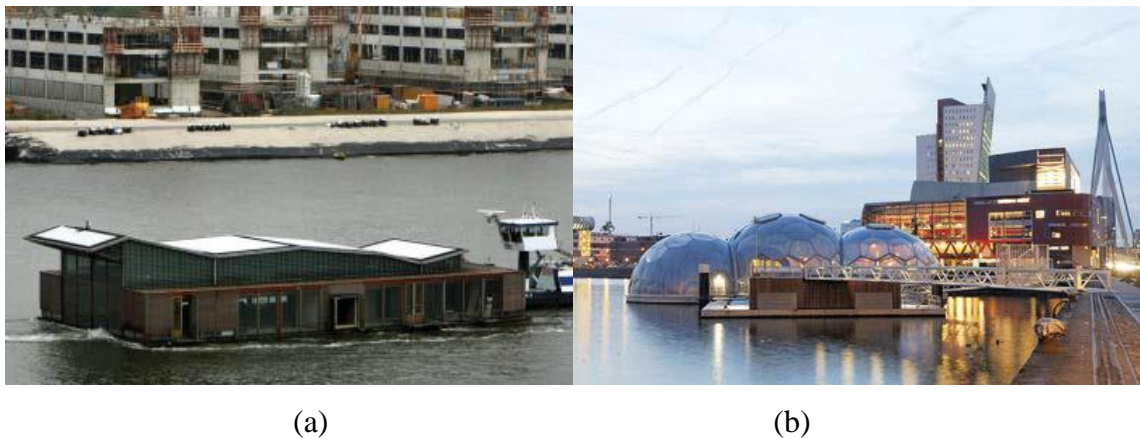


Fig. 1.10: (a) Transportable Information Centre Amsterdam and, (b) A complex of three hemispheres Rotterdam (Shuku et al., 2001).

As the floating structure can be of any shape and size, it is necessary to analyze the floating platform with arbitrary shapes. There is a need to study the behaviour of floating platform with arbitrary shapes. The above stated structures can not be developed by using a regular rectangular or square planform, but, are made to float as a complete structure by attaching many arbitrary planforms. Literature lags in the

study or analysis of arbitrary shape planforms. Analysis of Ice berg with arbitrary shape is the front runner in the analysis of floating VLFS. The present thesis mainly deals with the study of VLFS with arbitrary shapes and the obtained results from a proposed numerical scheme will be compared with the available literature.

## **1.2 NUMERICAL METHODS**

Numerical method or a numerical simulation plays an important role in the design of engineering structures. The importance of numerical methods is increasing day by day due to its computational power, software quality and decrease in cost for simulating the model on computers as compared with experiments of high costs. However, numerical models must fulfill the strong requirement on efficiency, reliability and accuracy. Figure 1.11 shows the schematic sketch and procedures involved to solve physical problems. Initially, a base theory which suits the problem has to be selected. Further, this theory is supplemented by additional assumptions like problem dimensions, material properties, type of analysis, loading, etc. so that all the prescribed features adopted can lead to sufficient accuracy. This is called as “Physical model”.

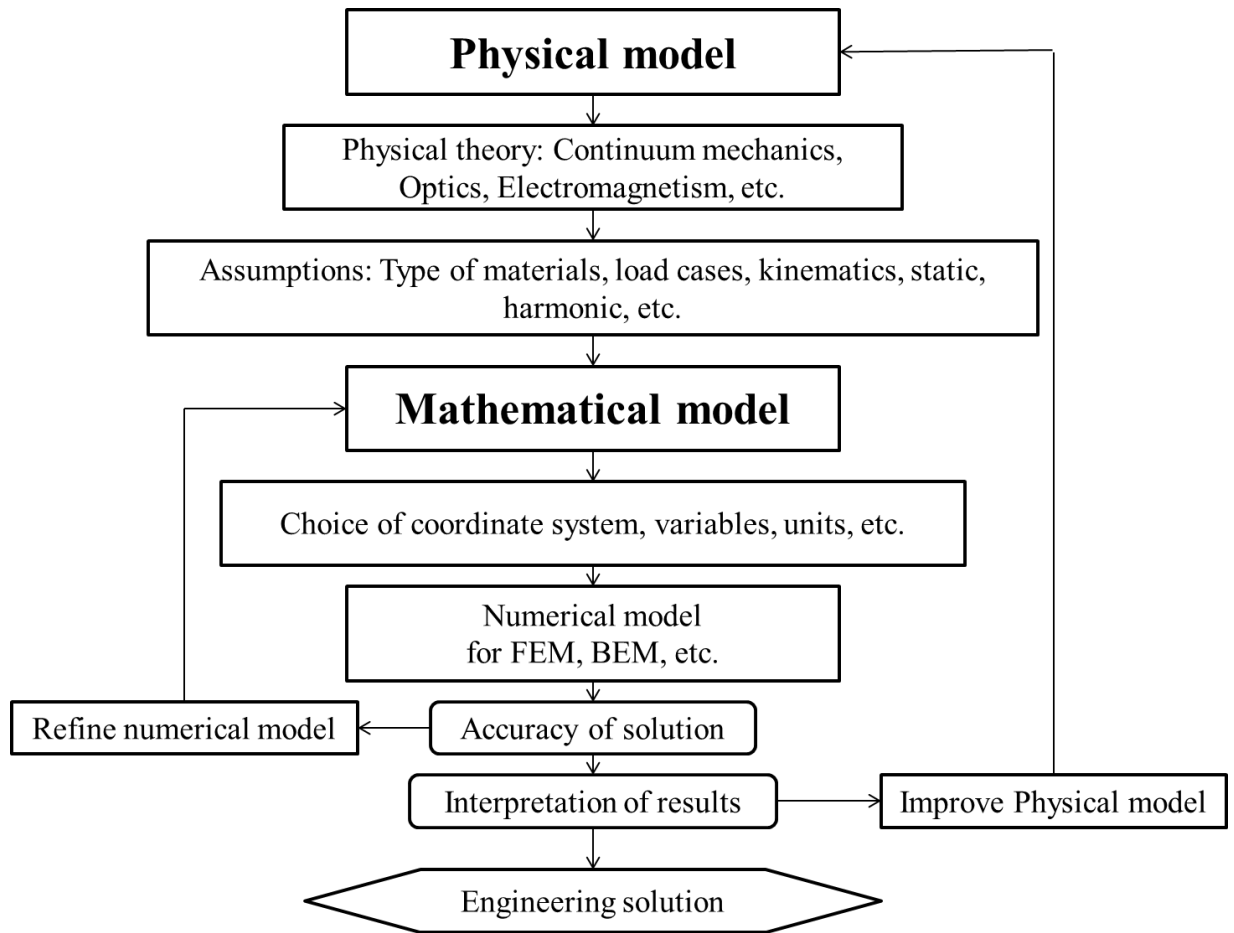


Fig. 1.11: Engineering solution of physical problem.

Subsequently, this physical model must be translated into the mathematical model. There are number of ways to express the physical model in terms of mathematical models. By selecting appropriate variables, units, coordinate systems, it can be represented in mathematical form. This leads to a particular mathematical description of physical problem with differential or integral equations, which are complemented by suitable mathematical descriptions of boundary and initial conditions. The modelling process plays a vital role in determining the best results to be obtained. The results can be obtained from a numerical tool, be it Finite Element Method (FEM), Boundary Element Method (BEM), Finite Volume Method (FVM), Finite Difference Method (FDM) or any other numerical methods. An appropriate solution scheme is as important as a good mathematical model, this helps to minimize the preparation and computational costs of the analysis. Thorough understanding of numerical tools is need to successfully solve the numerical problem. Few of the chosen solution

parameters may speed up the solution process, while few can yield erroneous results if applied incorrectly. After completion of the numerical analysis, the results must be analyzed and should be judged by experience and common sense, and should be always compared to other numerical models or any experimental models. First, it has to be assured that the accurate solution for the developed numerical model has been found. For instance, the use of inapproximate time-stepping or time-step size for the analysis of wave propagation can lead to unwanted oscillations or divergence and thus leading to useless results, even though after choosing the correct mathematical model for the analysis. Once convinced with the results obtained are accurate, then the interpretation of the obtained results from a physical point of view will be carried out to check whether it is a good or bad approximation. If the results are bad in physical point, then the analysis conducted ought to be modified or replace the physical model on which the analysis was based. At the end of the modelling, one should obtain a gratified solution for the real problems.

### **1.2.1 Boundary Element Method**

Boundary Integral Equations (BIE) are classical tools for the analysis of Boundary Value Problems (BVP) consisting of partial differential equations (Costabel, 1986). In general, any approximate numerical solution of the Boundary Integral Equation is termed as “Boundary Element Method” (BEM). By using BEM, the Boundary Value Problem must be solved to get an approximate solution. The obtained approximate solution has the eminent feature which may be an exact solution of the partial differential equation. Some of the advantages of BEM over the other methods like Finite Element Method (FEM) or Finite Difference Method (FDM) are as follows:

- Discretization will be carried out only at the boundary of the domain. When a boundary is just like a curve, i.e. two dimensional domain, this allows very simple data input and storage methods.
- Exterior problems such as unbounded domains with bounded boundaries are handled easily.
- Due to the usage of integrals and semi-analytical methods in BEM, the accuracy of the model can be increased.

- Due to the reduction in dimension, the modelling can be done more easily and effectively.
- Problems involving semi-infinite and infinite domain can be modelled accurately.

Few of the main difficulties associated with BEM are as follows:

- A clear knowledge of a fundamental solution of the differential equation is necessary.
- This method is available for linear partial differential equation with unknown constants. In case of pure BEM, nonlinear differential equations are generally not possible to solve.
- Several approximate methods exist to solve different Boundary Value Problems or Boundary Integral Equations.
- The Kernels are generally singular, whereas, Boundary Integral Equations are of the first kind. These type of problems leads to singularity.
- The BEM matrices are non-symmetrical and dense in nature.

The origin of Boundary Element Method can be seen in early Eighties. Using Green's third identity, the direct Boundary Integral Equation for potential problems was carried out by Jaswon (1963) and Symm (1963). Further, Rizzo (1967) and Cruse (1969) developed BIE approaches for 2-D and 3-D electrostatic problems using Somigliana's identity. Lachat and Watson (1976) has made breakthrough in the field of BIE and introduced algorithms for weakly singular and quasi-singular integrals. Further, the researchers introduced the sub region technique to handle large scale problems. Guiggiani and Gigante (1990) presented an algorithm for solving the Cauchy principal integral values. Further, The quasi arbitrary Lagrangian-Eulerian finite element method (QALEFEM) was used by Yan et al. (2010) which is based on the fully nonlinear potential theory (FNPT). Brebbia and Dominguez (1977) coined the name BEM and detailed in Brebbia (1978).

### **1.2.2 Finite Element Method**

Finite Element Method (FEM) is one of the numerical techniques which is used to find approximate solutions of partial differential equations. It was originated from the necessity to solve the complex engineering problems, such as elasticity and structural

analysis problems in Civil, Mechanical and Aerospace engineering. The main advantage of FEM is that it allows for detailed visualization and distribution of stresses and strains in the structure. Before the conceptual design, analysis using FEM allows for redefining and optimization of the design to be constructed. Hrennikoff (1941) initially worked on Finite Element Analysis and the plane elastic plate was represented by collections of bars and beams. Clough (1960) termed or coined the word “Finite Element Method” and the first conference was held in 1965. Zienkiewicz and Cheung (1967) authored the first book on Finite Element Method and the commercial FEM software packages (ABAQUS and ANSYS) originated in the early Seventies. Algorithms on fluid flow, thermal and electromagnetic analysis were developed in 1980s and the researchers started using FEM to analyze the vibration of the structures. Further, the technique is improvised to analyze flexible structures.

## **CHAPTER 2**

### **LITERATURE SURVEY**

#### **2.0 GENERAL**

The present chapter describes the various methods used for the problem of VLFS interacting with waves, sea bed profiles, breakwaters and mooring systems. Different VLFS models and their shapes are explored. This chapter also includes reports and research articles which give the basic theory for wave propagation and diffraction. Further, studies on the interaction between floating bodies and water waves are noted. In hydrodynamics, fluid-structure interaction problem is a known topic which deals with water wave interaction with fixed or floating structures. Herein, an attempt has been made to explore the studies on interaction between water waves and VLFS during past and present scenarios.

The innovative works of John (1949, 1950) and Stoker (1957) on the motion of a floating rigid plate provided a new dimension for the analysis of floating structures. Kashiwagi (1999) reviewed the most recent (till 1990s) studies and developments on the prediction of hydroelastic responses of VLFS. A very detailed survey of pontoon type VLFSs can be seen in Watanabe et al. (2004a, 2004b). Due to its small thickness compared to its horizontal dimensions (length and width), the Very Large Floating Structure can be modelled as a thin elastic plate. The depth of water plays a vital role in solving hydroelasticity problems. Three cases would be considered viz, very deep water (Infinite water depth), finite water depth (Intermediate water depth) and shallow water. It is difficult to solve the fluid structure problem in finite and infinite depths using analytical method, whereas, it can be solved by numerical approaches.

Few of the notorious books are referred here, which are commonly used in fluid-structure interaction. Hydrodynamics and its general information are given in “Hydrodynamics” by Lamb (1945). The interaction of a floating entity with water waves is described by Stoker (1957) in “Water Waves”. The problem of fluid motion and its solutions is given by Wehausen and Laitone (1960) in “Surface Waves” and Newman (1977) in “Marine Hydrodynamics”. The basic theory and their solution for

plates in shallow water region are given in Stoker (1957). Finite and infinite water depth models with their basic theory, boundary conditions and equations are described in Newman (1977). The study involving Green's functions and equation of motion of plate is given in John (1949, 1950) and the extended works can be seen in Stoker(1957), Wehausen and Laitone (1960) and Newman (1977). Green's function method was used to model the fluid and FEM was used to model the structure in the earliest works on VLFS. Basic theories involving wave propagation, diffraction, radiation is described by various authors (Landau and Lifshits, 1959; Kochin et al., 1964; Phillips, 1966; Huntley, 1977; Lighthill, 1978). Further, the works of Gehring (1860), Kirchhoff (1876), Love (1906), Mindlin (1951), Timoshenko and Woinowsky-Krieger (1959), Weaver Jr et al. (1990) and Wang et al. (2010) are known for analysis of VLFS as a thin plate. The theories described in the aforementioned books are referred in this thesis.

## **2.1 BASIC ASSUMPTIONS IN THE ANALYSIS OF VLFS**

The following assumptions are made in the hydroelastic analysis of Pontoon type floating structures (Watson, 1944; Lewis and Keller, 1964; Newman, 1977; Watanabe et al., 2004a, 2004b).

- The VLFS with free edges is modelled as a thin elastic plate.
- The fluid is ideal, inviscid, incompressible and the fluid motion is irrotational, so that the velocity potential exists.
- Vertical motion of the structure alone is considered. The amplitude of incident wave and VLFS motions are small.
- There won't be any gap exist between fluid and the VLFS i.e. VLFS is always in contact with the fluid floating freely on the free surface.
- Sea bottom is assumed to be horizontal.

In this thesis, the above mentioned assumptions have been considered. Further, the details about boundary conditions, governing equations, etc. can be found in Chapter 3.

## **2.2 DIFFERENT APPROACHES TO ANALYSE HYDROELASTICITY PROBLEM**

The problem of fluid structure interaction can be solved by different approaches. Modal expansion method and Direct method are the two basic methods used for the analysis of VLFS in the frequency domain and are studied in detail by various researchers. Numerical determination of eigen functions using Eigen Function Expansion Method is carried out by Wu et al. (1995), Kim (1998) and Ohmatsu (2000). The Ray method and the Geometrical Optics approach were studied by Takagi and Kohara (2000), Takagi and Nagayasu (2001) and Hermans (2001, 2003, 2004). Furthermore, the Wiener-Hopf technique (Evans and Davies, 1968; Tkacheva, 2001a, 2001b, 2001c, 2002) is the widely used technique. The Galerkin method (Kashiwagi, 1998) and the boundary element method (Hermans, 2000) with the accelerated Green's function can be seen in Utsunomiya and Watanabe (2001). The hybrid methods, combination of BEM-FEM and coupled higher order BEM-FEM were explored by Seto (1998), Wang and Meylan (2004), Yoon et al. (2014), Pan et al. (2016) and Jagite et al. (2018).

Mei and Tuck (1980) studied hydroelastic analysis by adopting the modal expansion method. The authors differentiated the method into two parts such as hydrodynamic analysis and the dynamic response of the plate. The deflection of the free-free edge plate is disintegrated into modes of vibration that can be chosen arbitrarily. Different methods of modal functions were studied by various authors. Researchers like Wu et al. (1995), Kashiwagi (1998) and Utsunomiya et al. (1998) studied the modal function for a free-free beam, Meylan and Squire (1996) and Meylan (2001) analyzed the modal functions of vibration for free plate in which the modal functions were calculated by using Green's function technique (Taylor and Ohkusu, 2000) and Cubic B-spline function. For each mode, unit amplitude is considered and hydrodynamic radiation forces are evaluated for freely vibrating plate. The modal amplitudes and responses of the governing equation is calculated by Galerkin's method. The model for thick plate analysis has been developed by Watanabe et al. (2006), and has studied the hydroelastic behaviour of a pontoon type VLFS. The study of fluid structure interaction has been carried out by using the modal expansion method in the

frequency domain. Using Mindlin theory, the circular thick plate with free edges have been analysed and the deflection is found to be in exact manner. Further, the study has been carried out to calculate the hydrodynamic diffraction and radiation forces using Eigenfunction Expansion Matching Method. Kim (1998) and Peter and Meylan (2004) used the modal expansion method to study the behavior of floating structures. The modes are divided into two types, namely dry and wet modes. Dry modes approach is the most commonly used method and the researchers Meylan and Squire (1996) and Kim (1998) adopted the dry modes approach because of its numerical efficiency and simplicity to solve the problem. Wet mode approaches are studied by Humamoto and Fujita (2002). The articulated floating plate was studied by Karmakar and Sahoo (2005). Further, the wave scattering by articulated floating elastic plate in infinite depth is studied by using the linearized water wave theory. The study was based on the geometrical symmetry of the articulated plate and the associated boundary value problem in the half plane is reduced to 2-D boundary value problem in the quarter plane. The solutions are derived by the direct application of a mixed type Fourier transform and the corresponding mode coupling relation.

In the direct method, the deflection of VLFS is determined by solving the governing equations directly without expanding into eigen modes and both, 2-D and 3-D geometries can be solved. Direct method and its solution for VLFS were pioneered by Mamidipudi (1994). In the solution obtained by Mamidipudi (1994), radiation and diffraction potentials were established first, then solving the combined hydroelastic equation by using finite difference scheme, the deflection of VLFS is determined.

Different types of direct methods were proposed by Ohkusu and Namba (1996, 1998). The authors perspective was based on the idea that the floating thin plate is also a part of free surface with properties differing from the fluid. In hydrodynamics, this problem is considered as a Boundary Value Problem (Babich and Kirpichnikova, 2003) rather than a problem determining the elastic response of the floating body. Meylan and Squire (1996) used the approach proposed by Ohkusu and Namba (1996) to analyze the problems of 2-D ice-floe dynamics. Further, Zilman and Miloh (2000) applied Boundary Value Problem proposed by Ohkusu and Namba (1996) to solve the circular floating plate problem. The main advantage of Boundary Value Problem is

that, in case of shallow water depth a closed form solution can be obtained. By using the approximation theory of Stoker (1957), the shallow water solution can be obtained. Kashiwagi (1998) proposed another type of direct method, in which, the deflection of the plate is derived from the vibration equation of the structure, using the pressure distribution method. Cubic B-spline function is used to achieve the accuracy in a very short wavelength regime. Further, cubic B-spline functions are used to represent the unknown pressure and to satisfy the boundary conditions, Galerkin method is applied. Babich and Buldyrev (1991) described the asymptotic theory for short waves. The same theory was applied by Ohkusu and Namba (1998) to analyze the VLFS problem using Wiener-Hopf technique (Morse and Feshbach, 1953; Noble 1958). Tkacheva (2001a, 2001b, 2001c, 2002, 2003) solved various problems in fluid-structure interaction. Vibrational equation method was proposed by Meylan (2002). Using Green's function, the problems related to crack were studied by Squire and Dixon (2000) and Williams and Squire (2002). Further, Evans and Porter (2003) considered multiple crack problems.

Using the geometrical-optics approach, Hermans (2000, 2001, 2003, 2004) solved the problem of diffraction of incident surface waves intercepted by floating platforms. Takagi and Kohara (2000) used the corresponding ray method to solve the VLFS problem. The improved ray method was proposed by Takagi (2001) and Takagi and Nagayasu (2002). Here, the authors have introduced and applied the parabolic approximations. The general ideas of geometric optics can be seen in Lewis and Keller (1964), Luneburg and Herzberger (1964) and Kay and Kline (1965). Kouzov (1963) studied the problem related to acoustics by using the Riemann-Hilbert technique. Evans and Davies (1968) presented the solution for evaluating transmission and reflection of waves in deep and semi-infinite regions. Kohout et al. (2007) and Kohout and Meylan (2008) studied the drift of complicated two dimensional model which consists of hundreds of elastic plates. The continuum mechanics-based finite element method was employed to model floating structures with arbitrary geometries, whereas, the boundary element method is used for the fluid by means of total potential formulation. According to Kim et al. (2013), an additional condensation procedure in conjunction with the modal superposition method, the

modified formulation can be linked to the conventional wave-structure interaction formulation. Further, Cho and Kim (2013) studied the interaction of oblique monochromatic incident waves with a submerged horizontal porous plate and has been investigated in the context of two-dimensional linear potential theory. Yoon et al. (2014) proposed a numerical procedure to analyze floating plate structures with multiple hinge connections in regular waves and investigated the maximum bending moment and deflection in the plate structures. The hinge connection was modelled by releasing the rotational degrees of freedom of the plate finite elements, in which, a complete condensation procedure is used considering structural mass, stiffness and fluid-structure interaction terms. As the number of hinge connections increases, the maximum bending moment in the floating plate decreases. The change in the maximum deflection due to hinge connections is large in the range of short wave. Also, it is reported that deflection becomes smaller as the wavelength becomes larger.

Kim et al. (2014) proposed a Hydroelastic Design Contour (HDC) that can be practically used for the preliminary design of pontoon type rectangular Very Large Floating Structures (VLFSs). Using this design contour, one can easily predict the maximum bending moment of VLFS in irregular waves. To develop the design contour, Hydroelastic Response Contours (HRCs) were developed by carrying out hydroelastic analyses considering various structural and wave conditions. Based on the pre-calculated HRCs, HDCs were developed considering irregular waves. The conclusion was made stating that the maximum bending moments which is predicted through HDC can be used for the preliminary design of VLFS. A theoretical model of water wave over wash of a thin floating plate was proposed by Skene et al. (2015). The nonlinear shallow-water equations were used to model the over wash, and the linear potential-flow. The model was shown to predict qualitative and quantitative over wash properties accurately for shallow over wash, which generally occurs for incident waves with relatively short lengths or low steepness. The hydroelastic responses of a mat - like, rectangular very large floating structure edged with dual horizontal / inclined perforated plates using analytical, numerical and experimental methods was performed by Cheng et al. (2016). In the analytical method, the Eigen function Expansion - Matching Method (EEMM) for multiple domains has been

applied to evaluate the diffraction and radiation potentials, and then the elastic equation of motion is solved by the Rayleigh – Ritz method. In the numerical model, the modal eigen vector equation of the VLFS with discrete Mindlin plate elements were obtained by using the Finite Element Method, whereas, the Boundary Element Method is applied to solve the water wave equation. The hybrid Finite Element Method-Boundary Element Method (FEM-BEM) solution is employed for more general cases with the inclusion of inclined perforated anti – motion plates. A series of experiments were conducted in order to validate analytical and numerical solutions.

Several experimental studies (Seto, 1998; Ohmatsu, 2000; Liet al., 2003) and numerical techniques were proposed by researchers in recent years. Direct integration method is the most common approach to analyze the VLFS in time domain and it uses Fourier transformation (Endo, 2000). Structural and fluid domain equations are both discretized in direct time integration method. Initially, the solution is obtained for fluid domain and the obtained solution/results are inserted into differential equations to capture elastic motion using Fourier transformation method. Coupling between Weakly Compressible Smooth Particle Hydrodynamics (WCSPH) and Total Lagrangian Smooth Particle Hydrodynamics (TLSPH) was carried out by He et al. (2017), to solve the hydroelastic problems. WCSPH and TLSPH methods are used to simulate fluid and structural dynamic equations, respectively. Mandal et al. (2017) studied the flexural gravity waves using eigen functions. Single layer and two layer fluids in both finite and infinite water depths are explored. The study concentrates to capture the scattering of gravity waves due to multiple articulations.

### **2.3 MODELS IN DIFFERENT WATER DEPTHS**

In hydrodynamics, there are three different models of water depth namely, shallow, finite and infinite water depths are available. One of the three models must be used for the fluid-structure interaction problem. Generally, it is very difficult to solve finite water depth models analytically. Approximation theories were developed to solve the shallow and infinite water depth models. Shallow and infinite water depth models can be modelled by taking the limits of depth as zero and infinity, respectively. By deriving an approximation theory, Stoker (1957) treated the shallow water problem.

John (1949, 1950) studied for water with finite depth, Kochinet al. (1964) studied the wave propagation and diffraction for infinite deep water and Wehausen and Laitone (1960) studied both infinite and finite water depths, and was continued by Newman (1977) as well.

Studies by authors such as Meylan and Squire (1996), Hermans (2000), Tkacheva (2001), Takagi (2002), Tkacheva (2001b) and Peter and Meylan (2004) consist of the problems of floating bodies in water waves for infinite water depth. The case of finite water depth was studied by different researchers like Mei and Black (1969), Fox and Squire (1994), Balmforth and Craster (1999), Takagi et al. (2000), Hermans (2001), Meylan (2001), Andrianov and Hermans (2003), Evans and Porter (2003), Tkacheva (2003), Hermans (2004) and Porter and Porter (2004). Few of the researchers have solved problems involving infinite water depth and later, they improved their technique to solve finite water depth (Guéret, 2003; Andrianov and Hermans, 2005, 2006a, 2006b). By using Stoker theory, solutions were derived for the problem of shallow water depth (Evans and Davies, 1968; Ohkusu and Namba, 1998; Zilman and Miloh, 2000; Sturova, 2000, 2001; Tsubogo, 2001; Ohkusu and Namba, 2004).

#### **2.4 APPLICATIONS AND PROBLEMS RELATED TO VLFS**

VLFS have many possible applications and therefore, researchers tend to take the problems according to the field requirements. For instance, the aircraft landing on and taking off effects on structures, different types of loads on VLFS and the connections and disconnections of several modules.

Endo (2000) and Guéret (2003) presented the analytical model of landing or taking off from VLFS. Yeung and Kim (2000) investigated the translation load applied on the floating structure. Further, Sturova (2002, 2003) studied the effect of external loading on a floating platform in shallow water.

The motions of air-cushioned Very Large Floating Platform (VLFP) were investigated by Pinkster (1998) and Guret and Hermans (2001, 2003). The obtained results of air-cushioned VLFP were further compared with the results of pontoon type VLFS. Cheung et al. (2000) considered a pneumatic floating platform. The buoyancy force to lift/carry the weight of the structure is provided by the air pressure acting on the

underside of the deck. The dynamic characteristics of the system are modified by the trapped air introduced between the platform and the water. Further, the transient response of a pontoon type VLFS subjected to moving load due to airplane landing/take-off was studied by Senjanovic et al. (2015). By using Rayleigh's quotient, Senjanovic et al. (2015) proposed an approximate solution which consists of set of natural vibrations/frequencies.

Traditionally, Very Large Floating Structures are considered as flat thin plates with uniform thickness at shallow water with the assumption of sea bed as a flat surface. But, usually the depth varies as it approaches near to the shore. The direct effect due to change in water depth and seabed can be seen in wave parameters, such as wave height, wave direction, wavelength, wave reflection and wave radiation. Hence, researchers like Takagi and Kohara (2000) have studied the non-flat bottom surface and non-uniform sea-bed. The topographical effects of the sea bed were studied by Murai et al. (2002). The solution has been derived by Porter and Porter (2004) by considering fluid of variable depth and variable thickness of floating structure for the case of finite water depth. The effect of irregular depth on floating structure was studied by Athanassoulis and Belibassakis (1999) and Belibassakis and Athanassoulis (2004 and 2005).

Very Large Mobile Offshore Structures (VLMOS) are the next generation of VLFS and can be used for different purposes in the marine environment. Japan is using VLMOS for wind and solar power plants (Takagi, 2004; Watanabe et al., 2004b; Takagi and Noguchi, 2005). Due to their mobile nature, complexity in analysis is increased. If the mobility of the structure is made to zero, then they can be analyzed as normal VLFS.

Sea ice-water interaction has been studied by various researchers. The principle approach remains same in both VLFS and sea-ice interactions. In general, the basic theory can be applied to solve both the problem as these two problems are very similar to each other. The reflection and transmission of waves with motion of ice sheets can be seen in Evans and Davies (1968), Doronin and Kheisin (1977), Fox and Squire (1994), Meylan and Squire (1996), Slepnyan and Fadeev (1988), Balmforth and

Craster (1999) and Linton and Chung (2003). Eigen function, Wiener-Hopf and BEM-FEM are widely used techniques to solve hydroelastic problems. The study of diffraction is an age old problem in optics, acoustics, electromagnetism, etc. The diffraction of various kinds of waves when encountered with structure was studied by, Kouzov (1963), Lewis and Keller (1964), Luneburg and Herzberger (1964), Jones (1965) and Kay and Kline (1965).

## **2.5 DIFFERENT SHAPES AND MODELS OF VLFS**

Classical thin plate theory or Kirchhoff theory (Gehring, 1860; Kirchhoff, 1876; Love, 1906), Mindlin theory (Mindlin 1951) and Timoshenko or Timoshenko-Reissner theory (Timoshenko and Woinowsky-Krieger, 1959) are the most commonly used plate theories. Kirchhoff plate theory has been used by many of the researchers (Ohkusu, 1996; Kashiwagi, 1998; Kim, 1998; Takagi et al., 2000; Tkacheva, 2001c; Zilman and Miloh, 2000; Andrianov and Hermans, 2003, 2005, 2006a; Meylan, 2001; Khabakhpasheva and Korobkin, 2002) to analyse mat like VLFSs as thin plates. The plate is said to be freely vibrating or freely floating on the water surface when it has free edges. VLFSs can be modelled as orthotropic plates by varying plate mass and stiffness and are explored by Mamidipudi (1994) and Hermans (2003). Mindlin's first order shear deformation theory is used to obtain the accurate stress results and the extended works can be seen in Andrianov and Hermans (2002), Watanabe et al. (2003), Wang et al. (2004) and Andrianov and Hermans (2005).

VLFS has been modelled as a floating beam by various researchers. Such a model does not describe the 2-D action of Pontoon type VLFS. VLFSs have also been modelled as different modules and are linked to each other to frame a VLFS. Sandwich grillage model, articulated plate, plane grillage mode, etc. are few of the examples. Based on characteristics of wave, ocean currents and sea currents, the choice of VLFS shape depends. Generally, the VLFS vary in their size and can have any shape (Yoneyama et al., 2004; Watanabe et al., 2004a; Riyansyah et al., 2010; Gao et al., 2011; Michailides and Angelides, 2012). Researchers like Mamidipudi (1994), Ohkusu and Namba (1998), Korobkin (2000), Taylor and Ohkusu (2000), Takagi et al. (2000), Hermans (2003), Usha and Gayathri (2005) and Papathanasiou

and Belibassakis (2014) have studied the rectangular plan form in shape. The plates having one or two infinite dimensions can be analyzed with analytical or numerical methods as described in the review articles by Kashiwagi (1999) and Watanabe et al. (2004a). Numerical methods are often used to solve the problems consisting of finite plates. Tkacheva (2001) and Linton and Chung (2003) have considered a half-plane problem with strip of infinite length and a quarter infinite plates (Ohkusu and Namba, 2004; Takagi, 2004). Hermans (2004) considered the floating platform with multiple plates connected to each other. A new model has been proposed by Lu et al. (2016) which is generally based on multi-body hydrodynamics and Euler-Bernoulli beam theory. A continuous VLFS has been divided into multiple modules and the section between two adjacent modules is considered as a beam element. Dry natural oscillation mode for hinged two-module flexible structure and hydrodynamic coefficients for each modes are evaluated by Sun et al. (2017). The finite gap that existed between two adjacent plates was studied by Chung and Linton (2003). Similarly, cracks in ice sheets was studied by Evans and Porter (2003).

Non-rectangular VLFS can serve the purposes like floating airports, power plants, floating storage facilities and floating cities. Meylan and Squire (1996), Zilman and Miloh (2000), Peter et al. (2003), Tsubogo (2001) and Sturova (2003) have analyzed the VLFS having a circular plan form. Humamoto and Fujita (2002) studied the arbitrary shapes such as L-shaped, X-shaped, C-shaped and T-shaped VLFSs. It is necessary to study the different shapes of floating structures to expand the floating structure with ease. This thesis concentrates on study of VLFS with different shapes (arbitrary shapes).

## **2.6 BREAKWATERS AND MOORING SYSTEMS**

Moorings systems, breakwaters and anti-motion devices are used to hold the VLFS in its place, to reduce its motion and keep it in its position. VLFS which are moored to shore are called as previous generations of VLFS and these are still in operating conditions in various countries. Breakwaters are used to reduce the energy of incoming waves and are usually constructed nearby the floating structures (Fig. 2.1). Special anti-motion devices can be used for this purpose as well. Studies have been

carried out on a VLFS moored in a reef or shore. Takagi (1996) studied the mooring force and elastic deformation of a VLFS on Tsunami waves. The hydroelastic analysis of the floating structure with mooring system has been analyzed by Watanabe et al. (2004a) and Yoneyama et al. (2004). By using a special mooring system which consists of the combination of dolphins with rubber fenders, the elastic motion of a VLFS can be reduced. Nagata et al. (1998), Utsunomiya et al. (1998), Ohmatsu (2000) and Nagata et al. (2003) studied the effect of breakwaters on the elastic motion of floating plate. Nagata et al. (1998) derived an analytical method to determine the motion of a VLFS in sea waves with breakwaters. Further, Nagata et al. (2003) analyzed the motion of VLFS which is surrounded by breakwater with the help of Higher-Order Boundary Element Method. Seto (1998) presented a numerical method for predicting the hydroelastic behaviour of VLFS in water region which is sheltered by breakwaters and land. Hybrid BEM-FEM method is employed to reduce the computational effort. Ohmatsu (2000) studied the effect of mutual interaction between the VLFS and the breakwater where the partial reflection coefficient is included. In the case of long waves, there is an effective reduction in the vertical deflection, whereas, for short waves the reduction is not always prominent. Usually all researchers and engineers consider the breakwaters as gravity type, anchored into the bottom. These types of breakwaters are not environmental friendly as they interrupt the water flow around VLFS. The construction cost may be higher for large depth installation as they are bottom mounted. Floating breakwaters are proposed such that they will allow the water to flow through openings at the bottom. This type of proposal is made to reduce the cost as well as to maintain the environmental friendly space.



Fig. 2.1: Existing breakwater in Latsi harbour.

In recent times, different breakwaters have been proposed, such as multilayered wave barriers, vertical barriers, Oscillating Water Column (OWC) type, structure embedded with an OWC type breakwater and floating breakwater using a submerged plate. Usha and Gayathri (2005) studied about a twin plate breakwater for the case of deep water. The mega-float was analyzed to capture elastic motions. In order to reduce the elastic motion, special antimotion devices and submerged plates are utilized by researchers. One of the anti-motion devices is a box-shaped structure which is attached to the edges of the VLFS. Takagi et al. (2000, 2001a), through his experimental and numerical studies showed that the performance of anti-motion devices are effective in reducing the deflection/elastic motion. It also reduces the deflection, bending moment and shear force of the floating structure. In order to reduce the deflection of the floating structure, Korobkin and Khabakhpasheva (2001) investigated the use of attaching the horizontal plate to the VLFS or attaching vertical plates at the edges of VLFS. Horizontal plates proved to be more effective when  $L/h \leq 1$ . As the vertical plate depth increases the effect of displacement reduces ( $d/w \leq 1$ ) and it is proven to be not economical as of horizontal plate. Korobkin and Khabakhpasheva (2001) and Watanabe et al. (2004a) have reported that there will be a sufficient reduction in the

motion of the VLFS if the mooring system is used together with plate attachments as an anti-motion device. It is also concluded that there is no need to use breakwaters, too. To reduce the hydroelastic responses, researchers have proposed other forms of plate attachments such as L-shape, reverse L-shape and T-shape. Watanabe et al. (2004a, 2004b) provided the details on anti-motion devices, mooring system, wave forces and breakwaters for the VLFS system.

## **2.7 SUMMARY OF LITERATURE REVIEW**

Studies on hydroelastic behaviour of VLFS were performed by various researchers by using analytical, numerical and experimental works. The main objective is to minimize or to optimize the deflection, bending moment and shear force imposed by wave loading. In the analytical work, the wave force is separated into diffraction and radiation components based on the problem of interest and VLFSs were analysed. VLFS with different support conditions such as free-free, simply supported, moored condition, etc, have been analysed by using Eigen function Expansion Matching Method. Further, VLFS of circular shape has been analysed using Bessel's function. In the numerical work, VLFS has been analysed as both beam and plate models. For the analysis of VLFS as a beam, Euler-Bernoulli's beam theory has been adopted. To analyse as a plate, classical thin plate and Mindlin's theories for thin and thick plates, respectively have been used. The floating platform has also been analysed by hybrid method (combination of FEM and BEM). However, the incident velocity potential is calculated using Boundary Element Method. The articulation of the VLFS has been carried out and optimum hinge stiffness between two beams has been investigated. Studies were carried out for three different water depths, such as shallow, finite and infinite water depths. The effect of bathymetry change on the performance of floating platform has also been analysed. In case of experimental works, it has been observed that researches have used Elastic modulus of 103MPa, draft of 10mm and Poisson's ratio of 0.35 to 0.40 and the results obtained were used for the validation of the analytical and numerical models developed by the researchers.

## **2.8 NECESSITY AND RELEVANCE OF THE PRESENT STUDY**

The literature showcases that the researchers have analyzed the hydroelastic analysis of VLFS both analytically and numerically. The reduction in the response of the floating structure has been analyzed by incorporating articulation and change in bathymetry through different methods and forms of Eigen function Expansion Matching Method. The researchers have used two and four noded elements in FEM to model the plate and to study the deflection of floating platform. The review of literature shows that the BEM model has not been modified and there is a need to explore this area. Further, the studies using Green's function in BEM is scanty. There is a need to develop a modified Green's function which will be suitable for finite and infinite depths, oblique wave attack and different shapes. Literature lags behind in the detailed explanation of Bessel's and Hankel functions and their respective orders. There is a necessity to study Bessel's and Hankel functions in order to modify the Green's function. The study on numerical integration must also be explored to support and to check the number of integration points per node of an FEM element. It is specified that the use of Bessel's function is limited/mostly used for circular platform. Hence, it is decided to include the functions like Bessel's or Hankel functions of different orders. Further, traditional Green's function has been modified to obtain comparably better results than the results reported in the available literature. In the present study, the use of Bessel's function combined with Hankel's function has been studied and adopted in the Green's function.

## **2.9 OBJECTIVES OF THE STUDY**

The present study is intended to demonstrate the effectiveness of the modified Green's function in order to capture the vertical deflection of the floating platform.

1. To develop a modified Green's function and to study hydroelastic analysis of VLFS, using coupled equation (coupling between structure and waves).
2. To develop a numerical model which is suited for finite and infinite water depths with variable bottom topography.
3. To study the response of the structure for different angle of wave attacks.

4. To study the number of integration points per node and number of panels required for the convergence of the model.
5. To study the response of different shapes (Rectangular, Triangular and Trapezoidal) of VLFSs.
6. Validation of the numerical model by available literature.

## CHAPTER 3

### MATHEMATICAL FORMULATION

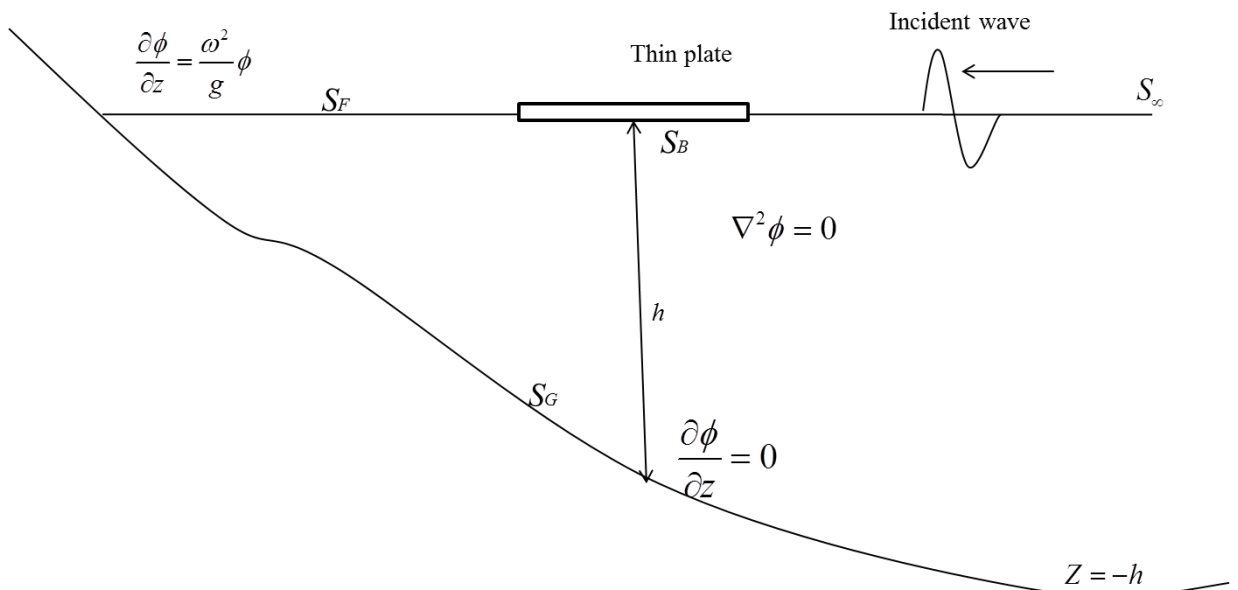
#### 3.1 GENERAL THEORY AND PROPOSED SOLUTION

This chapter deals with the formulation of mathematical model for the analysis of hydroelastic behaviour of VLFS under marine environment. Compared to horizontal dimensions, the thickness of the VLFS is considered to be small. The thickness/ draft is in the order of several meters, whereas, the horizontal dimensions are about several hundred meters to kilometers. Since the VLFS behave as a thin plate, hence forward in this thesis standard classical thin plate theory has been considered. A modified Green's function has been developed and its justification is done. Further, it is incorporated in hybrid BEM-FEM method. The present work describes the solution for three different shapes of thin elastic plate. In addition, the numerical studies are presented for finite and infinite water depths with sloping bathymetry. Perhaps, horizontal dimensions of plate to have the order of thousand meters, the wavelength is of order from ten to hundred meters in practical circumstances. Therefore, similar conditions are adopted in the present work in order to develop the numerical model. The numerical simulation can further be applied to small plates whose length is same or smaller than the wavelength. The present work is desired to capture the vertical displacement of the floating plate by considering frequency domain approach. Ocean engineering containing the problems related to infinite series and motivated for the use of Green's function. The primary use of Green's functions is to solve non-homogeneous boundary value problems. In the available literature, researchers have considered a delta function with parameter  $\xi$ , and a fixed value of  $\xi$   $G(x, \xi)$ . The Green's function which is available has been modified by the researchers using first order of Bessel's function in order to obtain deflection. Literature lags behind in explaining the use of Bessel's functions and Hankel function of different orders to obtain the deflection of a structure. The present work concentrates on using the Bessel's function and Hankel function of different order to obtain deflection. Further the obtained results have been validated with the results available in the literature. The mathematical formulation is based on BEM-FEM hybrid methodology with modified

Green's function. Subsection 3.2 gives the details about the general theory and proposed solution method. Initially, physical and mathematical formulation of the problem is studied and is transferred into a numerical model by applying various boundary conditions. The proposed model is capable of analysing thin plates with arbitrary shapes.

### 3.2 MATHEMATICAL FORMULATION

Mathematical formulation for the fluid-structure interaction, herein, water waves – VLFS interaction is described as follows. Very Large Floating Flexible Structure of arbitrary shape, freely floating in an open sea, always in contact with the water surface and meets the incoming regular water waves is considered. Very Large Floating Structure is modelled as a thin plate and Figure 3.1 shows the general geometry and coordinate system of the floating elastic plate. The plate occupies (covered) a certain part of the water surface which is denoted by  $S_B$ . Further,  $S_F$ ,  $S_\infty$  and  $S_G$  to represent the open free surface, open free surface towards infinity and seabed, respectively. The vertical coordinate  $z$ , points upwards with the water surface at zero and sea floor at  $z=-h$ . The horizontal co-ordinates  $x$  and  $y$  are denoted by the vector  $X$ . With negligible draft, the plate is considered to be freely floating on the surface of the water with wave encountering at different angles.



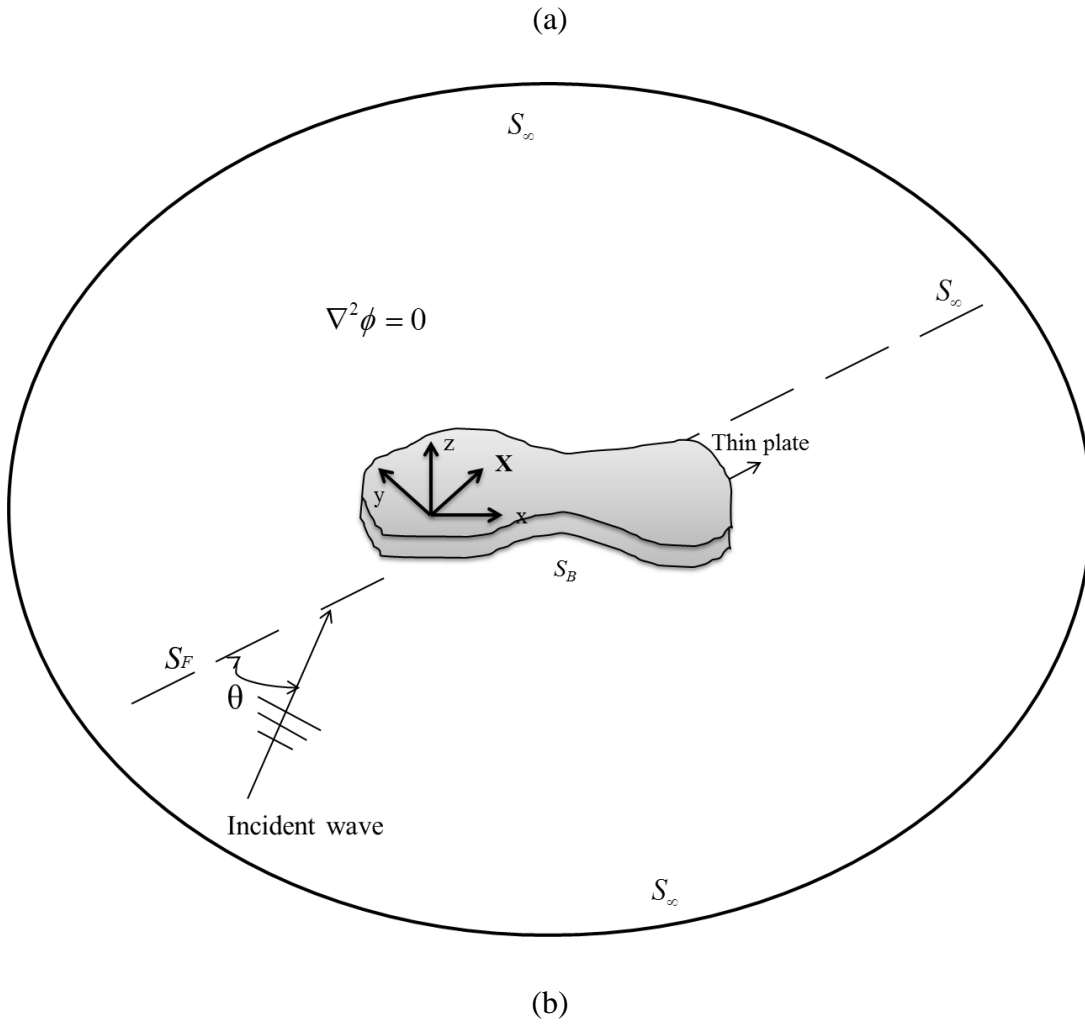


Fig. 3.1: Schematic diagram of floating structure. (a) Sectional View and (b) Plan view.

The structural and fluid properties considered in the problem are as follows. The plate which has the density  $\rho_i$  is considered to have the total length  $L$ , breadth  $B$  and thickness  $d$ , which freely floats on the water surface at a water depth  $h$ , and fluid density  $\rho_w$ . The structure is assumed to be elastic, homogeneous and isotropic in nature with  $D$  and  $\nu$  as flexural rigidity and Poisson's ratio, respectively. To satisfy the Laplace equation, fluid is assumed to be ideal, irrotational and inviscid in nature. With angular frequency  $\omega$ , and wavelength  $\lambda$  the incident wave is assumed to be coming continuously with an angle  $\theta$ . The equation of motion of elastic plate [Equation (1)] can be solved with boundary conditions as mentioned in Equation (2) (Wu. et al., 1995).

$$D\nabla^4 W + \rho_i h \frac{\partial^2 W}{\partial t^2} = P \quad (1)$$

$$\frac{\partial^2 W}{\partial n^2} + \nu \frac{\partial^2 W}{\partial s^2} = 0 \text{ and } \frac{\partial^3 W}{\partial n^3} + (2 - \nu) \frac{\partial^3 W}{\partial s^3} = 0 \quad (2)$$

where,  $W(x, y, z, t)$  is the plate displacement. Pressure at the interface of the water surface and the plate is denoted by  $P$  and  $n$  and  $s$  denote the normal and tangential directions, respectively. The pressure at the water surface can be obtained from the linearized Bernoulli's equation (Newman, 1977).

$$P = -\rho_w g W - \rho_w \left. \frac{\partial \phi}{\partial t} \right|_{z=0} \text{ on } S_B \quad (3)$$

Further, Equation (1) and Equation (3) are equated to get the fluid plate interaction.

$$D\nabla^4 W + \rho_i h \frac{\partial^2 W}{\partial t^2} = -\rho_w \left. \frac{\partial \phi}{\partial t} \right|_{z=0} - \rho_w g W \quad (4)$$

where,  $\phi(x, y, z, \lambda)$  is the velocity potential of water wave and  $g$  is the gravitational acceleration constant. The variables are non-dimensionalised and are represented as follows

$$\bar{x} = \frac{x}{L}, \bar{y} = \frac{y}{L}, \bar{z} = \frac{z}{L}, \bar{w} = \frac{w}{L}, \bar{d} = d \sqrt{\frac{y}{L}} \text{ and } \bar{\phi} = \frac{\phi}{L \sqrt{xy}}.$$

where,  $L$  is the longest dimension of the arbitrary shape. Substituting dimensionless variables in Equation (4), it is modified as follows,

$$\beta \nabla^4 \bar{W} + \gamma \frac{\partial^2 \bar{W}}{\partial \bar{t}^2} = -\left. \frac{\partial \bar{\phi}}{\partial \bar{t}} \right|_{\bar{z}=0} - \bar{W} \quad (5)$$

where, the constants  $\beta(\text{Stiffness}) = \frac{D}{\rho_i L^4 g}$  and  $\gamma(\text{Mass}) = \frac{\rho_i h}{\rho_w L}$

### 3.2.1 Reduction to single frequency problem

Assuming an incident wave with potential  $\phi_I$  and angular frequency  $\omega$  which enters the computational domain leads to vibrate the plate in a steady state harmonic motion in the same frequency  $\omega$ . Therefore, the fluid structure interaction problem can be considered at a single frequency which allows to represent the time dependence by  $exp(i\omega t)$ , where  $i$  is the imaginary number. Thus, the displacement and potential can be presented as the real parts of complex function as follows.

$$\bar{W}(\bar{x}, \bar{y}, \bar{t}) = \text{Re}[\bar{w}(\bar{x}, \bar{y})e^{-i\omega\bar{t}}] \quad (6a)$$

$$\phi(\bar{x}, \bar{y}, \bar{z}, \bar{t})_{z=0} = \text{Re}[\phi(\bar{x}, \bar{y})e^{-i\omega\bar{t}}] \quad (6b)$$

$$P(\bar{x}, \bar{y}, \bar{t}) = \text{Re}[(-\rho_w g \bar{w} + i\omega \rho_w \phi)e^{-i\omega\bar{t}}] \quad (7)$$

By substituting Equations (6a & 6b) and (7) in Equation (5) and omitting  $e^{i\omega t}$ , Equation (5) becomes

$$\beta \nabla^4 w(\bar{x}, \bar{y}) - \omega^2 \gamma w(\bar{x}, \bar{y}) = i\omega \phi(\bar{x}, \bar{y}) - w(\bar{x}, \bar{y}) \quad (8)$$

For the sake of convenience, the bar over the non-dimensional parameters are eliminated henceforth.

### 3.2.2 Equation of motion for water wave

The single frequency velocity potential of water wave must satisfy the Laplace equation.

$$\nabla^2 \phi(x, y, z) = 0, \quad (9)$$

and boundary conditions (Hermans, 2000).

$$\frac{\partial \phi}{\partial z}(x, y, z) = 0, \text{ on } S_G \quad (10)$$

$$\frac{\partial \phi}{\partial z}(x, y, z) = -i\omega w(x, y), \text{ on } S_B \quad (11)$$

$$\frac{\partial \phi}{\partial z}(x, y, z) = \frac{\omega^2}{g} \phi, \text{ on } S_F \quad (12)$$

Equation (10) implies the boundary condition at the sea bed which expresses impermeability i.e. no fluid enters or leaves the sea bed and hence, the velocity component normal to the sea bed is zero. Equation (11) shows that no gap exists

between the plate and the water free surface. Equation (12) is called as combined kinematic and dynamic free surface boundary condition. The wave velocity potential must also satisfy the Sommerfeld Radiation (Seto, 1998) condition as  $|X| \rightarrow \infty$   $|X| \rightarrow \inf$

$$\lim_{|x| \rightarrow \infty} \sqrt{|X|} \left[ \frac{\partial}{\partial |X|} - i\omega^2 \right] (\phi - \phi_i) = 0, \text{ on } S_\infty \quad (13)$$

Assumption is made that the incident potential is a plane wave and is given by,

$$\phi^{in} = \frac{A}{\omega} e^{ik(x \cos \theta + y \sin \theta) e^{kz}}, \text{ for infinite depth} \quad (14)$$

$$\phi^{in} = \frac{A}{\omega} e^{ik(x \cos \theta + y \sin \theta)} \frac{\cosh k(z+h)}{\cosh kh}, \text{ for finite depth} \quad (15)$$

$$\frac{\omega^2}{g} = k \tanh kh, \quad (16)$$

### 3.2.3 Boundary Element Method for solving fluid motion

In order to determine the fluid motion, the Boundary Element Method is adopted to the Laplace equation together with the boundary conditions [Eqns. (10-12)] into a boundary integral equation. This transformation reduces the modelling dimensionality from a 3-D fluid volume domain to 2-D fluid surface boundaries, thereby, requiring only the boundaries of the solution domain to be discretized. In carrying out the transformation, the 3-D fundamental solution and 3-D free surface Green's function are used. The 3-D fundamental solution of Laplace equation based on a concentrated potential or source at the point  $\xi$  is given as (Brebbia, 1978).

$$G(X, \xi) = C_s \left[ \frac{1}{R(X, \xi)} \right] \quad (17)$$

$C_s$  is the strength of the potential at the point  $X$  and it is convenient to set the source strength  $C_s = 1$ . Considering  $X = (x, y, z)$  as the field point and  $\xi = (\xi, \eta, \zeta)$  as the source point, the distance between source point and field point  $R(X, \xi)$  is given as

$$R(X, \xi) = \sqrt{(x-\xi)^2 + (y-\eta)^2 + (z-\tau)^2} \quad (18)$$

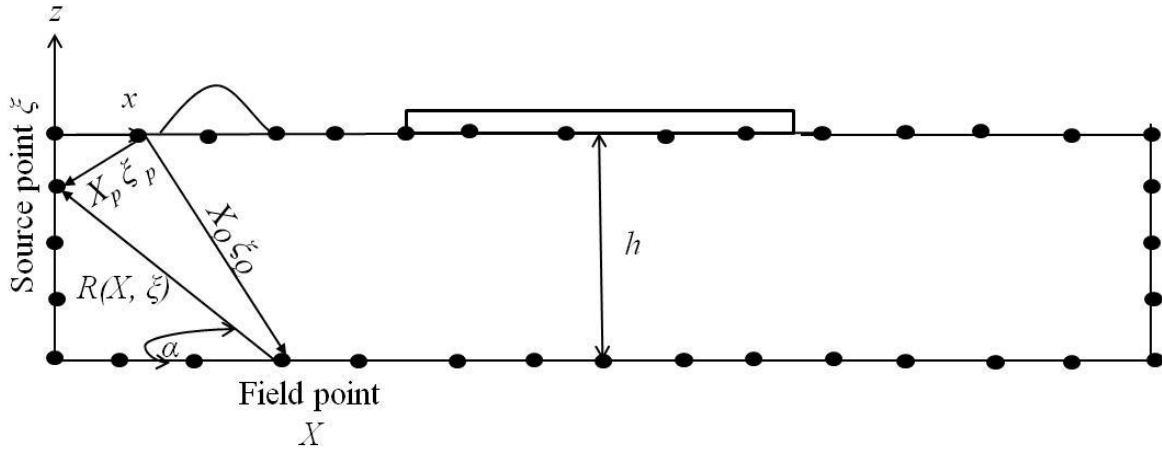


Fig. 3.2: Discrete version of BEM.

where,  $X_P \zeta_P$  and  $X_Q \zeta_Q$  are the symbolic representation of distances from source point to free surface and field point to free surface, respectively.

The 3-D free surface Green's function satisfies the seabed, water surface and Sommerfeld boundary condition. Therefore, the remaining unknown variables for the fluid part are only associated with the wetted bottom surface of the floating surface. The application of the Green's second identity to the Laplace equation and the boundary conditions results in the following boundary Integral Equation (BIE) for the velocity potential (Brebbia and Dominguez, 1977).

$$2\pi\phi_l + \int_{S_B} \phi \frac{\partial G}{\partial n} dS_B = \int_{S_B} G \frac{\partial \phi}{\partial n} dS_B + 2\pi\phi \quad (19)$$

The procedure (Brebbia, 1978) is to be followed to obtain the Boundary Integral Equation (Eqn. 19) is explained in detailed manner as given below. The Green's second identity for velocity potential is given as.

$$\int_{\Omega} (\phi \nabla^2 G - G \nabla^2 \phi) d\Omega = \int_S \left( \phi \frac{\partial G}{\partial n} - G \frac{\partial \phi}{\partial n} \right) dS \quad (20)$$

where,  $S$ ,  $n$  and  $G$  are boundary surface of the fluid domain, unit outward normal and as fundamental solution Green's function, respectively. The velocity potential  $\phi$  satisfies  $\nabla^2 \phi = 0$  everywhere in the solution domain. The fundamental solution  $G$ , however, satisfies  $\nabla^2 \phi = 0$  everywhere except at the source point  $\zeta$ , where, it is singular. To deal with this problem, one can surround the source point  $\zeta$  by a very

small sphere of radius  $\varepsilon$  and surface  $S_\varepsilon$ , and examine the solution in the limit as  $\varepsilon \rightarrow 0$ . By excluding this small sphere, the new volume is  $(\Omega - \Omega_\varepsilon)$  and the new surface is  $(S + S_\varepsilon)$ , hence, Equation (20) becomes,

$$\int_{\Omega - \Omega_\varepsilon} (\phi \nabla^2 G - G \nabla^2 \phi) d\Omega = \int_{S + S_\varepsilon} \left( \phi \frac{\partial G}{\partial n} - G \frac{\partial \phi}{\partial n} \right) dS \quad (21)$$

Within the volume  $(\Omega - \Omega_\varepsilon)$ ,  $\nabla^2 \phi = \nabla^2 G = 0$  everywhere, which makes the left hand side of Equation (21) equal to zero. The boundary surface  $S$  can be further decomposed into  $S + S_\varepsilon$  where,  $S_\varepsilon$  is small sphere of radius  $\varepsilon$  around the source point  $\zeta$ .

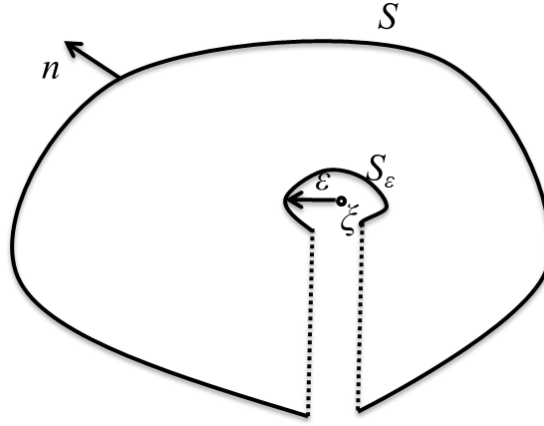


Fig. 3.3: Decomposition of a 3-D fluid domain.

The surface integral in Equation (21) can now be splitted into two surface integrals resulting in the following equation,

$$0 = \int_S \left( \phi \frac{\partial G}{\partial n} - G \frac{\partial \phi}{\partial n} \right) dS + \int_{S_\varepsilon} \left( \phi \frac{\partial G}{\partial n} - G \frac{\partial \phi}{\partial n} \right) dS \quad (22)$$

Referring to the sphere centered at  $\zeta$  (Figure 3.3), the second integral in Equation (22) can be rewritten as,

$$\int_{S_\varepsilon} \left( \phi \frac{\partial G}{\partial n} - G \frac{\partial \phi}{\partial n} \right) dS = \int_0^\pi \left( \frac{\partial G}{\partial n} - G \frac{\partial \phi}{\partial n} \right) 2\pi\varepsilon^2 \sin \alpha d\alpha \quad (23)$$

$\alpha$  is the angle measured from the x-axis at the source point  $\zeta$ . By substituting for  $G$  from the Equation (17) and using  $\frac{\partial}{\partial n} = -\frac{\partial}{\partial s}$  on the surface  $S_\varepsilon$ , the integral of Equation (23) becomes,

$$\begin{aligned}
& \int_0^\pi \left( \phi \frac{\partial}{\partial n} \left( \frac{1}{s} \right) - \frac{1}{s} \frac{\partial \phi}{\partial n} \right) 2\pi \varepsilon^2 \sin \alpha d\alpha \\
&= \int_0^\pi \left( \phi \frac{\partial}{\partial s} \left( -\frac{1}{s} \right) - \frac{1}{s} \frac{\partial \phi}{\partial n} \right) 2\pi \varepsilon^2 \sin \alpha d\alpha \quad (24) \\
&= \int_0^\pi \left( \phi \frac{1}{\varepsilon^2} - \frac{1}{\varepsilon} \frac{\partial \phi}{\partial n} \right) 2\pi \varepsilon^2 \sin \alpha d\alpha \\
&= \int_0^\pi \left( \phi - \varepsilon \frac{\partial \phi}{\partial n} \right) 2\pi \sin \alpha d\alpha
\end{aligned}$$

Taking each term in the limit as  $\varepsilon \rightarrow 0$  results in the following

$$\phi \int_0^\pi 2\pi \sin \alpha d\alpha = 2\pi \phi [-\cos \alpha]_0^\pi = 4\pi \phi \quad (25)$$

Substituting Equation (25) in Equation (22) and rearranging the terms, the Boundary Integral Equation for the fluid part is obtained as

$$4\pi \phi + \int_S \frac{\partial G}{\partial n} \phi dS = \int_S G \frac{\partial \phi}{\partial n} dS \quad (26)$$

If the source point  $\zeta$  in the Figure (3.3) is on the boundary  $S$ ,  $S_\varepsilon$  will become a small hemisphere with a surface area of  $2\pi \varepsilon^2$ . Hence, the BIE for the fluid is given as

$$2\pi \phi + \int_S \frac{\partial G}{\partial n} \phi dS = \int_S G \frac{\partial \phi}{\partial n} dS \quad (27)$$

By decomposing the boundary surface  $S$  into  $S_F$ ,  $S_B$ ,  $S_G$  and  $S_\infty$  and applying boundary conditions on these surfaces, Equation (27) can be written as,

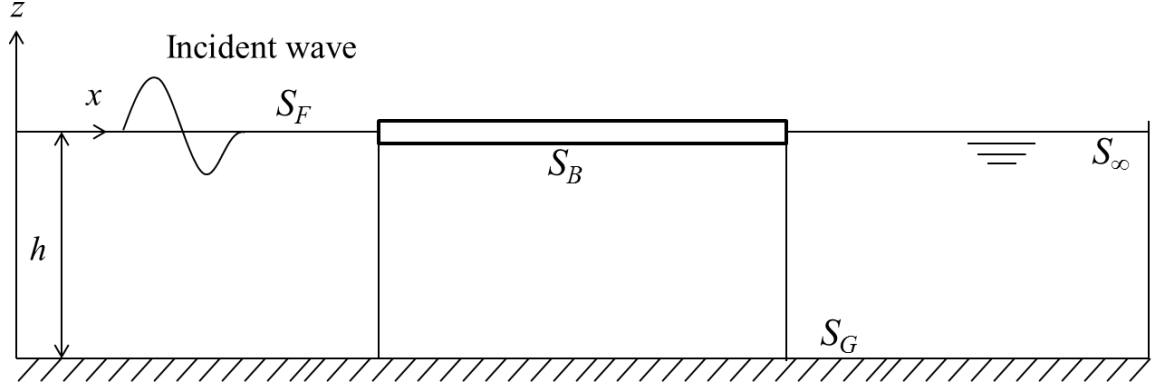


Fig. 3.4: Schematic diagram of coupled plate–water problem.

$$\begin{aligned}
-2\pi\phi &= \int_{S_F \cup S_B \cup S_G \cup S_\infty} \left[ \phi \frac{\partial G}{\partial n} - G \frac{\partial \phi}{\partial n} \right] dS \\
&= \int_{S_F} \left[ \phi \frac{\partial G}{\partial n} - G \frac{\partial \phi}{\partial n} \right] dS_F + \int_{S_B} \left[ \phi \frac{\partial G}{\partial n} - G \frac{\partial \phi}{\partial n} \right] dS_B + \int_{S_G} \left[ \phi \frac{\partial G}{\partial n} - G \frac{\partial \phi}{\partial n} \right] dS_G + \int_{S_\infty} \left[ \phi \frac{\partial G}{\partial n} - G \frac{\partial \phi}{\partial n} \right] dS_\infty \\
&= (\phi\alpha G - G\alpha\phi) dS_F + \int_{S_B} \left[ \phi \frac{\partial G}{\partial n} - G \frac{\partial \phi}{\partial n} \right] dS_B + (\phi(0) - G(0)) dS_G + \int_{S_\infty} \left[ \phi \frac{\partial G}{\partial n} - G \frac{\partial \phi}{\partial n} \right] dS_\infty \\
&= \int_{S_B} \phi \frac{\partial G}{\partial n} dS_B - \int_{S_B} G \frac{\partial \phi}{\partial n} dS_B + \int_{S_\infty} \left[ \phi \frac{\partial G}{\partial n} - G \frac{\partial \phi}{\partial n} \right] dS_\infty \tag{28}
\end{aligned}$$

By further decomposing the velocity potential  $\phi$  into incident potential  $\phi_I$ , the scattered potential  $\phi_S$  and radiation potential  $\phi_R$ , the integral on the right hand side of Equation (28) over the boundary surface at infinity  $S_\infty$  can be written as (Brebbia, 1978),

$$\int_{S_\infty} \left[ \phi \frac{\partial G}{\partial n} - G \frac{\partial \phi}{\partial n} \right] dS_\infty = \int_{S_\infty} \left[ (\phi_I + \phi_S + \phi_R) \frac{\partial G}{\partial n} - G \frac{\partial (\phi_I + \phi_S + \phi_R)}{\partial n} \right] dS_\infty$$

$$= \int_{S_\infty} \left[ \phi_I \frac{\partial G}{\partial n} - G \frac{\partial \phi_I}{\partial n} \right] dS_\infty + \int_{S_\infty} \left[ \phi_S \frac{\partial G}{\partial n} - G \frac{\partial \phi_S}{\partial n} \right] dS_\infty + \int_{S_\infty} \left[ \phi_R \frac{\partial G}{\partial n} - G \frac{\partial \phi_R}{\partial n} \right] dS_\infty \quad (29)$$

As the scattered and radiated potential satisfy the Sommerfeld condition given in Equation (13), the integral on the right hand side of Equation (29) which involves of  $\phi_S$  and  $\phi_R$  vanish at  $S_\infty$ . Hence, equation (29) can be written as,

$$\int_{S_\infty} \left[ \phi \frac{\partial G}{\partial n} - G \frac{\partial \phi}{\partial n} \right] dS_\infty = \int_{S_\infty} \left[ \phi_I \frac{\partial G}{\partial n} - G \frac{\partial \phi_I}{\partial n} \right] dS_\infty \quad (30)$$

$\phi_I$  and  $G$  in Equation (30) are harmonic everywhere at  $S_\infty$ , with an exception at the point where the wave source  $\zeta$  is located. Consider a small hemisphere of radius  $\varepsilon$  with surface  $S_\varepsilon$ .

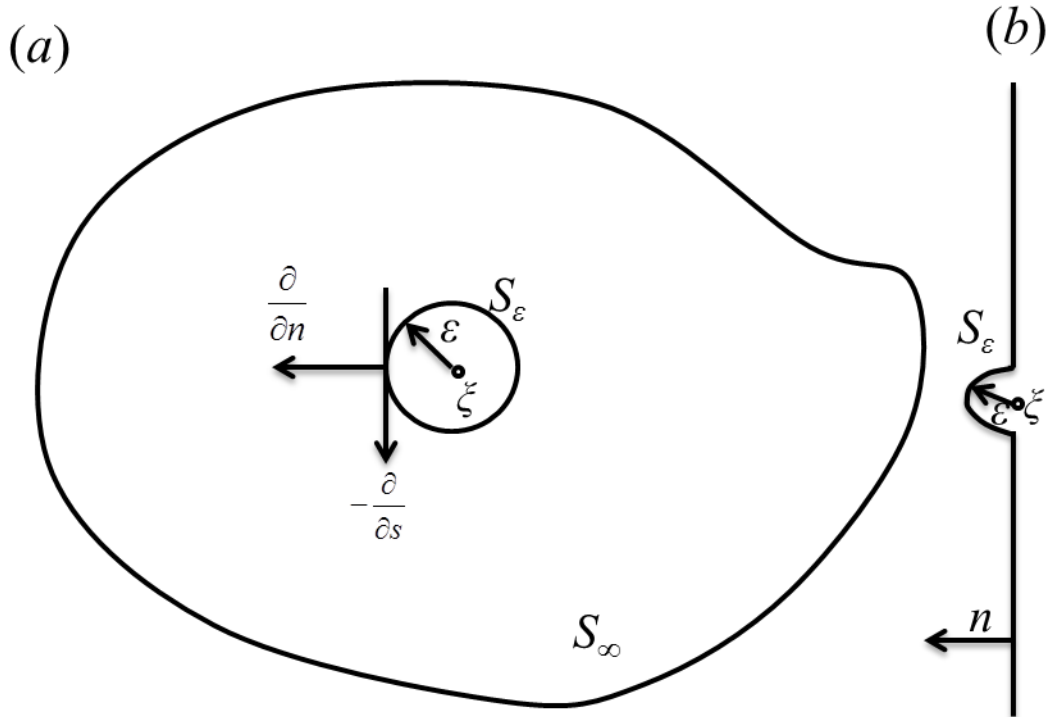


Fig. 3.5: Decomposition of 2-D surface  $S_\infty$  into  $S_\infty \cup S_\varepsilon$  (a) plan view (b) side view. In

case  $\partial/\partial n = -\partial/\partial s$ .

Equation (30) is then given by,

$$\begin{aligned}
\int_{S_\infty} \left[ \phi_I \frac{\partial G}{\partial n} - G \frac{\partial \phi_I}{\partial n} \right] dS_\infty &= \int_{S_{\infty-\varepsilon}} \left[ \phi_I \frac{\partial G}{\partial n} - G \frac{\partial \phi_I}{\partial n} \right] dS_{\infty-\varepsilon} + \int_{S_\varepsilon} \left[ \phi_I \frac{\partial G}{\partial n} - G \frac{\partial \phi_I}{\partial n} \right] dS_\varepsilon \\
&= \int_{S_\varepsilon} \left[ \phi_I \frac{\partial G}{\partial n} - G \frac{\partial \phi_I}{\partial n} \right] dS_\varepsilon \\
&= \int_{S_\varepsilon} \phi_I \frac{\partial G}{\partial n} dS_\varepsilon - \int_{S_\varepsilon} G \frac{\partial \phi_I}{\partial n} dS_\varepsilon \\
&= \int_{S_\varepsilon} \phi_I \frac{\partial}{\partial r} \left( \frac{1}{r} \right) dS_\varepsilon - \int_{S_\varepsilon} \frac{1}{r} \frac{\partial \phi_I}{\partial n} dS_\varepsilon \\
&= -\phi_I \left[ \frac{1}{\varepsilon^2} \right] \int_{S_\varepsilon} dS_\varepsilon - \frac{1}{\varepsilon^2} \frac{\partial \phi_I}{\partial n} \int_{S_\varepsilon} dS_\varepsilon \\
&= -\phi_I \left( \frac{1}{\varepsilon^2} \right) 2\pi\varepsilon^2 - \frac{1}{\varepsilon^2} \left( \frac{\partial \phi_I}{\partial n} \right) 2\pi\varepsilon^2 \\
&= -2\pi\phi_I \tag{31}
\end{aligned}$$

The second term in the right hand side vanishes because  $\varepsilon$  is very small. By substituting Equation (31) in (28) we obtain the final equation.

$$2\pi\phi_I + \int_{S_B} \phi \frac{\partial G}{\partial n} dS_B = \int_{S_B} G \frac{\partial \phi}{\partial n} dS_B + 2\pi\phi$$

### 3.2.4 Discrete versions of the plate using Finite Element Method

Equation of motions (Equ. 8) for plate and water wave (Equ. 19) are discretized using FEM and BEM, respectively. Each node contains three degrees of freedom, namely displacement ( $w$ ), rotation degree  $\theta_x$  ( $\partial w/\partial x$ ) and rotation degree  $\theta_y$  ( $\partial w/\partial y$ ). The displacement  $w(x)$  is represented as shown below as a vector of functions.

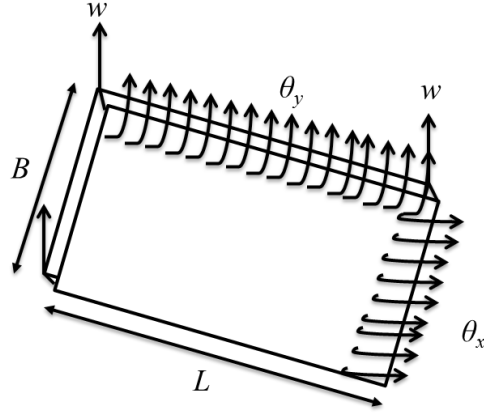


Fig. 3.6: FEM panel showing three degree of freedom system.

$$w(x) = N_d(X) w_d, X \in S_d \quad (32)$$

The basis vector is defined by Love (1906)

$$N_d(X) = [N_{11} N_{12} N_{13} N_{21} N_{22} N_{23} N_{31} N_{32} N_{33} N_{41} N_{42} N_{43}] \quad (33)$$

$N_{j1} = N_{j1}(x, y)$ ,  $N_{j2} = N_{j2}(x, y)$ ,  $N_{j3} = N_{j3}(x, y)$ , ( $j=1, 2, 3, 4$ ) and are detailed further as given below.

$$N_{j1}(x, y) = \frac{1}{8}(1 + x_j x)(1 + y_j y)(2 + x_j x + y_j y - x^2 - y^2)$$

$$N_{j2}(x, y) = \frac{a}{16}(1 + x_j x)(y_j + y)(y^2 - 1)$$

$$N_{j3}(x, y) = -\frac{a}{16}(x_j + x)(x^2 - 1)(1 + y_j y)$$

The vector  $w_d$  is a vector of elements, which is given by

$$w_d = [w_i^{(d)} \frac{\partial w_1^{(d)}}{\partial x} \frac{\partial w_1^{(d)}}{\partial y} w_i^{(d)} \frac{\partial w_2^{(d)}}{\partial x} \frac{\partial w_2^{(d)}}{\partial y} w_j^{(d)} \frac{\partial w_3^{(d)}}{\partial x} \frac{\partial w_3^{(d)}}{\partial y} w_4^{(d)} \frac{\partial w_4^{(d)}}{\partial x} \frac{\partial w_4^{(d)}}{\partial y}]$$

$$\text{where, } w_j^{(d)} = w(x_j), \frac{\partial w_j^{(d)}}{\partial x} = \frac{\partial}{\partial x} w(X_j) \text{ and } \frac{\partial w_j^{(d)}}{\partial y} = \frac{\partial}{\partial y} w(X_j)$$

Now, both the basis vector  $N_d$  and constant vector  $w_d$  are of dimensions  $1 \times 12$  and  $12 \times 1$ , respectively. The potential can be expanded in an identical manner (Riyansyah et al., 2010) to the displacement i.e.

$$\phi(x) = N_d(X) \hat{\phi}_d, X \in S_d \quad (34)$$

where,  $\phi_d$  is vector of constant and is defined as follows.

$$\phi_d = [\phi_1^{(d)} \frac{\partial \phi_1^{(d)}}{\partial x} \frac{\partial \phi_1^{(d)}}{\partial y} \phi_2^{(d)} \frac{\partial \phi_2^{(d)}}{\partial x} \frac{\partial \phi_2^{(d)}}{\partial y} \phi_3^{(d)} \frac{\partial \phi_3^{(d)}}{\partial x} \frac{\partial \phi_3^{(d)}}{\partial y} \phi_4^{(d)} \frac{\partial \phi_4^{(d)}}{\partial x} \frac{\partial \phi_4^{(d)}}{\partial y}] \quad (35a)$$

$$\text{where, } \phi_j^{(d)} = \phi(x_j), \frac{\partial \phi_j^{(d)}}{\partial x} = \frac{\partial}{\partial x} \phi(X_j) \text{ and } \frac{\partial \phi_j^{(d)}}{\partial y} = \frac{\partial}{\partial y} \phi(X_j)$$

Likewise  $\phi^{in}(X)$  can be written as

$$\phi^{in}(X) = N_d(X) \widehat{\phi}_d^{in} \quad (35b)$$

where,

$$\widehat{\phi}_d^{in} = \left[ \phi_1^{in} \quad \frac{\partial \phi_1^{in}}{\partial x} \quad \frac{\partial \phi_1^{in}}{\partial y} \quad \phi_2^{in} \quad \frac{\partial \phi_2^{in}}{\partial x} \quad \frac{\partial \phi_2^{in}}{\partial y} \quad \phi_3^{in} \quad \frac{\partial \phi_3^{in}}{\partial x} \quad \frac{\partial \phi_3^{in}}{\partial y} \quad \phi_4^{in} \quad \frac{\partial \phi_4^{in}}{\partial x} \quad \frac{\partial \phi_4^{in}}{\partial y} \right]^T$$

Representing the potential and displacement in the finite element basis function, Equation (8) will be solved. Further, Equation (8) is reduced to form the equivalent equation which is applied to analyze the panels.

$$\beta \nabla^4 (N_d w_d) - \omega^2 \gamma (N_d w_d) = i \omega (N_d \phi_d) - (N_d w_d).$$

$$\int_{\Delta_d} \left\{ \beta \left[ \frac{\partial^2 N_d^T}{\partial x^2} \frac{\partial^2 N_d}{\partial x^2} + \frac{\partial^2 N_d^T}{\partial y^2} \frac{\partial^2 N_d}{\partial y^2} + 2(1-\nu) \frac{\partial^2 N_d^T}{\partial x \partial y} \frac{\partial^2 N_d}{\partial x \partial y} + 2\nu \frac{\partial^2 N_d}{\partial x^2} \frac{\partial^2 N_d}{\partial y^2} \right] \right\} dX^{(d)} w_d - \int_{\Delta_d} (\omega^2 \gamma N_d^T N_d) dx^{(d)} w_d = \int_{\Delta_d} [i \omega N_d^T N_d \widehat{\phi}_d - N_d^T N_d w_d] dX^{(d)} \quad (36)$$

According to Meylan (2002) the mass and stiffness matrices are as follows.

$$\langle N_d, N_d \rangle_{\Delta_d} = \int_{\Delta_d} N_d^T N_d dX^{(d)}$$

$$\text{where, } \langle N_d, N_d \rangle_{\Delta_d} = [m_d] \quad (37)$$

$$\int_{\Delta_d} \left[ \frac{\partial^2 N_d^T}{\partial x^2} \frac{\partial^2 N_d}{\partial x^2} + \frac{\partial^2 N_d^T}{\partial y^2} \frac{\partial^2 N_d}{\partial y^2} + 2(1-\nu) \frac{\partial^2 N_d^T}{\partial x \partial y} \frac{\partial^2 N_d}{\partial x \partial y} + 2\nu \frac{\partial^2 N_d}{\partial x^2} \frac{\partial^2 N_d}{\partial y^2} \right] dX^{(d)} = [k]_d \quad (38)$$

where,  $[k]_d$  is the stiffness matrix and  $[m]_d$  is the mass matrix (Wang and Meylan, 2004). Equation (36) is simplified by incorporating mass and stiffness matrices and is given as

$$\beta[k]_d w_d - \omega^2 \gamma[m]_d w_d = i\omega[m]_d \phi_d - [m]_d w_d \quad (39)$$

### 3.2.5 Higher Order Boundary Element Method [HOBEM]

Without separating the velocity potential, Equation (34) can be discretized directly by using the Higher Order Boundary Element Method (Meylan, 2001). By substituting the boundary conditions and making use of the free-surface Green's function, it can

$$\text{be obtained as } \phi(x) = \phi_l(x) - \int_{S_B} G(X, \xi) \left[ \frac{\omega^2}{g} \phi(\xi) + i\omega w(\xi) \right] d\xi \quad (40)$$

Equation (40) is referred as water wave equation. It can be solved using the representation of the displacement and potential in the Finite Element basis functions. In HOBEM, the fluid potential is expressed as a function by using the nodal potentials. Substituting Equations (35a & 35b) into Equation (40) it is obtained as,

$$N_d(X)\phi_d = N_d(X)(\phi_l)_d - \frac{\omega^2}{g} \sum_{e=1}^p (G_{de} N_e) \phi_e - i\omega \sum_{e=1}^p (G_{de} N_e) w_e \quad (41)$$

where,

$$G_{de} N_e = \int_{\Delta_e} G(X; \xi) N_e(\xi) d\xi$$

Following Wang and Meylan (2004) and applying an inner product  $N_d$  to both sides of the Equation (41) resulting in,

$$\langle N_d, N_d \rangle_{\Delta_d} \phi_d = \langle N_d, N_d \rangle_{\Delta_d} (\phi_l)_d - \frac{\omega^2}{g} \sum_{e=1}^p \langle N_d, (G_{de} N_e) \rangle_{\Delta_d} \phi_e - i\omega \sum_{e=1}^p \langle N_d, (G_{de} N_e) \rangle_{\Delta_d} w_e, \quad (42)$$

$$\langle N_d, N_d \rangle_{\Delta_d} = \int_{\Delta_d} N_d^T N_d dX \quad (43a)$$

$$\langle N_d, (G_{de}, N_d) \rangle_{\Delta_d} = \int_{\Delta_d} N_d^T G_{de} N_e dX \quad (43b)$$

Analogous to the definitions of the mass and stiffness matrix, the Green's matrix  $[G]_{de}$  is defined as (Brebbia, 1978)

$$\int_{\Delta_e} N_d^T (G_{de} N_e) dX = [G]_{de} \quad (44)$$

The calculation of  $[G]_{de}$  is separated into two cases, depending on whether  $d = e$  or not. This is because the free surface Green's function is singular at  $|X - \xi| = 0$ . Since  $X$  lies in element, the singularity occurs when  $d = e$ . It can be noticed from Equation (44) that Green's function occurs in the integral  $G_{de} N_e$  and therefore it is needed to separate the solution  $G_{de} N_e$  into the singular and the non-singular cases. By evaluating the integral  $G_{de} N_e$  using a numerical integration method i.e., Gauss quadrature, it is obtained as.

$$G_{de} N_e = \int_{\Delta_e} G(\mathbf{X}; \xi) N_e(\xi) d\xi = \sum_{j=1}^M v_j G(\mathbf{X}; \xi_j) N_e(\xi_j) \quad (45)$$

where  $\xi_j$  and  $v_j$  are sets of  $M$  integration points and their corresponding weights. Note that  $\xi_j$  needs to be determined from the corresponding Gauss points  $r_j(r_j, q_j)$  by isoparametric coordinate transformation using basis function. Also, both the field element  $\Delta_d(x, y)$  and source element  $\Delta_e(\xi, \eta)$  are transformed into a parametric element  $\Delta_r$  with natural coordinates  $(r, q)$  for integration (Wang and Meylan, 2004). The integral part in the Equation (44) is calculated in a similar way with the possibility of choosing different points and weights can be given as

$$\int_{\Delta_d} N_d^T(x) (G_{de} N_e) dX^{(d)} = \sum_{i=1}^N u_i N_d^T(r_i, q_i) (G_{de} N_e) \quad (46)$$

where,  $x_i$  and  $u_i$  are sets of  $N$  integration points and their corresponding weights. By combining Equations (45) and (46), the numerical set of Green's matrix  $[G]_{de}$  is given by,

$$[G]_{de} = \sum_{i=1}^N u_i N_d^T(r_i, q_i) \sum_{j=1}^M v_j G^{(ij)} N_e(\xi_j) = [N_N][G_{NM}][N_M] \quad (47)$$

$$[G]_{de} = \begin{cases} N_1 G_1 N_2 & \text{if } d=e \\ N_1 G_2 N_1^T & \text{if } d \neq e \end{cases}$$

where,  $G_1$  and  $G_2$  are rectangular matrix of  $N \times M$  and square matrix of  $N \times N$ , respectively.

$$G_1 = \begin{bmatrix} G^{(11)} & G^{(12)} & \dots & G^{(1N)} \\ G^{(21)} & G^{(22)} & \dots & G^{(2N)} \\ \vdots & \vdots & \ddots & \vdots \\ G^{(M1)} & G^{(M2)} & \dots & G^{(MN)} \end{bmatrix} \quad (48a)$$

$$G_2 = \begin{bmatrix} G^{(11)} & G^{(12)} & \dots & G^{(1N)} \\ G^{(21)} & G^{(22)} & \dots & G^{(2N)} \\ \vdots & \vdots & \ddots & \vdots \\ G^{(N1)} & G^{(N2)} & \dots & G^{(NN)} \end{bmatrix} \quad (48b)$$

$N_1$  is  $12 \times N$  matrix and  $N_2$  is  $M \times 12$  matrix

$$N_1 = \begin{bmatrix} v_1 N_d^{(1)T} \\ v_2 N_d^{(2)T} \\ \vdots \\ v_N N_d^{(d)T} \end{bmatrix} \quad \text{and} \quad N_2 = \begin{bmatrix} v_1 N_d^{(1)T} \\ v_2 N_d^{(2)T} \\ \vdots \\ v_N N_d^{(d)T} \end{bmatrix} \quad (49)$$

To avoid the singularity when  $X_i$  coincides  $\zeta_j$ , Equation (34) is solved by using set of distinct points ( $x_i$ ) and ( $\zeta_j$ ). For the case of  $d = e$ , it is necessary to use more integration points because of singularity. There are several methods to calculate the singularity integral, however, coordinate transformation is widely used method and is described by Hamamoto et al. (1997). The same set of integration points and their corresponding weights will be employed for the case of non-singular Green's function.

$$[K_w]_d \phi_d = [K_w]_d \phi_d^{in} + \frac{\omega^2}{g} \sum_{e=1}^P [G]_{de} \phi_e - i\omega \sum_{e=1}^P [G]_{de} w_e, \quad (50)$$

which is discretized version of the water wave Equation (40) for a single element. After assembling all the elements, the equation for the entire plate domain is expressed as,

$$[K_w] \{\phi\} = [K_w] \{\phi^{in}\} + \frac{\omega^2}{g} [G] \{\phi_e\} - i\omega [G] \{w_e\}, \quad (51)$$

Herein, the fluid potential  $\phi$  is coupled with plate displacement  $w$ . The direct solution method is adopted for solving the water plate interaction.

According to Wang and Meylan (2004) and Kim et al. (2013), the force surface Green's function at infinite depth is given as

$$G(X, \xi) = \frac{-1}{4\pi} \left( \frac{2}{(X - \xi)} - \pi\omega^2 [H_0(\omega^2 |X - \xi|) + Y_0(\omega^2 |X - \xi|) - 2i\pi J_0(\omega^2 |X - \xi|)] \right) \quad (52)$$

where,  $H_0$ , denotes Struve function of order zero,

$Y_0$  and  $J_0$  denote Bessel function of first and second kind with order of zero, respectively.

The forcing function at finite water depth is given by Yiew et al. (2016) is as follows,

$$G(X, \xi) = \frac{-i}{2} \frac{\omega^4 - k^2}{(\omega^4 - k^2)h - \omega^2} \cosh^2(kh) H_0^{(1)}(k|X - \xi|) - \frac{1}{\pi} \sum_{m=1}^{\infty} \frac{k_m^2 + \omega^4}{(k_m^2 + \omega^4)h - \omega^2} \cos^2(k_m h) K_0(k_m |X - \xi|) \quad (53)$$

where,  $H_0^{(1)}$  and  $K_0$ , denote Hankel function of first kind and Bessels function of the second kind, both of order zero. Further,  $k$  is taken as the positive real solution to dispersion relation for free surface and  $k_m$  as the imaginary parts of the solutions with positive imaginary part.

The modified simple equation which differs from Wang and Meylan (2004) and Yiew et al. (2016) is given below and has been further used in the numerical model.

$$G(X, \xi) = G(X, \xi) - \left[ \frac{H_0^{(1)}}{2\pi C} \right] (\cosh(kh)h)^2 \quad (54)$$

$$\text{where, } C = \frac{h}{2} \left[ \frac{1 + (\sin(2 \cosh(Ch)h))}{2 \cosh(Ch)h} \right]$$

By expressing the integral operator  $Gf(X) = \int_{\Delta} G(X, \xi) f(\xi) d\xi$  and rewriting it as,

$$\phi(X) = \phi^{in}(X) + \omega^2 G\phi(X) + \lambda\omega G(X) \quad (55)$$

Solving Equations (51) and (55), the deflection of the floating platform can be obtained in finite and infinite water depths.

## CHAPTER 4

### RESULTS AND DISCUSSION

#### 4.0 GENERAL

The proposed numerical model can be applied to analyse hydroelasticity of floating thin plate for any arbitrary shapes at finite and infinite water depths. The efficacy of the numerical model is studied for rectangular, triangular and trapezoidal shapes and are described in this chapter. The discussion is mainly focused on maximum deflection that occurs on floating elastic plate, simulation time to calculate the deflection and the error in convergence rate for integration points of  $N = M = 2$ ,  $N = M = 4$  and,  $N = 4$   $M = 8$ . MATLAB 2015 has been used to calculate the maximum deflection and time required for the simulation. Initially, the results for rectangular plate at finite and infinite water depths are discussed and are followed by the results of triangular and trapezoidal plates. To validate the proposed numerical model, the obtained results are compared with the numerical results of Wang and Meylan (2004), analytical results of Wu et al. (1995) and experiment results of Utsunomiya et al. (1995). The simulation time is expected to reduce, as the developed model consists of same number of the basis functions in both BEM and FEM. Further, by increasing the number of integration points ( $N$  and  $M$ ), the accuracy of the model is also expected to be increased. The above said aspects are discussed in the forthcoming sections by considering the plate dimensions as given in Figure 4.1 and parameters reported in Table 4.1.

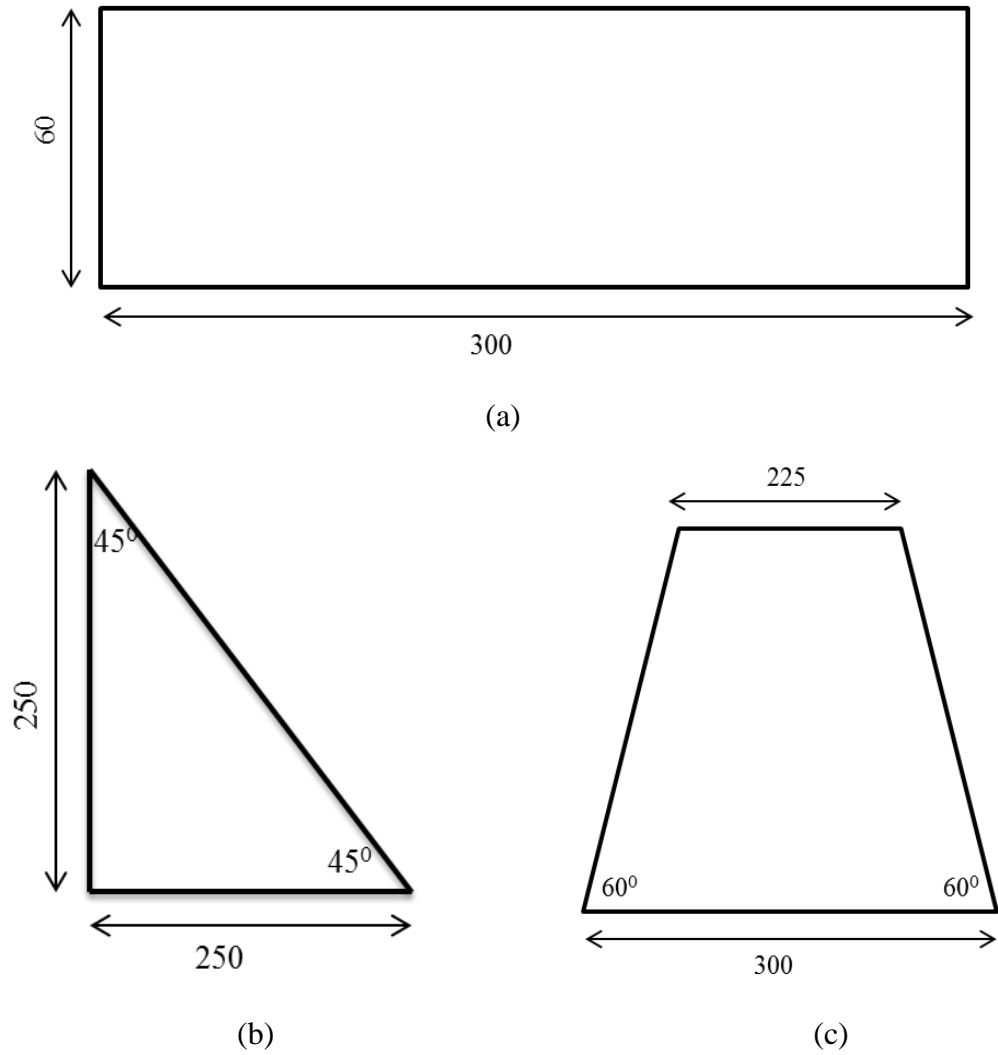


Fig. 4.1: Different shapes of the floating plate (non dimensional) (a) Rectangular, (b) Triangular and (c) Trapezoidal.

Table 4.1: Plate parameters used in the model

|  |                         |
|--|-------------------------|
| Thickness, $d$                             | 2m                      |
| Draft, $T$                                 | 0.5m                    |
| Poisson's ratio                            | 0.2                     |
| Density of plate, $\rho_i$                 | 922.5kg/m <sup>3</sup>  |
| Wavelength, $\lambda$                      | 2m                      |
| Non-dimensional rigidity of plate, $\beta$ | 5.828x10 <sup>-3</sup>  |
| Non-dimensional Mass, $\nu$                | 1.507 x10 <sup>-3</sup> |

#### 4.1 HYDROELASTIC BEHAVIOUR OF RECTANGULAR PLATE

This subsection describes the vertical displacement of rectangular plate, subjected to oblique wave attack at finite and infinite water depths. Vertical displacement, simulation time and error in the model for integration points  $N = M = 2$  and  $N = M = 4$  are discussed here.

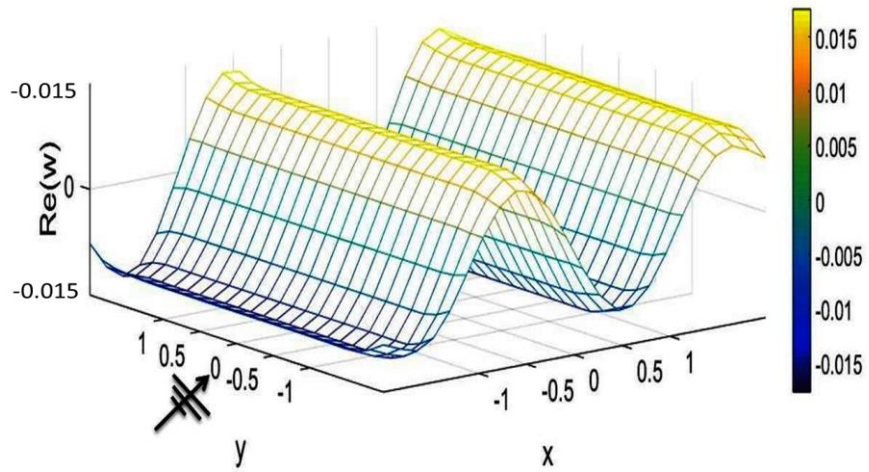
The time period required to run the model in order to capture the elastic motion or vertical deflection of the floating rectangular plate is recorded. The model is analyzed by increasing the number of panels from 100 to 900 and by considering equal integration points ( $N = M = 4$ ). The panel dependency of the proposed numerical work is observed to be absent when the number of panels crosses 900. Hence, the error is considered to be zero when the panel number is 900 and above. Based on this condition, the error is estimated for the considered panels with wave angle  $\theta = 0$  and Table 4.2 explains the details regarding error and simulation time for different number of panels.

Table 4.2: Time and error as the function of panels with wave angle  $\theta = 0$ .

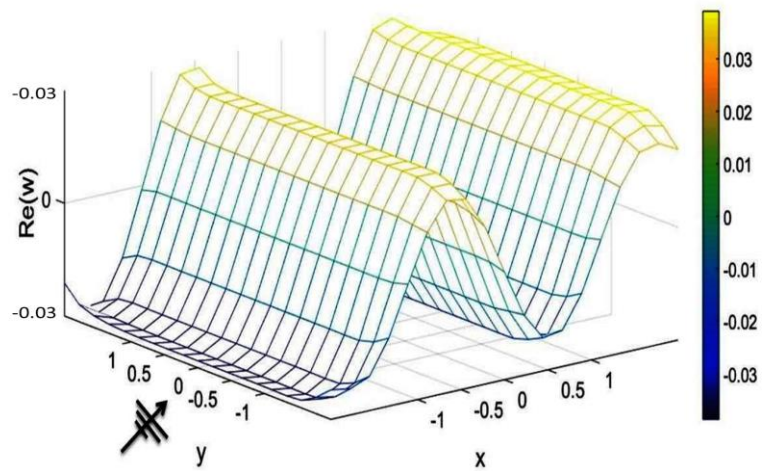
| <b>Number of panels</b> | <b>Time(s)</b> | <b>% Error</b> |
|-------------------------|----------------|----------------|
| 100                     | 66.144         | 0.3959         |
| 225                     | 334.032        | 0.1013         |
| 400                     | 1051.107       | 0.0216         |
| 625                     | 2532.635       | 0.0111         |
| 900                     | 5742.102       | 0.0010         |
| 1089                    | 8932.165       | 0.0010         |

It is observed that as the number of panels in the plate increases the time required for the simulation increases, whereas, the error in deflection profile reduces. Figures 4.2 (a) – 4.2 (d) depict the elastic motions or deflected profiles in the rectangular plate at finite water depth with angle of wave attack  $\theta = 0$ . The maximum vertical deflection for 100 panels is 0.25, whereas, for 625 panels it is 0.012. It is observed that as the

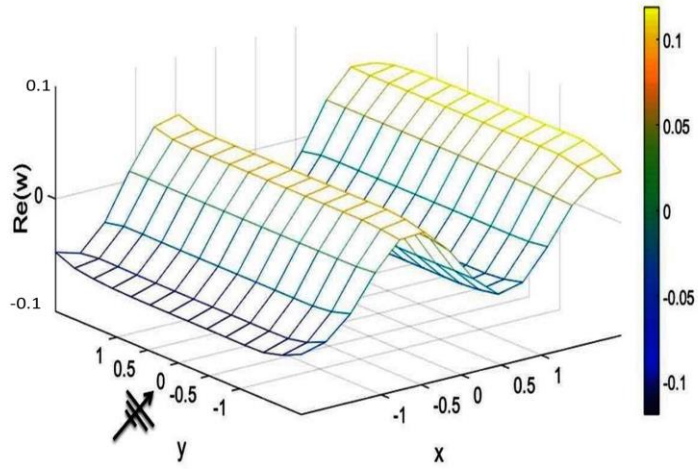
number of panels increases, the deflection profile of the rectangular plate becomes smooth and provide accurate vertical deflection.



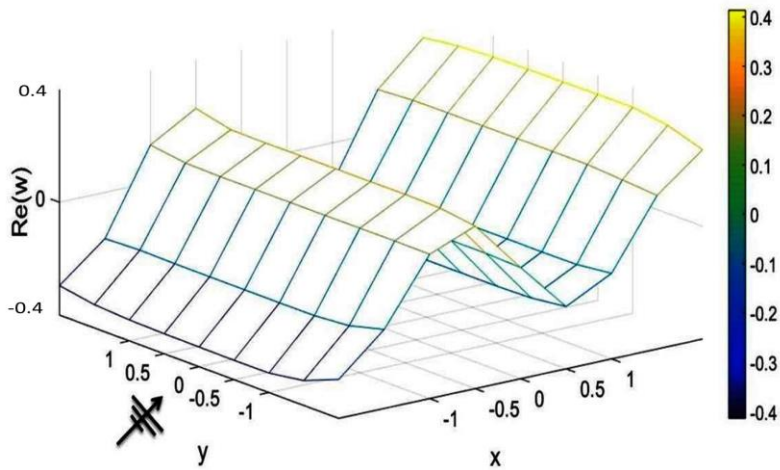
(a)



(b)



(c)

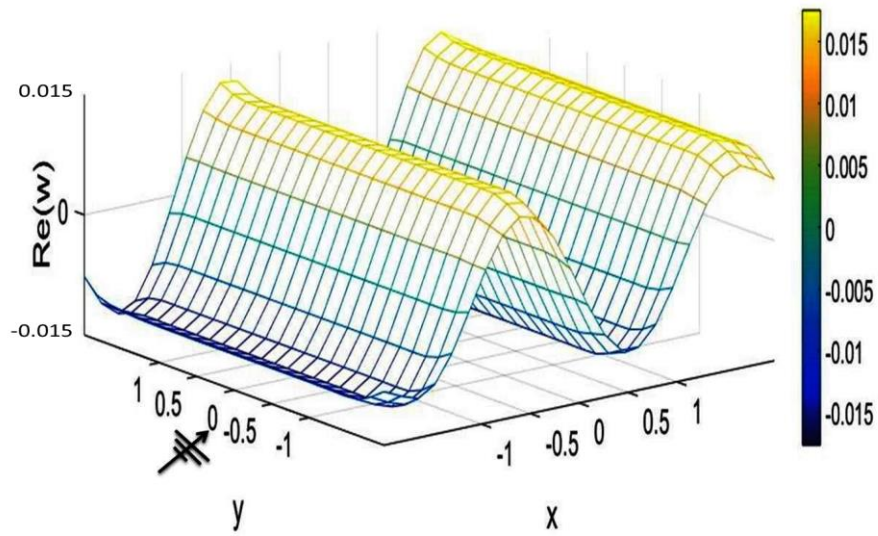


(d)

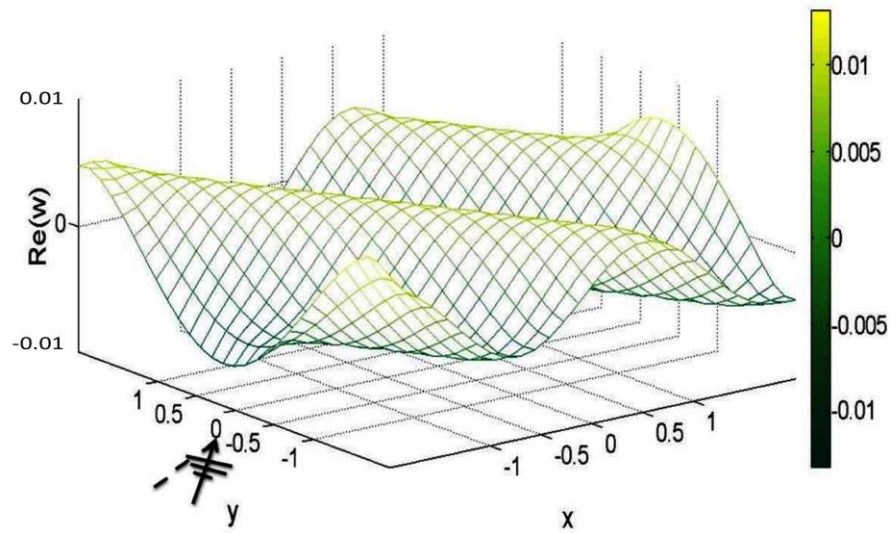
Fig. 4.2: Deflection of rectangular plate for different number of panels and wave angle of  $\theta = 0$ : (a) 625, (b) 400, (c) 225 and (d) 100 panels.

Figures 4.3 (a) – 4.3 (d), exhibit the simulation of elastic motions at finite water depth at the depth of  $1/4$  for different angles of wave attack ( $\theta = 0, \pi/6, \pi/4$  and  $\pi/2$ ) by keeping constant integration points ( $N = M = 4$ ) and number of panels 900. It can be seen that the elastic motion is captured elegantly over the entire plate as well as at the corners of the plate. Further, the simulation time for different number of panels is recorded and the error in deflection of the floating elastic plate is presented in Tables 4.3 – 4.6 for  $\theta = 0, \pi/6, \pi/4$  and  $\pi/2$ , respectively. For the usage of 625 panels and for

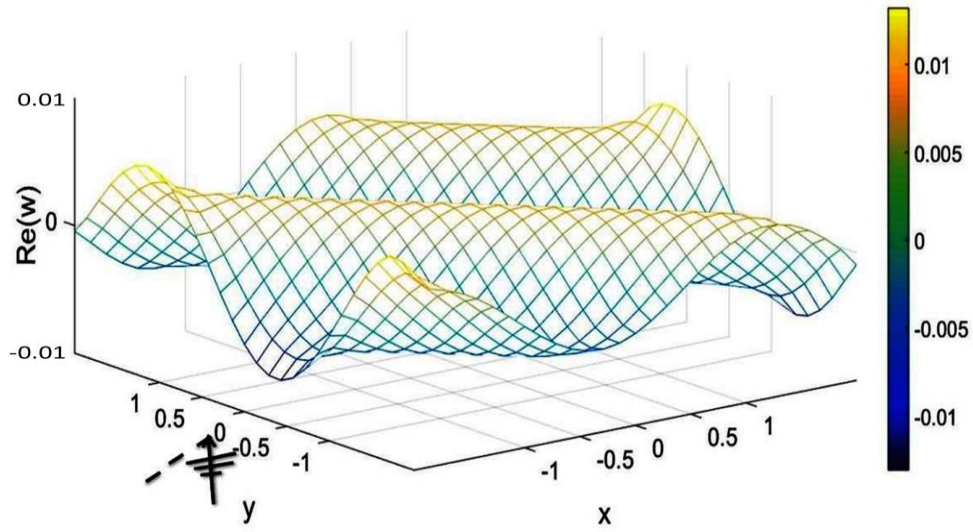
wave angle of attack  $\theta = 0$ , the error is on the higher side when compared with  $\theta = \pi/2$ .



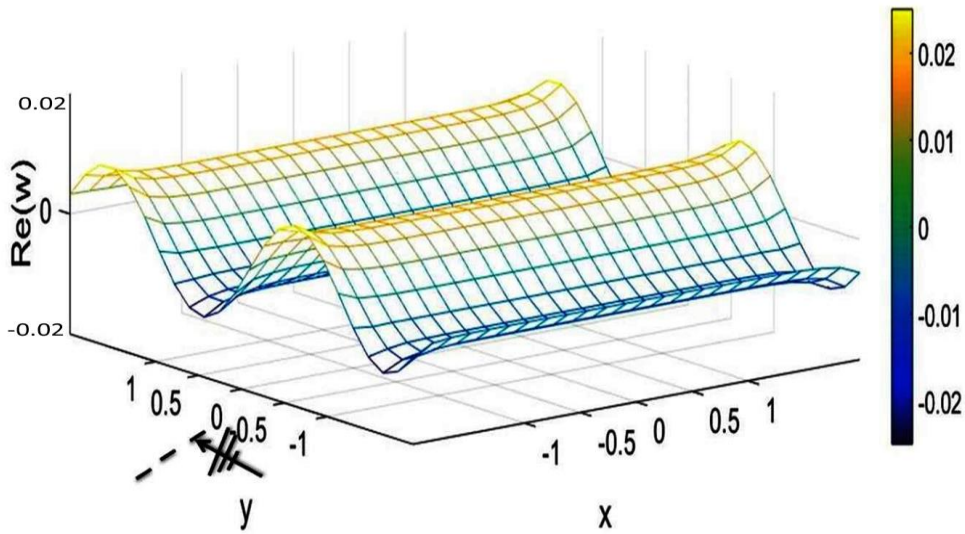
(a)



(b)



(c)



(d)

Fig. 4.3: Deflection of rectangular plate for different wave angle attack (a)  $\theta = 0$ , (b)  $\theta = \pi/6$ , (c)  $\theta = \pi/4$  and (d)  $\theta = \pi/2$ .

This is due to the fact that when the wave propagation is aligned with length of the plate, the bending effect is more due to its larger dimension. As the angle of wave attack increases and reaches  $\theta = \pi/2$ , the wave propagation is aligned with shorter dimension of plate. At this situation, the bending effect is observed to be less and hence, the error is also less when compared with  $\theta = 0$ .

Table 4.3: Time and error as the function of panels for integration points  $N$ ,  $M = 4$  and wave angle  $\theta = 0$ .

| <b>Number of panels</b> | <b>Time(s)</b> | <b>% Error</b> |
|-------------------------|----------------|----------------|
| 100                     | 66.144         | 0.4254         |
| 225                     | 336.144        | 0.1365         |
| 400                     | 1051.107       | 0.0498         |
| 625                     | 2532.635       | 0.0131         |
| 900                     | 5712.012       | 0              |

Table 4.4: Time and error as the function of panels for integration points  $N$ ,  $M = 4$  and wave angle  $\theta = \pi/6$ .

| <b>Number of panels</b> | <b>Time(s)</b> | <b>% Error</b> |
|-------------------------|----------------|----------------|
| 100                     | 65.740         | 0.4108         |
| 225                     | 326.054        | 0.1293         |
| 400                     | 1050.88        | 0.0435         |
| 625                     | 2640.409       | 0.0126         |
| 900                     | 5385.264       | 0              |

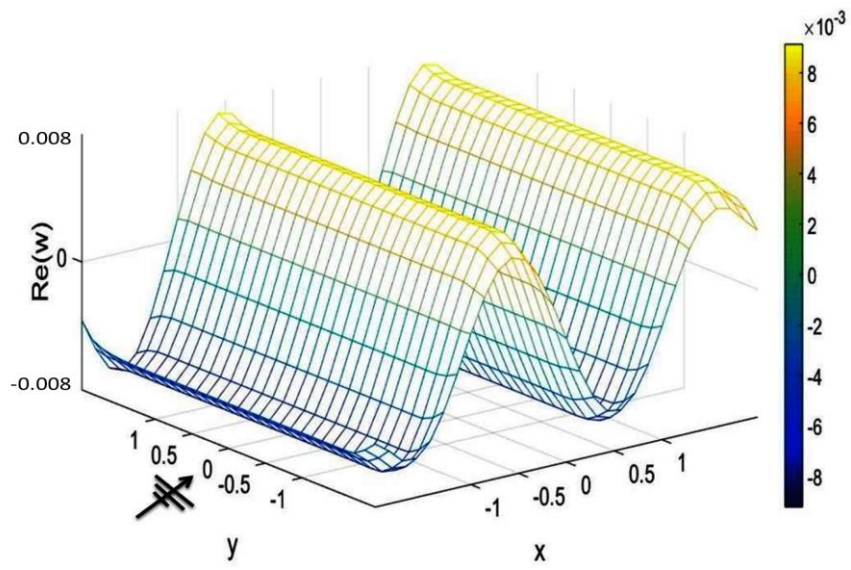
Table 4.5: Time and error as the function of panels for integration points  $N$ ,  $M = 4$  and wave angle  $\theta = \pi/4$ .

| <b>Number of panels</b> | <b>Time(s)</b> | <b>% Error</b> |
|-------------------------|----------------|----------------|
| 100                     | 65.46          | 0.4086         |
| 225                     | 328.028        | 0.1340         |
| 400                     | 1060.461       | 0.0442         |
| 625                     | 2695.860       | 0.0127         |
| 900                     | 5692.205       | 0              |

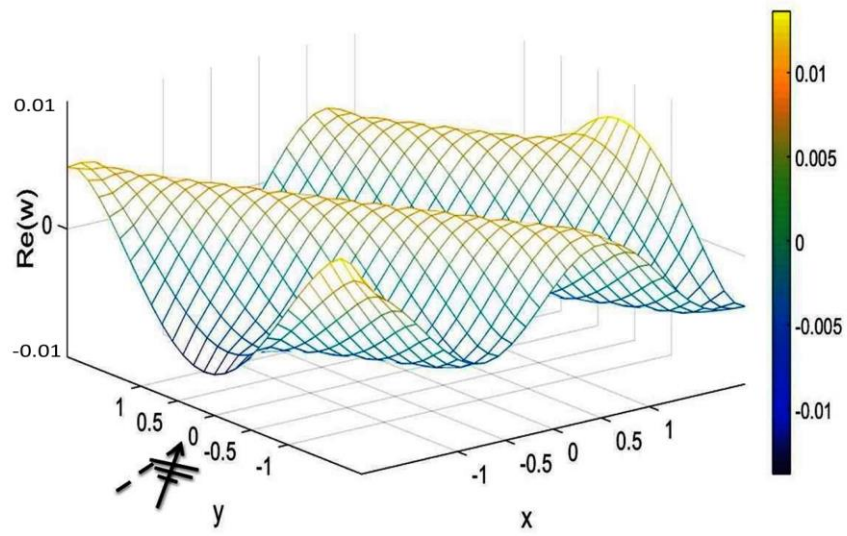
Table 4.6: Time and error as the function of panels for integration points  $N, M = 4$  and wave angle  $\theta = \pi/2$ .

| <b>Number of panels</b> | <b>Time(s)</b> | <b>% Error</b> |
|-------------------------|----------------|----------------|
| 100                     | 67.253         | 0.4125         |
| 225                     | 326.757        | 0.1296         |
| 400                     | 1011.846       | 0.0496         |
| 625                     | 2537.883       | 0.0112         |
| 900                     | 5687.23        | 0              |

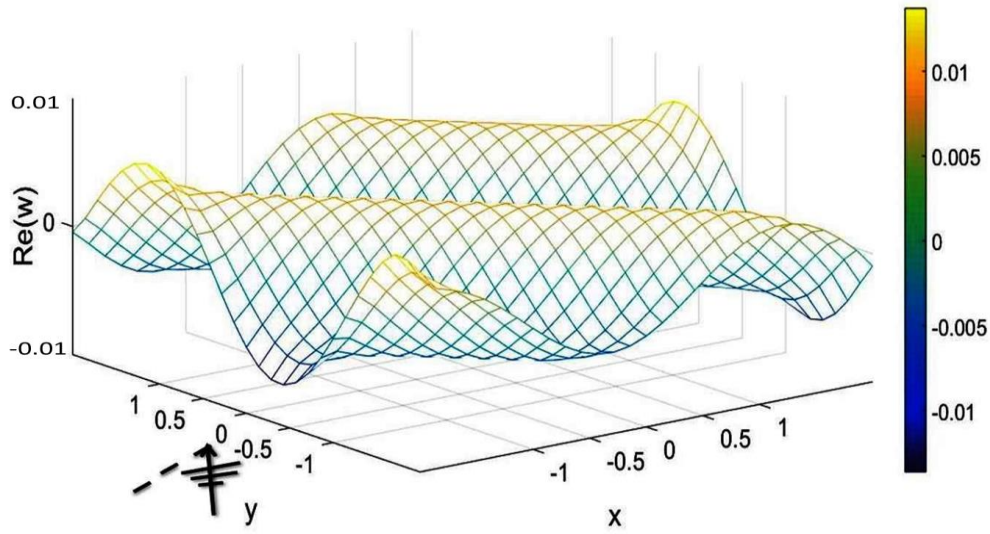
Deflected profiles of the plate when subjected to different wave angles ( $\theta = 0, \pi/6, \pi/4$  and  $\pi/2$ ) of attack with integration points  $N, M = 2$  and are shown in Figure 4.4. In order to understand the effect of number of integration points, the results are compared with integration points  $N, M = 4$ . Tables 4.7 – 4.10 explain the time required for the simulation and error in the model for the number of panels considered, subjected to different angles of wave attack ( $\theta = 0, \pi/6, \pi/4$  and,  $\pi/2$ ). It is observed that the error obtained using integration points  $N = M = 2$  is lesser than the error obtained using integration points  $N = M = 4$  subjected to wave angle of attack  $\theta = 0$ . It is also inferred that the error is less by an average of 3% for  $N = M = 4$  when compared with  $N = M = 2$ . The simulation time for integration points  $N = M = 4$  is three times higher than the simulation time required for integration points of  $N = M = 2$ .



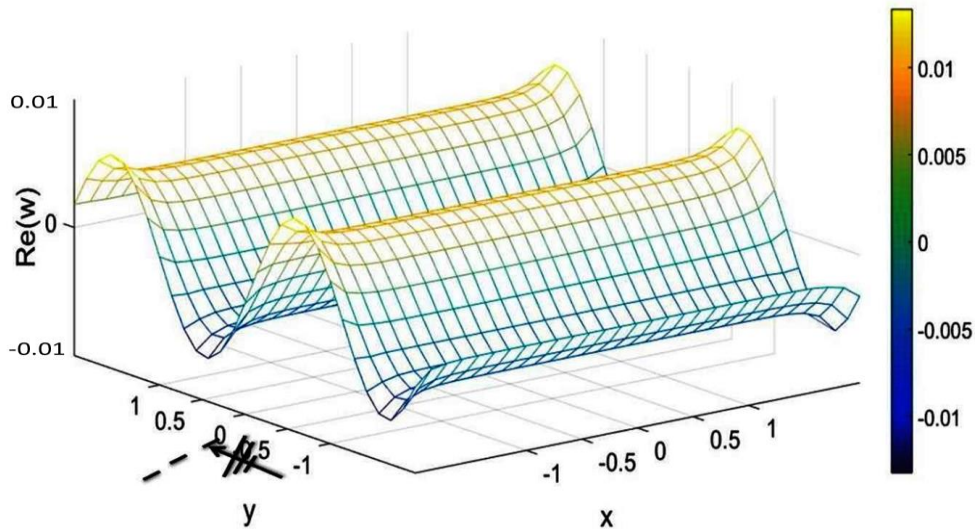
(a)



(b)



(c)



(d)

Fig. 4.4: Deflection of rectangular plate for different wave angles of attack: (a)  $\theta = 0$ , (b)  $\theta = \pi/6$ , (c)  $\theta = \pi/4$  and, (d)  $\theta = \pi/2$ .

By analyzing the integration points,  $N = M = 2$ , it is learnt that the error obtained at  $\theta = 0$  (in line with the length of the plate) is lesser than the error observed for the other angles of wave attack ( $\theta = \pi/6, \pi/4, \pi/2$ ). By considering number of panels as 225, 400 and 625, the error observed for wave propagation in  $\theta = \pi/6$  is lesser than  $\theta = \pi/4$ .

Table 4.7: Time and error as the function of panels for integration points  $N, M = 2$   
and  
wave angle  $\theta = 0$ .

| <b>Number of panels</b> | <b>Time(s)</b> | <b>% Error</b> |
|-------------------------|----------------|----------------|
| 100                     | 32.841         | 0.4191         |
| 225                     | 113.355        | 0.1158         |
| 400                     | 353.636        | 0.0316         |
| 625                     | 907.434        | 0.0091         |
| 900                     | 1989.565       | 0              |

Table 4.8: Time and error as the function of panels for integration points  $N, M = 2$   
and wave angle  $\theta = \pi/6$ .

| <b>Number of panels</b> | <b>Time(s)</b> | <b>% Error</b> |
|-------------------------|----------------|----------------|
| 100                     | 20.465         | 0.4214         |
| 225                     | 103.9953       | 0.1338         |
| 400                     | 332.914        | 0.0451         |
| 625                     | 898.959        | 0.0131         |
| 900                     | 1960.811       | 0              |

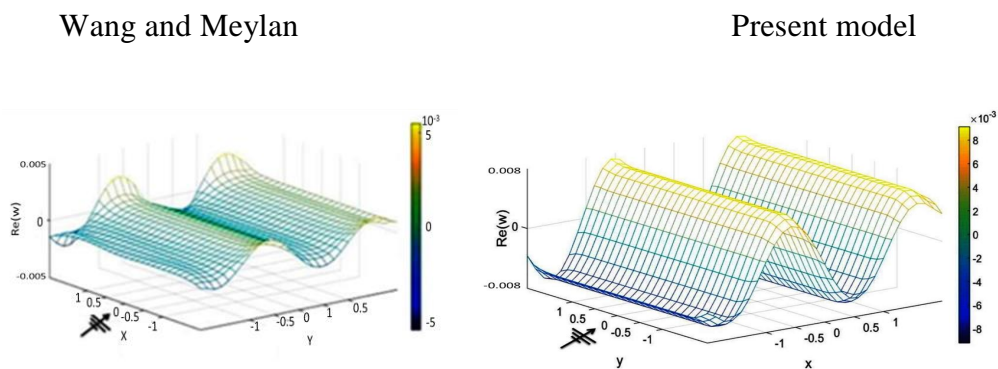
Table 4.9: Time and error as the function of panels for integration points  $N, M = 2$   
and wave angle  $\theta = \pi/4$ .

| <b>Number of panels</b> | <b>Time(s)</b> | <b>% Error</b> |
|-------------------------|----------------|----------------|
| 100                     | 21.214         | 0.4204         |
| 225                     | 106.627        | 0.1386         |
| 400                     | 345.691        | 0.0458         |
| 625                     | 961.570        | 0.0132         |
| 900                     | 1872.529       | 0              |

Table 4.10: Time and error as the function of panels for integration points  $N$ ,  $M = 2$   
 and  
 wave angle  $\theta = \pi/2$ .

| Number of panels | Time(s)   | % Error |
|------------------|-----------|---------|
| 100              | 20.182    | 0.3809  |
| 225              | 103.807   | 0.1328  |
| 400              | 362.531   | 0.0442  |
| 625              | 904.001   | 0.0126  |
| 900              | 1897.6193 | 0       |

The efficacy of the present numerical model at finite water depth is explored by comparing with the results of Wang and Meylan (2004) and the surface profiles are presented in Figure 4.5 for different angles of wave attack. It can be seen that the present model captures the elastic motions smoother than Wang and Meylan (2004). Also, examining the deflection profiles, it is understood that the proposed numerical model simulates the edges of the plates smoothly due to the usage of modified Green's function. Further, it is noticed that a smooth transition of surface mode is captured by the present model which is in accordance with practical sense.



(a)

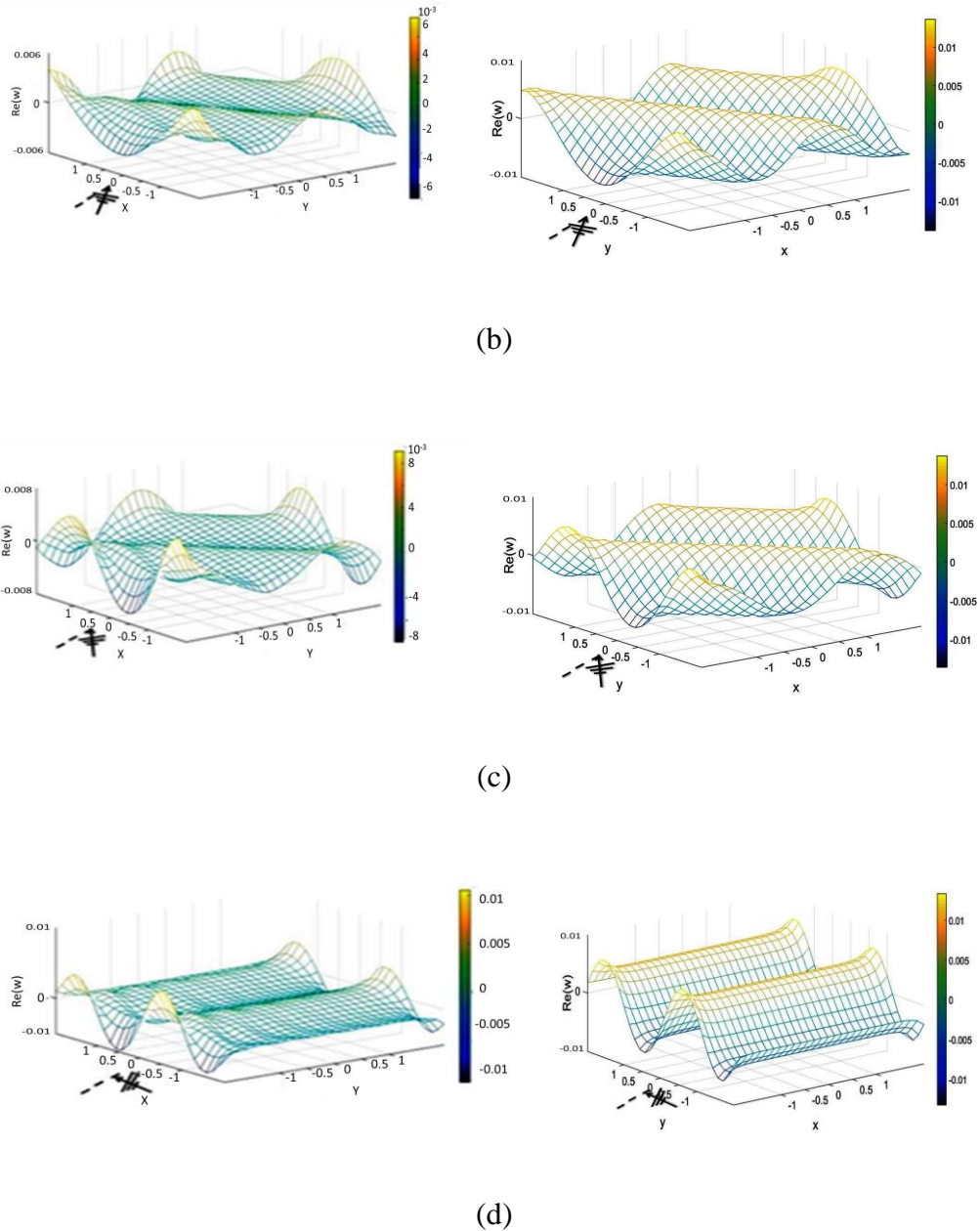


Fig. 4.5: Deflection of rectangular plate for different wave angles of attack: (a)  $\theta = 0$ , (b)  $\theta = \pi/6$ , (c)  $\theta = \pi/4$  and, (d)  $\theta = \pi/2$  for  $N, M = 2$ .

Tables 4.11 – 4.14 provide the comparison of Wang and Meylan (2004) and the developed numerical model with respect to simulation time and error in simulation for integration points of  $N, M = 2$ . In general, it is observed that the simulation time for the present model is lesser than the simulation time of Wang and Meylan (2004). Further, it is learnt that as the number of panel increases, there is a considerable time

saving is observed. For the number of panels as 900, the time saving is about 3%, 9% and an average of 12% for  $\theta = 0$ ,  $\theta = \pi/6$  and  $\theta = \pi/4$  &  $\theta = \pi/2$ , respectively. Further, for the usage of 625 panels, the increase in percentage of error is found to be about 50%, 66%, 15% and -30% for the wave excitation angles  $\theta = 0$ ,  $\theta = \pi/6$ ,  $\theta = \pi/4$  and  $\theta = \pi/2$ , respectively. The negative sign indicates that the present model works better than Wang and Meylan (2004).

Table 4.11: Time and error as the function of panels for integration points  $N$ ,  $M = 2$  and wave angle  $\theta = 0$ .

| <b>Present model</b>    |                |                | <b>Wang model</b> |                |
|-------------------------|----------------|----------------|-------------------|----------------|
| <b>Number of panels</b> | <b>Time(s)</b> | <b>% Error</b> | <b>Time(s)</b>    | <b>% Error</b> |
| 100                     | 32.841         | 0.4191         | 21.775            | 0.2357         |
| 225                     | 113.355        | 0.1158         | 113.354           | 0.0548         |
| 400                     | 353.636        | 0.0316         | 369.544           | 0.0169         |
| 625                     | 907.434        | 0.0091         | 925.887           | 0.0044         |
| 900                     | 1989.565       | 0              | 2036.955          | 0              |

Table 4.12: Time and error as the function of panels for integration points  $N$ ,  $M = 2$  and wave angle  $\theta = \pi/6$ .

| <b>Present model</b>    |                |                | <b>Wang model</b> |                |
|-------------------------|----------------|----------------|-------------------|----------------|
| <b>Number of panels</b> | <b>Time(s)</b> | <b>% Error</b> | <b>Time(s)</b>    | <b>% Error</b> |
| 100                     | 20.465         | 0.4214         | 20.655            | 0.2357         |
| 225                     | 103.9953       | 0.1338         | 110.216           | 0.0542         |
| 400                     | 332.914        | 0.0451         | 380.003           | 0.0169         |
| 625                     | 898.959        | 0.0131         | 978.376           | 0.0044         |
| 900                     | 1960.811       | 0              | 2134.043          | 0              |

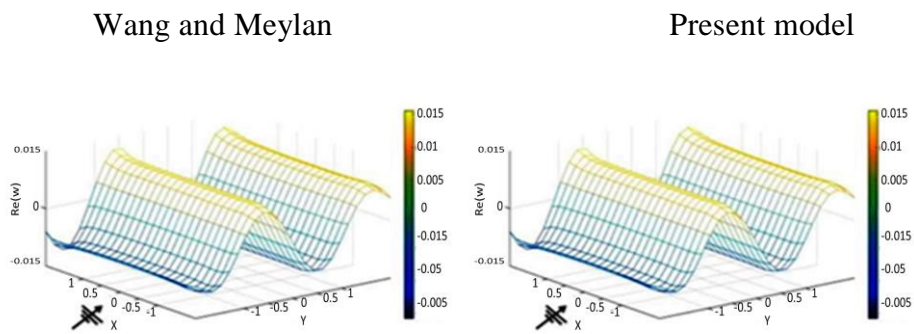
Table 4.13: Time and error as the function of panels for integration points  $N$ ,  $M = 2$  and wave angle  $\theta = \pi/4$ .

| <b>Present model</b>    |                |                | <b>Wang model</b> |                |
|-------------------------|----------------|----------------|-------------------|----------------|
| <b>Number of panels</b> | <b>Time(s)</b> | <b>% Error</b> | <b>Time(s)</b>    | <b>% Error</b> |
| 100                     | 21.214         | 0.4204         | 20.545            | 0.2377         |
| 225                     | 106.627        | 0.1386         | 106.521           | 0.0793         |
| 400                     | 345.691        | 0.0458         | 359.234           | 0.0239         |
| 625                     | 961.570        | 0.0132         | 945.527           | 0.0112         |
| 900                     | 1872.529       | 0              | 2082.876          | 0              |

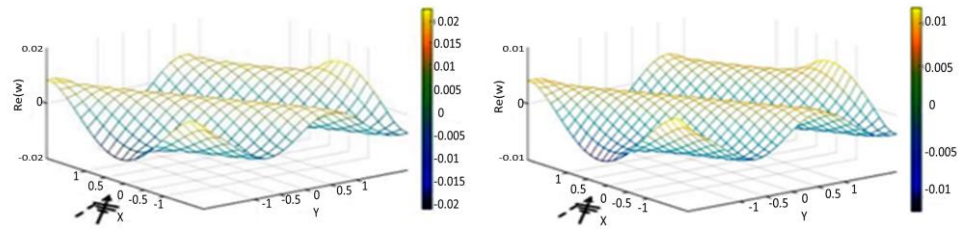
Table 4.14: Time and error as the function of panels for integration points  $N, M = 2$  and wave angle  $\theta = \pi/2$ .

| Present model    |           |         | Wang model |         |
|------------------|-----------|---------|------------|---------|
| Number of panels | Time(s)   | % Error | Time(s)    | % Error |
| 100              | 20.182    | 0.3809  | 21.047     | 0.2233  |
| 225              | 103.807   | 0.1328  | 108.958    | 0.0579  |
| 400              | 362.531   | 0.0442  | 367.448    | 0.0803  |
| 625              | 904.001   | 0.0126  | 949.028    | 0.0454  |
| 900              | 1897.6193 | 0       | 2144.247   | 0       |

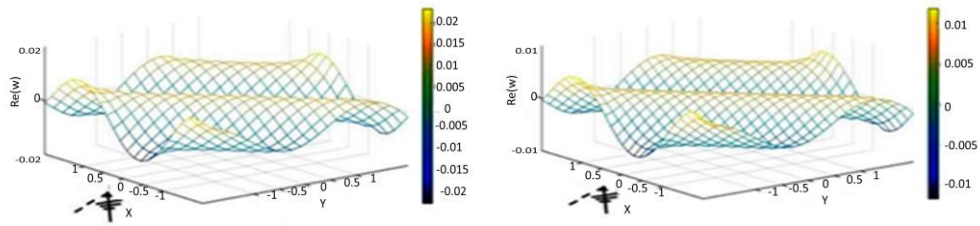
Figure 4.6 captures the deflection of the plate at infinite water depth from the present model with different wave attack angles for  $N, M = 4$ . Also, it compares the surface profile captured by Wang and Meylan, (2004). It is noticed that both the models are equally competitive in capturing the surface modes and the deflection at the corners of the plate.



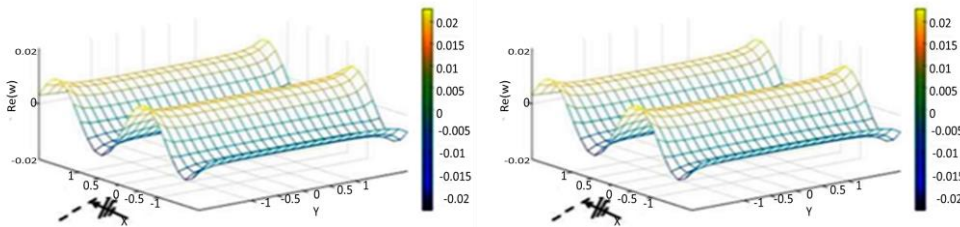
(a)



(b)



(c)



(d)

Fig. 4.6: Deflection of rectangular plate in infinite water depth for different wave angles of attack: (a)  $\theta = 0$ , (b)  $\theta = \pi/6$ , (c)  $\theta = \pi/4$  and, (d)  $\theta = \pi/2$  for  $N, M = 4$ .

Tables 4.15 – 4.18 give the comparison in the aspect of time required for simulation and error in the deflection of both models. It is understood that the present model gives lesser error than Wang and Meylan (2004). However, the simulation time is on the higher side for most of the test conditions. The percentage of error is found to be lesser in the present model for all the angles of wave attack. The said percentage

decrease in error is about 30%, 80%, 74% and 19% for excitation angles  $\theta = 0$ ,  $\theta = \pi/6$ ,  $\theta = \pi/4$  and  $\theta = \pi/2$ , respectively.

Table 4.15: Time and error as the function of panels for integration points  $N, M = 4$  in infinite water depth and wave angle  $\theta = 0$ .

| <b>Present model</b>    |                |                | <b>Wang model</b> |                |
|-------------------------|----------------|----------------|-------------------|----------------|
| <b>Number of panels</b> | <b>Time(s)</b> | <b>% Error</b> | <b>Time(s)</b>    | <b>% Error</b> |
| 100                     | 23.012         | 0.384          | 22.937            | 0.411          |
| 225                     | 122.199        | 0.0915         | 128.108           | 0.1025         |
| 400                     | 402.622        | 0.0267         | 408.996           | 0.0315         |
| 625                     | 1043.968       | 0.0076         | 1040.267          | 0.0099         |
| 900                     | 2260.613       | 0              | 2134.043          | 0              |

Table 4.16: Time and error as the function of panels for integration points  $N, M = 4$  in infinite water depth and wave angle  $\theta = \pi/6$ .

| <b>Present model</b>    |                |                | <b>Wang model</b> |                |
|-------------------------|----------------|----------------|-------------------|----------------|
| <b>Number of panels</b> | <b>Time(s)</b> | <b>% Error</b> | <b>Time(s)</b>    | <b>% Error</b> |
| 100                     | 24.585         | 0.3858         | 23.927            | 0.4125         |
| 225                     | 125.861        | 0.1180         | 124.203           | 0.1598         |
| 400                     | 405.896        | 0.0388         | 414.360           | 0.0421         |
| 625                     | 1056.352       | 0.0110         | 1053.640          | 0.0195         |
| 900                     | 2321.061       | 0              | 2231.190          | 0              |

Table 4.17: Time and error as the function of panels for integration points  $N, M = 4$  in infinite water depth and wave angle  $\theta = \pi/4$ .

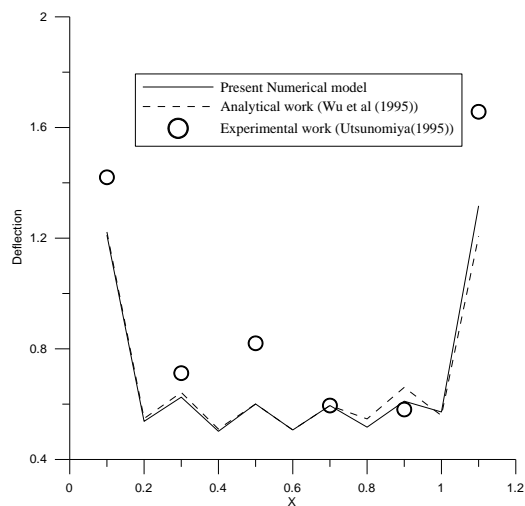
| <b>Present model</b>    |                |                | <b>Wang model</b> |                |
|-------------------------|----------------|----------------|-------------------|----------------|
| <b>Number of panels</b> | <b>Time(s)</b> | <b>% Error</b> | <b>Time(s)</b>    | <b>% Error</b> |
| 100                     | 24.4553        | 0.3789         | 24.184            | 0.3995         |
| 225                     | 123.403        | 0.1218         | 121.550           | 0.1289         |
| 400                     | 407.082        | 0.0398         | 406.328           | 0.0412         |
| 625                     | 1048.909       | 0.0114         | 928.149           | 0.0198         |
| 900                     | 2379.090       | 0              | 2306.478          | 0              |

Table 4.18: Time and error as the function of panels for integration points  $N, M = 4$  in infinite water depth and wave angle  $\theta = \pi/2$ .

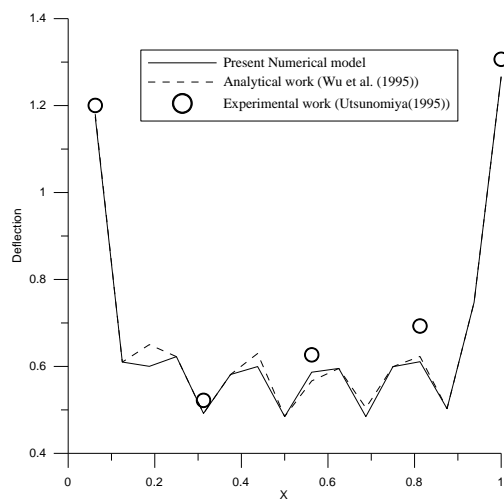
| <b>Present model</b>    |                |                | <b>Wang model</b> |                |
|-------------------------|----------------|----------------|-------------------|----------------|
| <b>Number of panels</b> | <b>Time(s)</b> | <b>% Error</b> | <b>Time(s)</b>    | <b>% Error</b> |
| 100                     | 24.231         | 0.3473         | 23.039            | 0.4128         |
| 225                     | 138.359        | 0.1175         | 113.368           | 0.1970         |
| 400                     | 422.657        | 0.0387         | 402.945           | 0.0410         |
| 625                     | 1043.968       | 0.0042         | 1020.984          | 0.00498        |
| 900                     | 2379.090       | 0              | 2134.043          | 0              |

The developed numerical model is compared with the analytical work of Wu et al. (1995) and experimental work of Utsunomiya et al. (1995) and are projected in Figure 4.7. The length of the model is 10 m, the model is made of polyurethane plates having

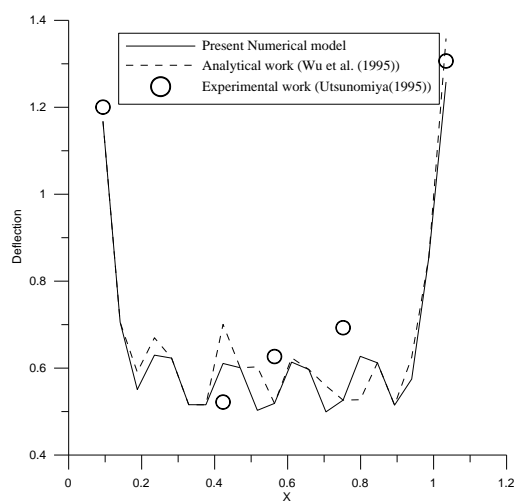
the width of 0.5 m, elastic modulus is 103 MPa, and the density is 0.22 g/cm<sup>3</sup>. The experiment has been carried under the conditions of the water depth of 1.1 m, the incident wave heights of 5, 10, and 20 mm. The predicted deflection profile by the developed numerical model is found to be reasonable agreement with the analytical and experimental works. It can be observed that as the number of panels increases the profile of the developed numerical model is having a good agreement with both the analytical and experimental works.



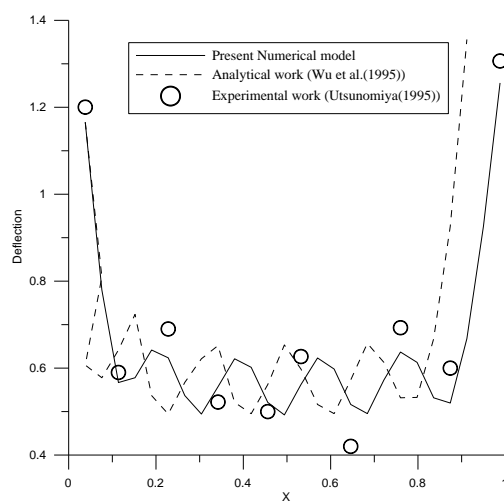
(a)



(b)



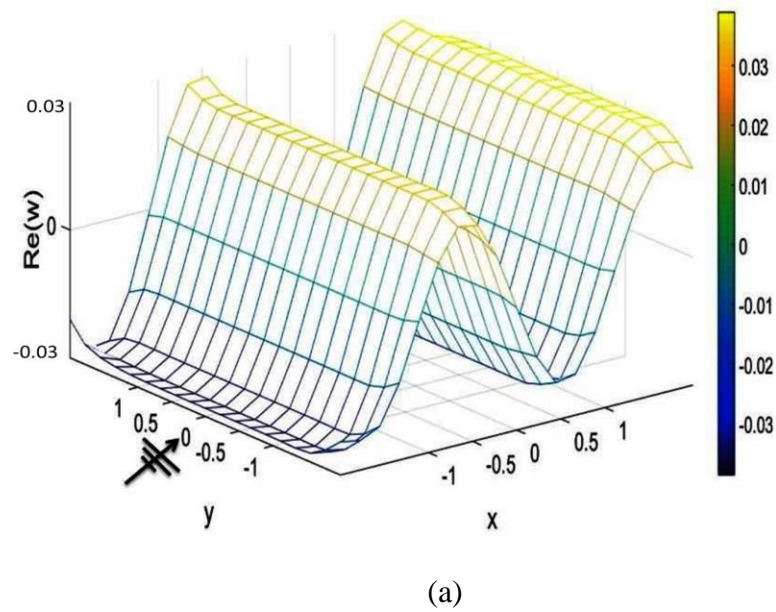
(c)

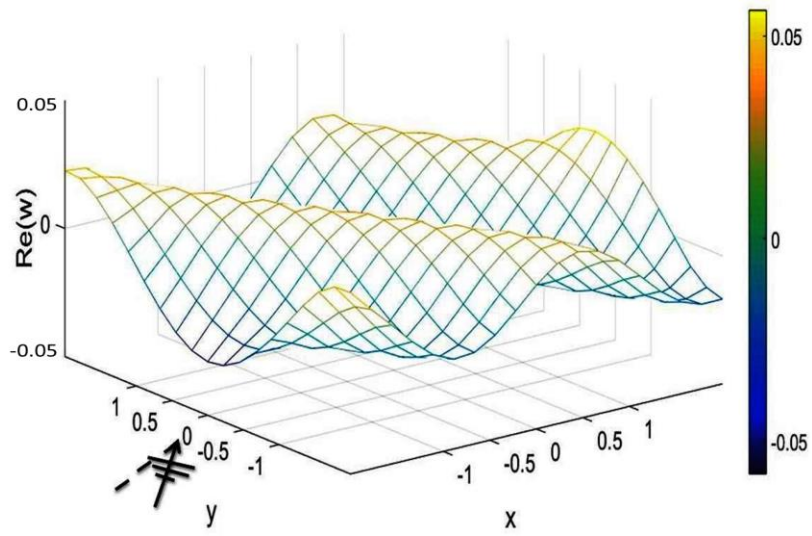


(d)

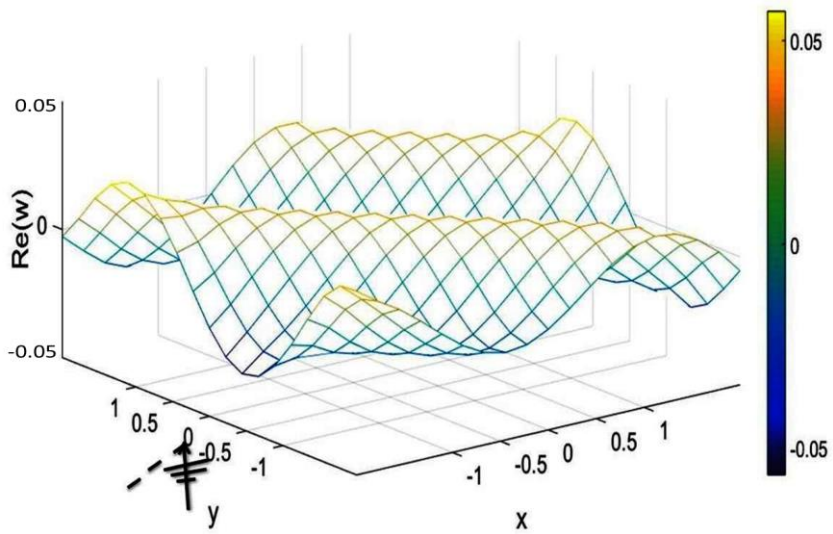
Fig. 4.7: Deflection of rectangular plate for integration points  $N, M = 4$  and  $\theta = 0^\circ$  (a) = 225, (b) = 400, (c) = 625 and, (d) = 900 panels.

The efficacy of the model has been checked for the higher integration points  $N = 4$  and  $M = 8$  at infinite water depth. Figure 4.8 gives the deflection of the floating thin elastic plate subjected to oblique wave angle and it can be seen that a smoother surface profile is observed for all the considered angles of wave attack. The time required for the simulation and error in the model as a function of panels has been studied and are shown in Tables 4.19 – 4.22.

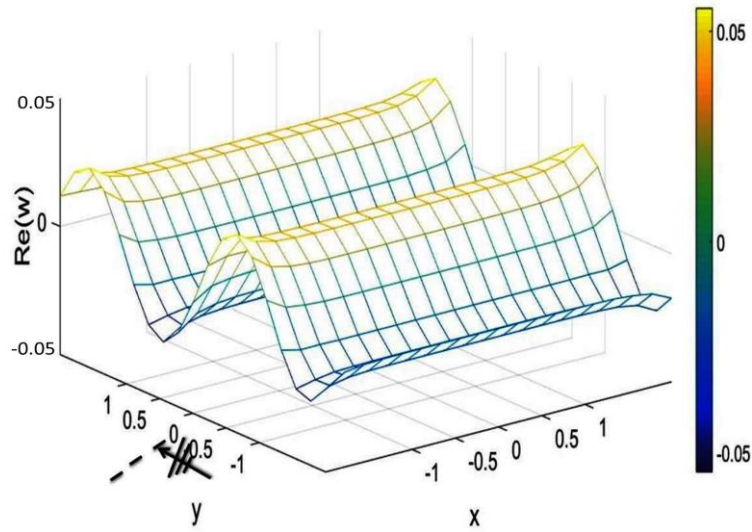




(b)



(c)



(d)

Fig 4.8: Deflection of rectangular plate in infinite water depth for different wave angles of attack (a)  $\theta = 0$ , (b)  $\theta = \pi/6$ , (c)  $\theta = \pi/4$  (d)  $\theta = \pi/2$  for  $N = 4$  and  $M = 8$ .

Table 4.19: Time and error as the function of panels for integration points  $N = 4$  and  $M = 8$  in infinite water depth and  $\theta = 0$ .

| Number of panels | Time(s) | % Error |
|------------------|---------|---------|
| 100              | 72.871  | 0.3766  |
| 225              | 353.683 | 0.0799  |
| 400              | 405.896 | 0       |

Table 4.20: Time and error as the function of panels for integration points  $N = 4$  and  $M = 8$  in infinite water depth and wave angle  $\theta = \pi/6$ .

| Number of panels | Time(s) | % Error |
|------------------|---------|---------|
| 100              | 72.81   | 0.3656  |
| 225              | 343.43  | 0.0856  |

|     |          |   |
|-----|----------|---|
| 400 | 1108.504 | 0 |
|-----|----------|---|

Table 4.21: Time and error as the function of panels for integration points  $N = 4$  and  $M = 8$  in infinite water depth and wave angle  $\theta = \pi/4$ .

| Number of panels | Time(s)  | % Error |
|------------------|----------|---------|
| 100              | 66.915   | 0.3635  |
| 225              | 350.898  | 0.0894  |
| 400              | 1108.900 | 0       |

Table 4.22: Time and error as the function of panels for integration points  $N = 4$  and  $M = 8$  in infinite water depth and wave angle  $\theta = \pi/2$ .

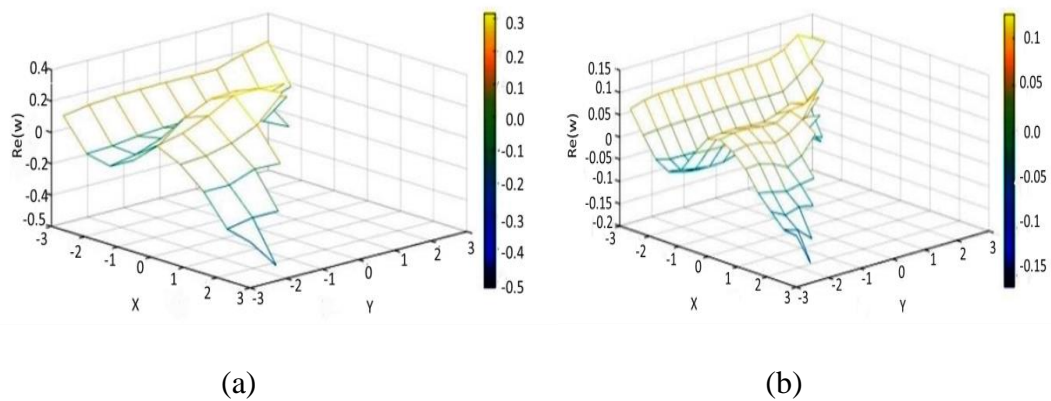
| Number of panels | Time(s) | % Error |
|------------------|---------|---------|
| 100              | 69.615  | 0.3275  |
| 225              | 348.891 | 0.0858  |
| 400              | 405.896 | 0       |

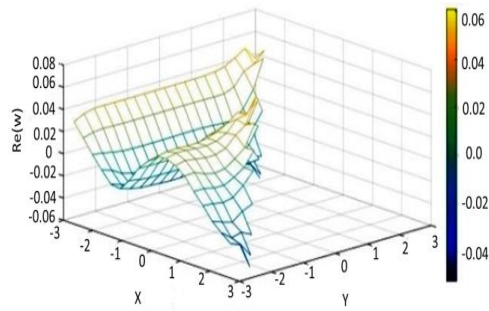
It is observed that as the integration points increases the time required for the simulation also increases and the error in deflection decreases. The model converges as the number of panels reach 400 for integration points  $N = 4$  and  $M = 8$ , whereas, the model converges at 900 panels for  $N = M = 2$  and  $N = M = 4$ . Usage of 100 number of panels at  $\theta = \pi/2$  gives less error when compared with other wave directions. A nominal variation in error is observed among different angles of attack for 225 panels. However, the error is less for the wave propagation in line ( $\theta = \pi/2$ ) with the breadth of the plate. This reduction in error considering different wave angles is due to increase in integration points from  $N = M = 2$  to  $N = 4$  and  $M = 8$ .

## 4.2 HYDROELASTIC BEHAVIOUR OF TRIANGULAR PLATE

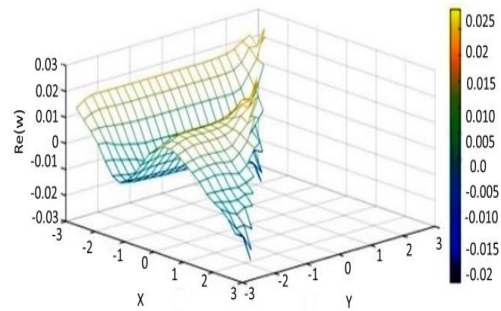
This subsection describes the vertical displacement of the triangular plate, subjected to oblique wave at finite and infinite water depths. Vertical displacement, simulation time and error in the model for integration points  $N = M = 2$  and  $N = M = 4$  are discussed here.

The simulation time necessary to run the model is recorded in order to represent the vertical deflection of the floating plate. Initially, by considering an equal number of integration points ( $N = M = 2$ ), the numerical model has been analysed at finite water depth. Further, the panel dependency of the model has been captured by increasing the number of panels from 77 to 527. The elastic modes or vertical deflection of the triangular plate for different panels have been represented in Figures 4.9 (a) – 4.9 (e) and it can be seen that as the panel number increases the smoothness in deflection profile is evident. It is experimented that the panel dependency is absent as the number of panels crosses 527. Based on this condition, the error is estimated for the panels 77 to 527 at different angles of wave attack.

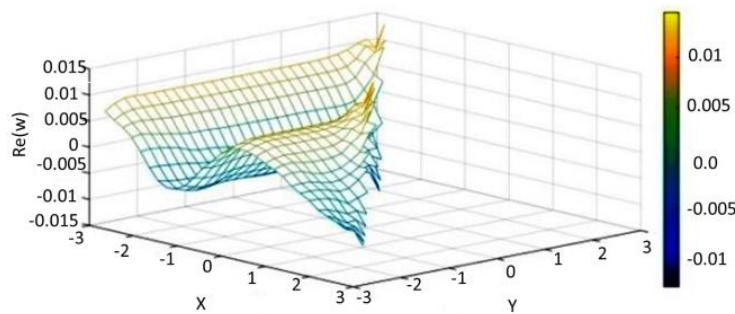




(c)



(d)



(e)

Fig 4.9: Deflection of triangular plate for different number of panels and wave angle of  $\theta=0$ : (a) 77, (b) 152, (c) 252, (d) 377 and (e) 577 panels.

The proposed model is experimented with different angles of wave attack  $\theta = 0, \pi/6$  and  $\pi/4$ . The elastic modes are analysed for simulation time and error in deflection. The obtained results are given in Tables 4.23, 4.24 and 4.25 for angles of wave attack  $\theta = 0, \pi/6$  and  $\pi/4$ , respectively. It is observed that as the number of panels increases, the time required for the simulation also increases. It is also noted that as the number of panels increases, the error in the elastic mode is reduced.

Table 4.23: Time and error as the function of panels for integration points  $N, M = 2$  and wave angle  $\theta = 0$ .

| <b>Number of panels</b> | <b>Time(s)</b> | <b>% Error</b> |
|-------------------------|----------------|----------------|
| 77                      | 5.705          | 0.8727         |
| 152                     | 29.027         | 0.4392         |
| 252                     | 91.402         | 0.1626         |
| 377                     | 228.151        | 0.048          |
| 527                     | 475.635        | 0              |

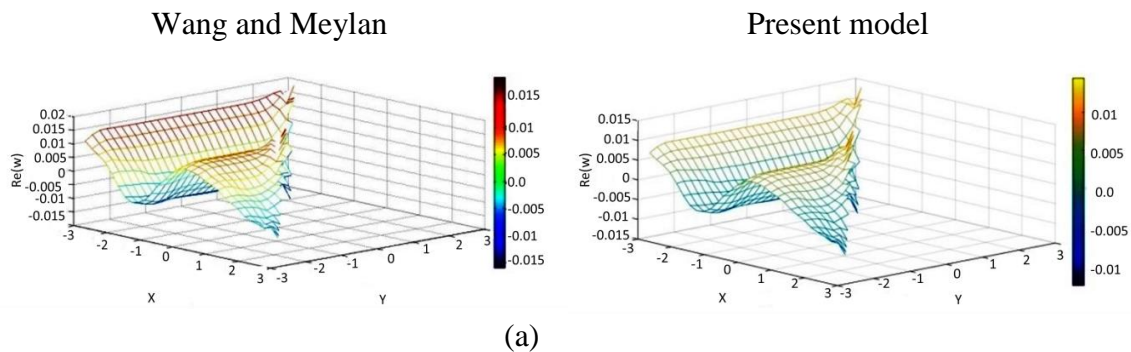
Table 4.24: Time and error as the function of panels for integration points  $N, M = 2$  and wave angle  $\theta = \pi/6$ .

| <b>Number of panels</b> | <b>Time(s)</b> | <b>% Error</b> |
|-------------------------|----------------|----------------|
| 77                      | 5.902          | 0.4889         |
| 152                     | 28.259         | 0.1424         |
| 252                     | 90.341         | 0.0529         |
| 377                     | 229.659        | 0.0168         |
| 527                     | 474.620        | 0              |

Table 4.25: Time and error as the function of panels for integration points  $N$ ,  $M = 2$  and wave angle  $\theta = \pi/4$ .

| Number of panels | Time(s) | % Error |
|------------------|---------|---------|
| 77               | 5.456   | 0.466   |
| 152              | 29.048  | 0.2022  |
| 252              | 95.920  | 0.0668  |
| 377              | 217.844 | 0.0193  |
| 527              | 463.550 | 0       |

The suitability of the developed numerical model is validated by using the results of Wang and Meylan (2004). Figure 4.10 depicts the comparison of surface modes between the present model and the model developed by Wang and Meylan (2004). It can be seen that the deflection profile is smooth at the corners and edges of the plate. The transition of surface mode obtained at the corners by the present numerical model is in accordance with practical sense. Also, the profile obtained from the developed numerical model gives the satisfactory results. It is due to the adaptation of modified Green's function in the present numerical model.



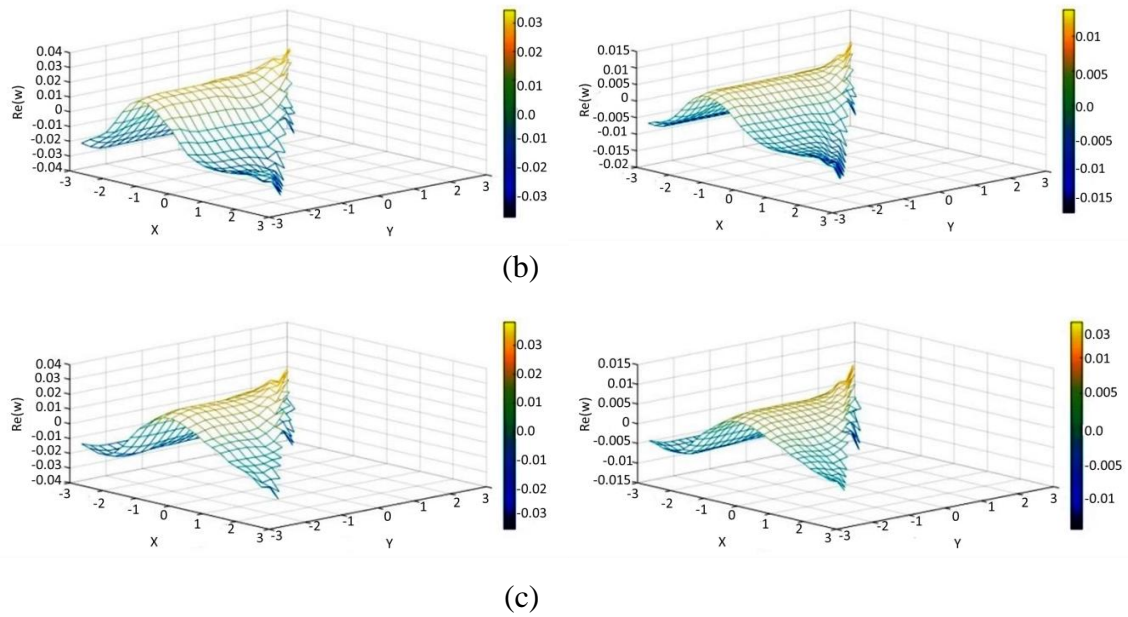


Fig 4.10: Deflection of triangular plate for different wave angles of attack: (a)  $\theta = 0$ ,  
 (b)  $\theta = \pi/6$ , (c)  $\theta = \pi/4$  for  $N, M = 2$ .

Tables 4.26 to 4.28 provide the details of the time required for the simulation and error in the models for the number of panels considered, subjected to different angles of wave attack ( $\theta = 0, \pi/6$  and  $\pi/4$ ). It is understood that the time saved by the present model is about an average of 20% when compared with Wang and Meylan (2004) model. The error in the present model decreases in proper intervals as the number of panels increases, whereas, in Wang and Meylan (2004) the decrease in error is not in proper intervals and it fluctuates as the number of panels increase. Also, it is observed that the error is higher for wave angle of attack  $\theta = 0$  by considering the cases of all number of panels.

Table 4.26: Time and error as the function of panels for integration points  $N, M = 2$  and wave angle  $\theta = 0$ .

| Present model    |         | Wang model |         |
|------------------|---------|------------|---------|
| Number of panels | Time(s) | % Error    | % Error |
|                  |         |            |         |

|     |         |        |         |        |
|-----|---------|--------|---------|--------|
| 77  | 5.705   | 0.8727 | 13.239  | 0.5494 |
| 152 | 29.027  | 0.4392 | 32.548  | 0.2648 |
| 252 | 91.402  | 0.1626 | 104.401 | 0.0971 |
| 377 | 228.151 | 0.048  | 271.689 | 0.0286 |
| 527 | 475.635 | 0      | 599.424 | 0      |

Table 4.27: Time and error as the function of panels for integration points  $N$ ,  $M = 2$  and wave angle  $\theta = \pi/6$ .

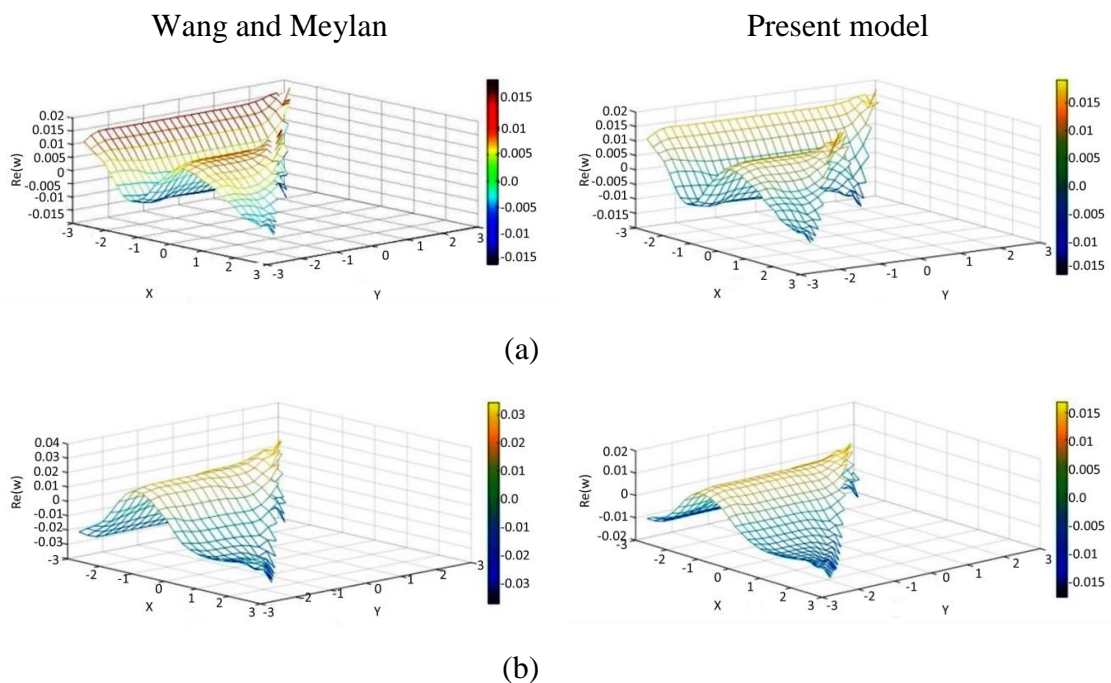
| <b>Present model</b>    |                |                | <b>Wang model</b> |                |
|-------------------------|----------------|----------------|-------------------|----------------|
| <b>Number of panels</b> | <b>Time(s)</b> | <b>% Error</b> | <b>Time(s)</b>    | <b>% Error</b> |
| 77                      | 5.902          | 0.4889         | 7.030             | 0.3192         |
| 152                     | 28.259         | 0.1424         | 34.118            | 0.0852         |
| 252                     | 90.341         | 0.0529         | 113.316           | 0.0442         |
| 377                     | 229.659        | 0.0168         | 258.660           | 0.0137         |
| 527                     | 474.620        | 0              | 548.819           | 0              |

Table 4.28: Time and error as the function of panels for integration points  $N$ ,  $M = 2$  and wave angle  $\theta = \pi/4$ .

| <b>Present model</b>    |                |                | <b>Wang model</b> |                |
|-------------------------|----------------|----------------|-------------------|----------------|
| <b>Number of panels</b> | <b>Time(s)</b> | <b>% Error</b> | <b>Time(s)</b>    | <b>% Error</b> |

|     |         |        |         |        |
|-----|---------|--------|---------|--------|
| 77  | 5.456   | 0.466  | 6.871   | 0.3256 |
| 152 | 29.048  | 0.2022 | 32.666  | 0.1463 |
| 252 | 95.920  | 0.0668 | 103.562 | 0.0516 |
| 377 | 217.844 | 0.0193 | 266.876 | 0.0155 |
| 527 | 463.550 | 0      | 545.946 | 0      |

The number of integration points has been increased from  $N = M = 2$  to  $N = M = 4$  and the salient results are reported. Figure 4.11 illustrates the comparison of surface modes between the present model and Wang and Meylan (2004) model for the integration points of  $N = M = 4$ . The smoothness is improved for the increased panels and as there is a better profile is obtained by the present model for all the wave angles of attack.



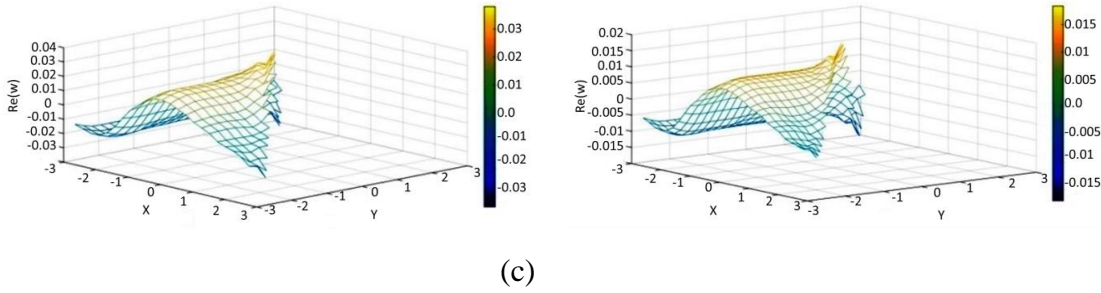


Fig 4.11: Deflection of triangular plate for different wave angles of attack: (a)  $\theta = 0$ , (b)  $\theta = \pi/6$ , (c)  $\theta = \pi/4$  for  $N, M = 4$ .

The time required for simulation and error in the model has been presented in Tables 4.29 – 4.31 and compared with the results of Wang and Meylan (2004). By introspecting the results obtained by the present model, the time required for the simulation is four times higher than that of integration points  $N = M = 4$ . Further, the error in deflection reduces considerably for integration points  $N = M = 4$ . On the aspect of simulation time Wang and Meylan (2004) model requires 1.2 times higher than that of present model. However, the error is on the higher side for the present model by an amount of 45% (average) for the number of panels as 377 and  $\theta = 0, \pi/6$ . The said increase in percentage of error is about 15% for  $\theta = \pi/2$ . By analysing the trend of percentage error, it is understood that there is a fluctuation in the trend of error in Wang and Meylan (2004) as observed for  $N = M = 2$ .

Table 4.29: Time and error as the function of panels for integration points  $N, M = 4$  and wave angle  $\theta = 0$ .

| Present model    |         |         | Wang model |          |
|------------------|---------|---------|------------|----------|
| Number of panels | Time(s) | % Error | Time(s)    | % Error  |
| 77               | 19.54   | 0.87    | 23.28      | 0.162    |
| 152              | 97.757  | 0.4365  | 112.943    | 0.012521 |

|     |          |        |          |         |
|-----|----------|--------|----------|---------|
| 252 | 293.249  | 0.1613 | 352.326  | 0.00079 |
| 377 | 735.292  | 0.0475 | 869.565  | 0.0265  |
| 527 | 1469.878 | 0      | 1259.744 | 0       |

Table 4.30: Time and error as the function of panels for integration points  $N$ ,  $M = 4$  and wave angle  $\theta = \pi/6$ .

| <b>Present model</b>    |                |                | <b>Wang model</b> |                |
|-------------------------|----------------|----------------|-------------------|----------------|
| <b>Number of panels</b> | <b>Time(s)</b> | <b>% Error</b> | <b>Time(s)</b>    | <b>% Error</b> |
| 77                      | 18.075         | 0.4869         | 23.330            | 0.0030         |
| 152                     | 89.025         | 0.141          | 118.785           | 0.0029         |
| 252                     | 276.041        | 0.0524         | 360.749           | 0.0004         |
| 377                     | 657.504        | 0.0165         | 860.591           | 0.00769        |
| 527                     | 1446.549       | 0              | 1845.036          | 0              |

Table 4.31: Time and error as the function of panels for integration points  $N$ ,  $M = 4$  and wave angle  $\theta = \pi/4$ .

| <b>Present model</b>    |                |                | <b>Wang model</b> |                |
|-------------------------|----------------|----------------|-------------------|----------------|
| <b>Number of panels</b> | <b>Time(s)</b> | <b>% Error</b> | <b>Time(s)</b>    | <b>% Error</b> |
| 77                      | 20.326         | 0.463          | 24.173            | 0.00711        |
| 152                     | 113.068        | 0.2005         | 122.010           | 0.00349        |

|     |          |        |          |         |
|-----|----------|--------|----------|---------|
| 252 | 310.974  | 0.0662 | 354.22   | 0.00529 |
| 377 | 741.488  | 0.0191 | 884.896  | 0.01571 |
| 527 | 1499.705 | 0      | 1759.534 | 0       |

Further, the developed numerical model is used to capture the elastic motions of triangular plate at infinite water depth subjected to different wave angles of attack, and for integration points of  $N = M = 2$ . The comparison between the developed numerical model and Wang and Meylan (2004) has been shown in Figure 4.12. It is noticed that both the models are equally competitive in capturing the surface modes and the deflection at the corners of the plate.

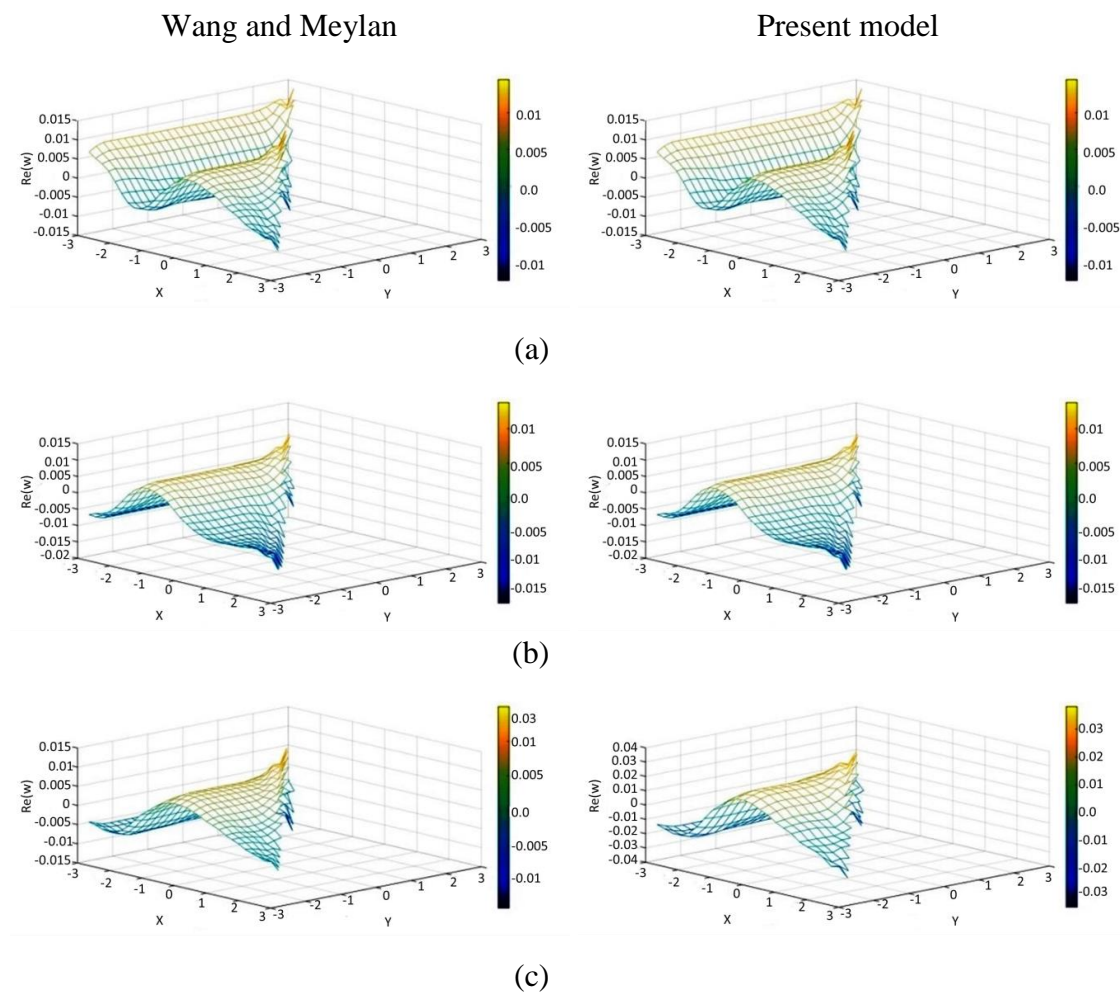


Fig 4.12: Deflection of triangular plate for different wave angles of attack in infinite water depth: (a)  $\theta = 0$ , (b)  $\theta = \pi/6$  and (c)  $\theta = \pi/4$  for  $N, M = 2$ .

Tables 4.32 – 4.34 provide the comparison in the aspect of time required for simulation and error in the deflection of both models. It is understood that the present model gives lesser error than Wang and Meylan (2004). However, the simulation time is on the higher side for most of the test conditions. A uniform decreasing trend in percentage of error is observed for both the models. By considering the number of panels as 377 and  $\theta = 0$  the percentage of error in the present model is about 4.5%, whereas, Wang and Meylan (2004) gives as 8%. The said percentage is about 1.27 & 2.7% and 1.9% & 6% for  $\theta = \pi/6$  and  $\theta = \pi/4$ , respectively.

Table 4.32: Time and error as the function of panels for integration points  $N, M = 2$  and wave angle  $\theta = 0$ .

| <b>Present model</b>    |                |                | <b>Wang model</b> |                |
|-------------------------|----------------|----------------|-------------------|----------------|
| <b>Number of panels</b> | <b>Time(s)</b> | <b>% Error</b> | <b>Time(s)</b>    | <b>% Error</b> |
| 77                      | 2.388          | 0.788          | 3.578             | 0.985          |
| 152                     | 11.971         | 0.409          | 12.325            | 0.562          |
| 252                     | 39.371         | 0.1516         | 42.321            | 0.195          |
| 377                     | 104.221        | 0.0451         | 110.896           | 0.0812         |
| 527                     | 221.452        | 0              | 229.458           | 0              |

Table 4.33: Time and error as the function of panels for integration points  $N$ ,  $M = 2$   
and wave angle  $\theta = \pi/6$ .

| <b>Present model</b>    |                |                | <b>Wang model</b> |                |
|-------------------------|----------------|----------------|-------------------|----------------|
| <b>Number of panels</b> | <b>Time(s)</b> | <b>% Error</b> | <b>Time(s)</b>    | <b>% Error</b> |
| 77                      | 2.374          | 0.4962         | 3.578             | 0.5236         |
| 152                     | 13.018         | 0.1384         | 12.325            | 0.2367         |
| 252                     | 43.920         | 0.0527         | 42.321            | 0.0912         |
| 377                     | 103.988        | 0.0168         | 110.896           | 0.027          |
| 527                     | 246.014        | 0              | 252.458           | 0              |

Table 4.34: Time and error as the function of panels for integration points  $N$ ,  $M = 2$   
and wave angle  $\theta = \pi/4$ .

| <b>Present model</b>    |                |                | <b>Wang model</b> |                |
|-------------------------|----------------|----------------|-------------------|----------------|
| <b>Number of panels</b> | <b>Time(s)</b> | <b>% Error</b> | <b>Time(s)</b>    | <b>% Error</b> |
| 77                      | 2.349          | 0.4505         | 3.578             | 0.585          |
| 152                     | 12.672         | 0.194          | 12.325            | 0.362          |
| 252                     | 40.132         | 0.0634         | 42.321            | 0.095          |
| 377                     | 101.816        | 0.0187         | 110.896           | 0.0612         |
| 527                     | 244.107        | 0              | 252.458           | 0              |

Further, the results are simulated for the integration points of  $N = M = 4$ . Figure 4.13 compares the results of the present model and Wang and Meylan (2004). The surface profiles of the triangular plate in both the models are same. Further, it can be observed that the profile of the elastic motions is smoother than that of integration points  $N = M = 2$ .

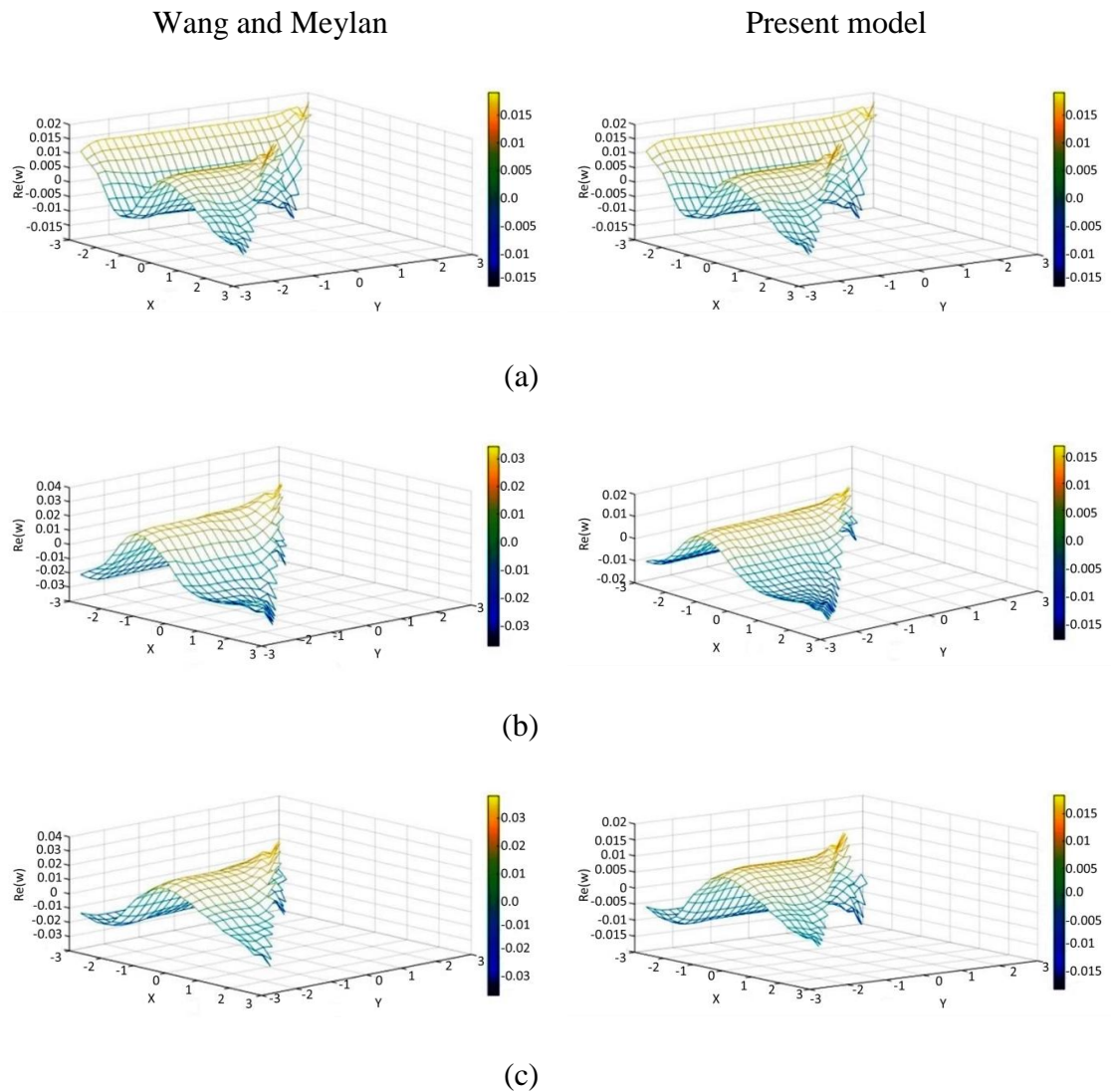


Fig 4.13: Deflection of triangular plate for different wave angles of attack in infinite water depth: (a)  $\theta = 0$ , (b)  $\theta = \pi/6$  and (c)  $\theta = \pi/4$  for  $N, M = 4$ .

Tables 4.35 – 4.37 provide the comparison in the aspect of time required for simulation and error in the deflection of both models. It is understood that the present model works better in terms of time saving and percentage of error. For  $\theta = 0$  and number of panels as 77, the time saving by the present model is about 50%. As the

panel number increases, the percentage of time saving keep decreasing, and it is about 2%, for panel number as 527. Similar trend is observed for the wave angles of attack  $\theta = \pi/6$  and  $\theta = \pi/4$ . It is learnt that as the panel number increases, the reduction in percentage of error increases when compared with Wang and Meylan (2004) for all the angles of wave attack. By considering the panel number as 377, the percentage of reduction in error is about 40% for all the angles of wave excitation.

Table 4.35: Time and error as the function of panels for integration points  $N, M = 4$  and wave angle  $\theta = 0$ .

| <b>Present model</b>    |                |                | <b>Wang model</b> |                |
|-------------------------|----------------|----------------|-------------------|----------------|
| <b>Number of panels</b> | <b>Time(s)</b> | <b>% Error</b> | <b>Time(s)</b>    | <b>% Error</b> |
| 77                      | 6.125          | 0.8723         | 9.214             | 0.9251         |
| 152                     | 29.508         | 0.4013         | 32.842            | 0.5217         |
| 252                     | 94.847         | 0.1411         | 103.952           | 0.32           |
| 377                     | 237.850        | 0.0414         | 248.74            | 0.09           |
| 527                     | 494.424        | 0              | 501.90            | 0              |

Table 4.36: Time and error as the function of panels for integration points  $N, M = 4$  and wave angle  $\theta = \pi/6$

| <b>Present model</b>    |                |                | <b>Wang model</b> |                |
|-------------------------|----------------|----------------|-------------------|----------------|
| <b>Number of panels</b> | <b>Time(s)</b> | <b>% Error</b> | <b>Time(s)</b>    | <b>% Error</b> |

|     |         |        |         |        |
|-----|---------|--------|---------|--------|
| 77  | 6.291   | 0.3912 | 7.235   | 0.5002 |
| 152 | 31.475  | 0.1151 | 32.365  | 0.195  |
| 252 | 97.725  | 0.047  | 100.32  | 0.0921 |
| 377 | 248.747 | 0.0144 | 251.089 | 0.0199 |
| 527 | 515.965 | 0      | 521.005 | 0      |

Table 4.37: Time and error as the function of panels for integration points  $N$ ,  $M = 4$  and wave angle  $\theta = \pi/4$ .

| <b>Present model</b>    |                |                | <b>Wang model</b> |                |
|-------------------------|----------------|----------------|-------------------|----------------|
| <b>Number of panels</b> | <b>Time(s)</b> | <b>% Error</b> | <b>Time(s)</b>    | <b>% Error</b> |
| 77                      | 6.143          | 0.3639         | 8.561             | 0.425          |
| 152                     | 31.529         | 0.8995         | 32.36             | 0.992          |
| 252                     | 101.423        | 0.0533         | 105.952           | 0.6257         |
| 377                     | 255.173        | 0.0149         | 257.482           | 0.0210         |
| 527                     | 496.356        | 0              | 501.102           | 0              |

### 4.3 HYDROELASTIC BEHAVIOUR OF TRAPEZOIDAL PLATE

This subsection describes the vertical displacement of the trapezoidal plate, subjected to oblique wave at finite and infinite water depths. Vertical displacement, simulation time and error in the model for integration points  $N = M = 2$  and  $N = M = 4$  are discussed here.

To check the efficacy of the proposed model on complex geometry, trapezoidal shape has been considered and simulation is carried out. Figure 4.14 illustrates the elastic modes of the trapezoidal plate for integration points  $N = M = 2$  subjected to different wave angles of attack. Also, it is compared with the results of Wang and Meylan (2004). It is learnt that both the profiles are almost similar.

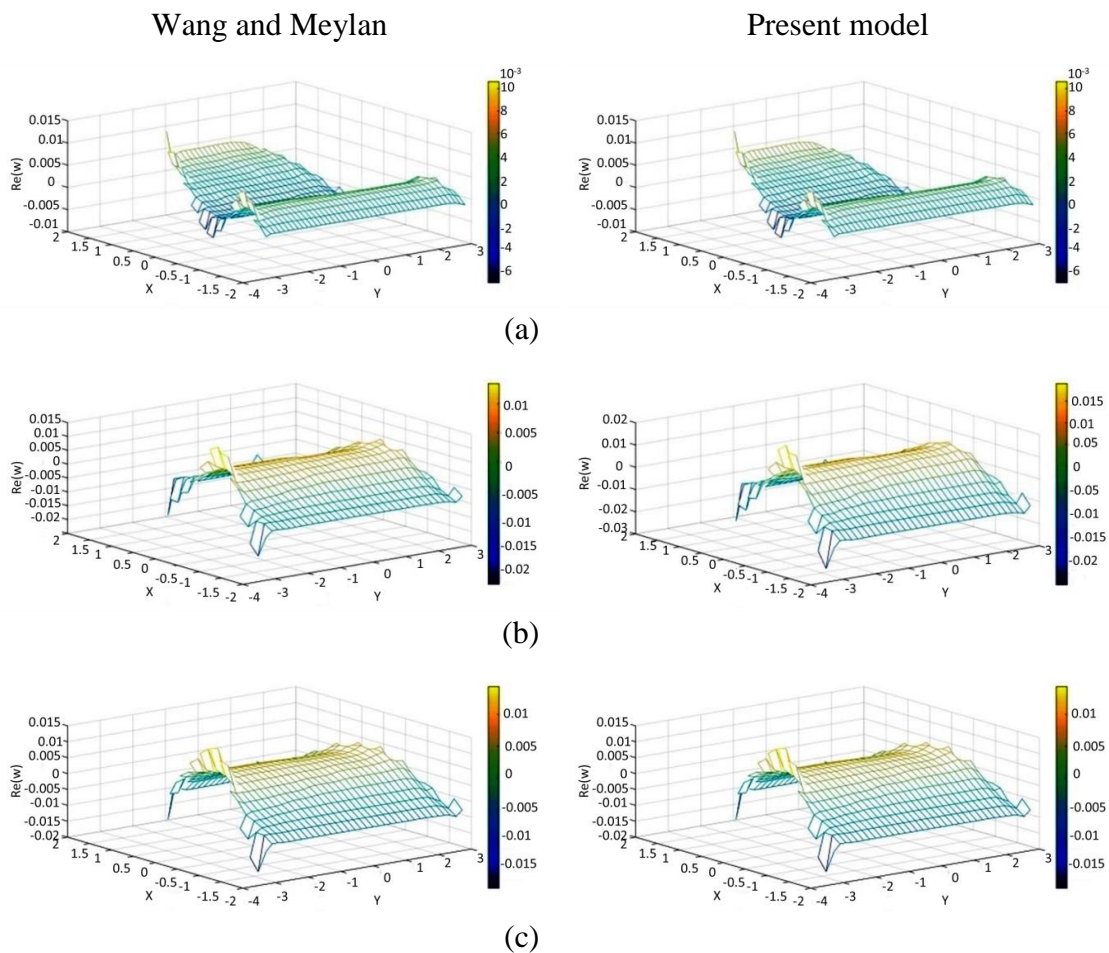


Fig 4.14: Deflection of trapezoidal plate for different wave angles of attack: (a)  $\theta = 0$ , (b)  $\theta = \pi/4$ , (c)  $\theta = \pi/6$  for  $N, M = 2$ .

Table 4.38: Time and error as the function of panels for integration points  $N$ ,  $M = 2$  and wave angle  $\theta = 0$ .

| <b>Present model</b>    |                |                | <b>Wang model</b> |                |
|-------------------------|----------------|----------------|-------------------|----------------|
| <b>Number of panels</b> | <b>Time(s)</b> | <b>% Error</b> | <b>Time(s)</b>    | <b>% Error</b> |
| 120                     | 32.078         | 0.4348         | 23.030            | 0.5323         |
| 304                     | 146.583        | 0.0693         | 177.569           | 0.0558         |
| 572                     | 580.193        | 0              | 708.349           | 0              |

Table 4.39: Time and error as the function of panels for integration points  $N$ ,  $M = 2$  and wave angle  $\theta = \pi/6$ .

| <b>Present model</b>    |                |                | <b>Wang model</b> |                |
|-------------------------|----------------|----------------|-------------------|----------------|
| <b>Number of panels</b> | <b>Time(s)</b> | <b>% Error</b> | <b>Time(s)</b>    | <b>% Error</b> |
| 120                     | 18.055         | 0.2821         | 22.511            | 0.2021         |
| 304                     | 140.055        | 0.0369         | 190.182           | 0.0285         |
| 572                     | 595.381        | 0              | 731.642           | 0              |

Table 4.40: Time and error as the function of panels for integration points  $N, M = 2$  and wave angle  $\theta = \pi/4$ .

| Present model    |         |         | Wang model |         |
|------------------|---------|---------|------------|---------|
| Number of panels | Time(s) | % Error | Time(s)    | % Error |
| 120              | 16.621  | 0.3102  | 23.366     | 0.2465  |
| 304              | 129.986 | 0.0483  | 169.222    | 0.0345  |
| 572              | 544.287 | 0       | 727.322    | 0       |

Initially, the simulation is carried out with 120 panels as mentioned in Wang and Meylan (2004). Also, the simulation is tried by increasing the panels to 304 and 572. A further increase in panels i.e. beyond 572, the dependency is observed to be absent. Tables 4.38 – 4.40 compare the results of present model and Wang and Meylan (2004) for  $N = M = 2$  subjected to wave angle of attack  $\theta = 0, \pi/6$  and  $\pi/4$ . It can be observed that the time required for the simulation is lesser than Wang and Meylan (2004) by an average of 130% for panels 120, 304 and 572. A decreasing trend is observed for all angles of wave attack in the present model, however, fluctuation in error is observed in Wang and Meylan (2004). By considering the number of panels as 304, the increase in error is about 19% and an average of 30% for  $\theta = 0$  and  $\theta = \pi/6$  &  $\pi/4$ , respectively.

Figure 4.15 shows deflection of the trapezoidal plate for increased number of integration points  $N = M = 4$  and the surface profile is compared with Wang and Meylan, (2004). Tables 4.41 – 4.43 provide the results for  $N = M = 4$  and for angle of wave attack  $\theta = 0, \pi/6$  and  $\pi/4$ . A thorough investigation reveals that there is 20% of time saving for all the angles of wave attack when compared with Wang and Meylan

(2004). However, the error in deflection profile is higher than Wang and Meylan (2004) and also fluctuates with respect to number of panels

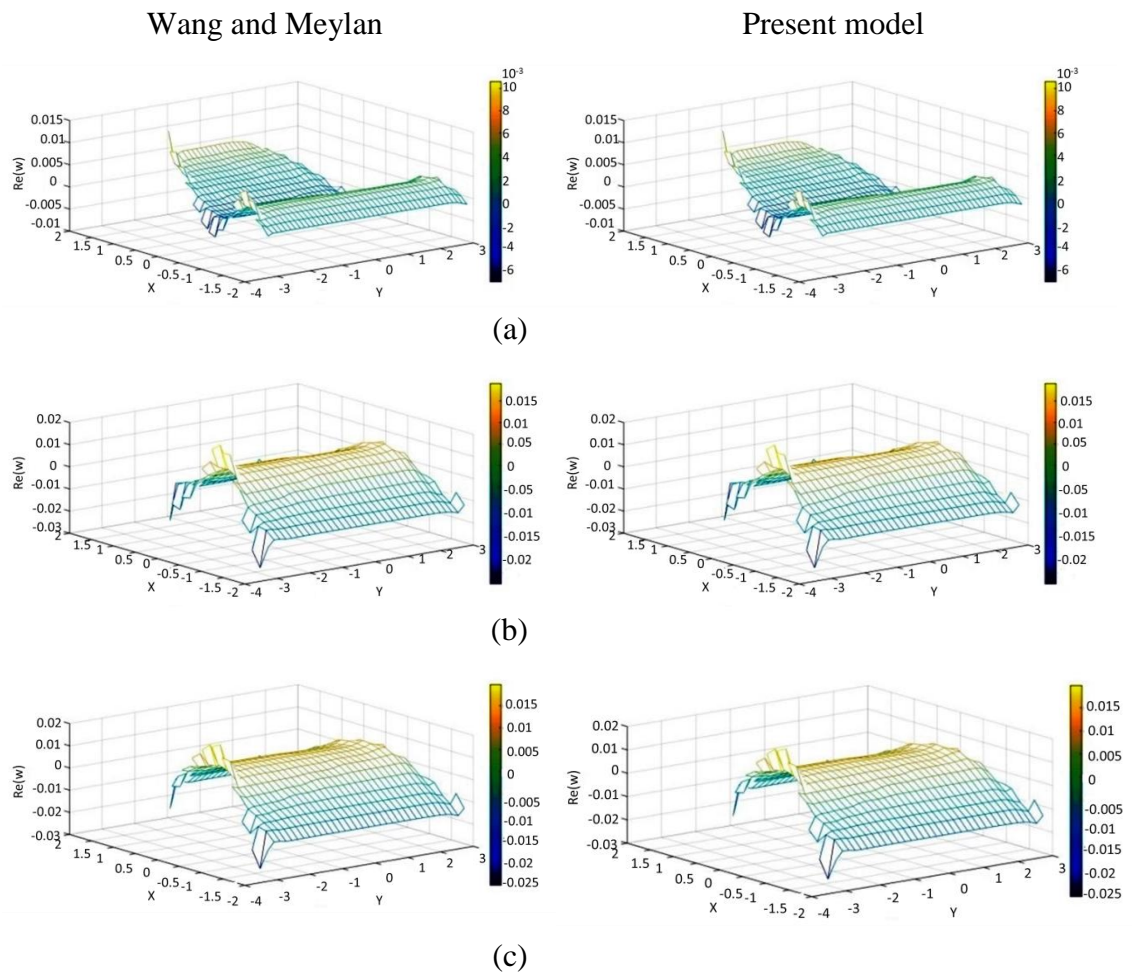


Fig 4.15: Deflection of trapezoidal plate for different wave angles of attack: (a)  $\theta = 0$ , (b)  $\theta = \pi/6$ , (c)  $\theta = \pi/4$  for  $N, M = 4$ .

Table 4.41: Time and error as the function of panels for integration points  $N$ ,  $M = 4$  and wave angle  $\theta = 0$ .

| <b>Present model</b>    |                |                | <b>Wang model</b> |                |
|-------------------------|----------------|----------------|-------------------|----------------|
| <b>Number of panels</b> | <b>Time(s)</b> | <b>% Error</b> | <b>Time(s)</b>    | <b>% Error</b> |
| 120                     | 55.106         | 0.6358         | 69.221            | 0.334          |
| 304                     | 425.550        | 0.0687         | 541.978           | 0.011          |
| 572                     | 1656.301       | 0              | 2205.208          | 0              |

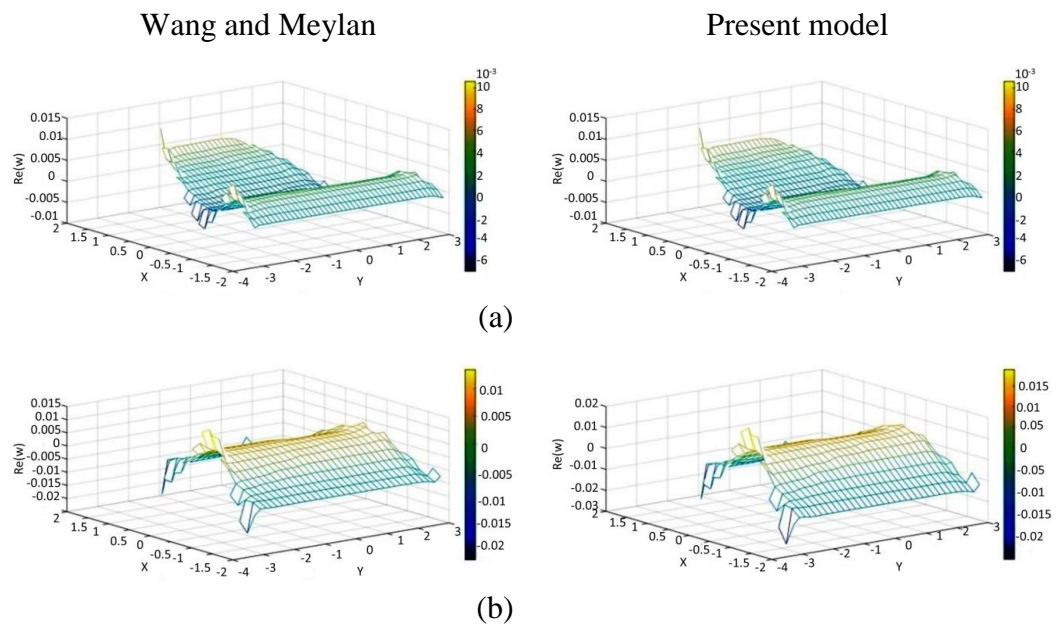
Table 4.42: Time and error as the function of panels for integration points  $N$ ,  $M = 4$  and wave angle  $\theta = \pi/6$ .

| <b>Present model</b>    |                |                | <b>Wang model</b> |                |
|-------------------------|----------------|----------------|-------------------|----------------|
| <b>Number of panels</b> | <b>Time(s)</b> | <b>% Error</b> | <b>Time(s)</b>    | <b>% Error</b> |
| 120                     | 59.337         | 0.2798         | 79.658            | 0.222          |
| 304                     | 442.093        | 0.0365         | 550.925           | 0.016          |
| 572                     | 1710.054       | 0              | 2253.355          | 0              |

Table 4.43: Time and error as the function of panels for integration points  $N, M = 4$  and wave angle  $\theta = \pi/4$ .

| Present model    |          |         | Wang model |         |
|------------------|----------|---------|------------|---------|
| Number of panels | Time(s)  | % Error | Time(s)    | % Error |
| 120              | 55.713   | 0.3071  | 71.726     | 0.441   |
| 304              | 429.326  | 0.0477  | 564.247    | 0.046   |
| 572              | 1698.675 | 0       | 2191.471   | 0       |

Further, the developed numerical model is used to capture the elastic motions of trapezoidal plate at infinite water depth. The plate has been analyzed for different wave attack angles with  $N = M = 2$ . The results obtained by the developed model are compared with the results of Wang and Meylan (2004) and is shown in Figure 4.16. It is noticed that both the models are equally competitive in capturing the surface modes and the deflection at the corners of the plate.



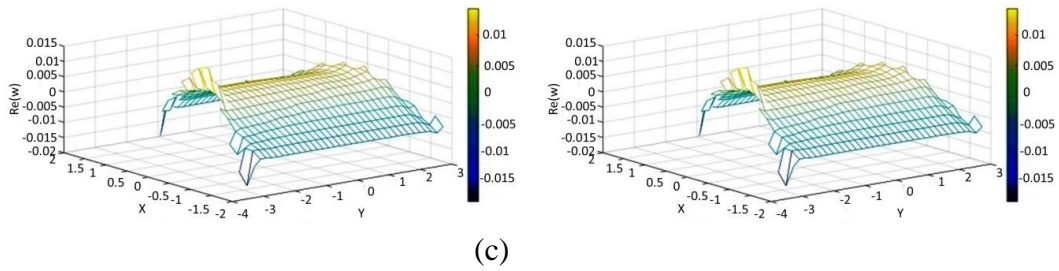


Fig 4.16: Deflection of trapezoidal plate for different wave angles of attack: (a)  $\theta = 0$ ,  
 (b)  $\theta = \pi/6$ , (c)  $\theta = \pi/4$  for  $N, M = 2$ .

Tables 4.44 – 4.46 provide the comparison in the aspect of time required for simulation and error in the deflection of both models. It is understood that the usage of present model saves simulation time by an average of 3% and 7% for  $\theta = 0$  &  $\pi/4$  and  $\theta = \pi/6$ , respectively. The percentage of error is lesser by an amount of 8% for  $\theta = 0$ . The said percentage is about 6% for  $\theta = \pi/6$ .

Table 4.44: Time and error as the function of panels for integration points  $N, M = 2$  and wave angle  $\theta = 0$ .

| Present model    |         |         | Wang model |         |
|------------------|---------|---------|------------|---------|
| Number of panels | Time(s) | % Error | Time(s)    | % Error |
| 120              | 7.675   | 0.4169  | 8.001      | 0.4201  |
| 304              | 63.212  | 0.0668  | 64.125     | 0.0721  |
| 572              | 284.734 | 0       | 285.1023   | 0       |

Table 4.45: Time and error as the function of panels for integration points  $N, M = 2$  and wave angle  $\theta = \pi/6$ .

| <b>Present model</b>    |                |                | <b>Wang model</b> |                |
|-------------------------|----------------|----------------|-------------------|----------------|
| <b>Number of panels</b> | <b>Time(s)</b> | <b>% Error</b> | <b>Time(s)</b>    | <b>% Error</b> |
| 120                     | 7.637          | 0.2471         | 8.235             | 0.257          |
| 304                     | 65.433         | 0.0375         | 69.415            | 0.04005        |
| 572                     | 312.208        | 0              | 314.612           | 0              |

Table 4.46: Time and error as the function of panels for integration points  $N, M = 2$  and wave angle  $\theta = \pi/4$ .

| <b>Present model</b>    |                |                | <b>Wang model</b> |                |
|-------------------------|----------------|----------------|-------------------|----------------|
| <b>Number of panels</b> | <b>Time(s)</b> | <b>% Error</b> | <b>Time(s)</b>    | <b>% Error</b> |
| 120                     | 8.147          | 0.2959         | 8.247             | 0.3001         |
| 304                     | 71.427         | 0.0439         | 72.321            | 0.0495         |
| 572                     | 298.242        | 0              | 299.555           | 0              |

Further, the results are simulated for the integration points of  $N = M = 4$ . It can be observed that the profile of the elastic mode is smoother than the surface modes obtained for  $N = M = 2$ . Figure 4.17 compares the results of the present model and Wang and Meylan (2004). Both the models are equally competitive in capturing the surface profiles.

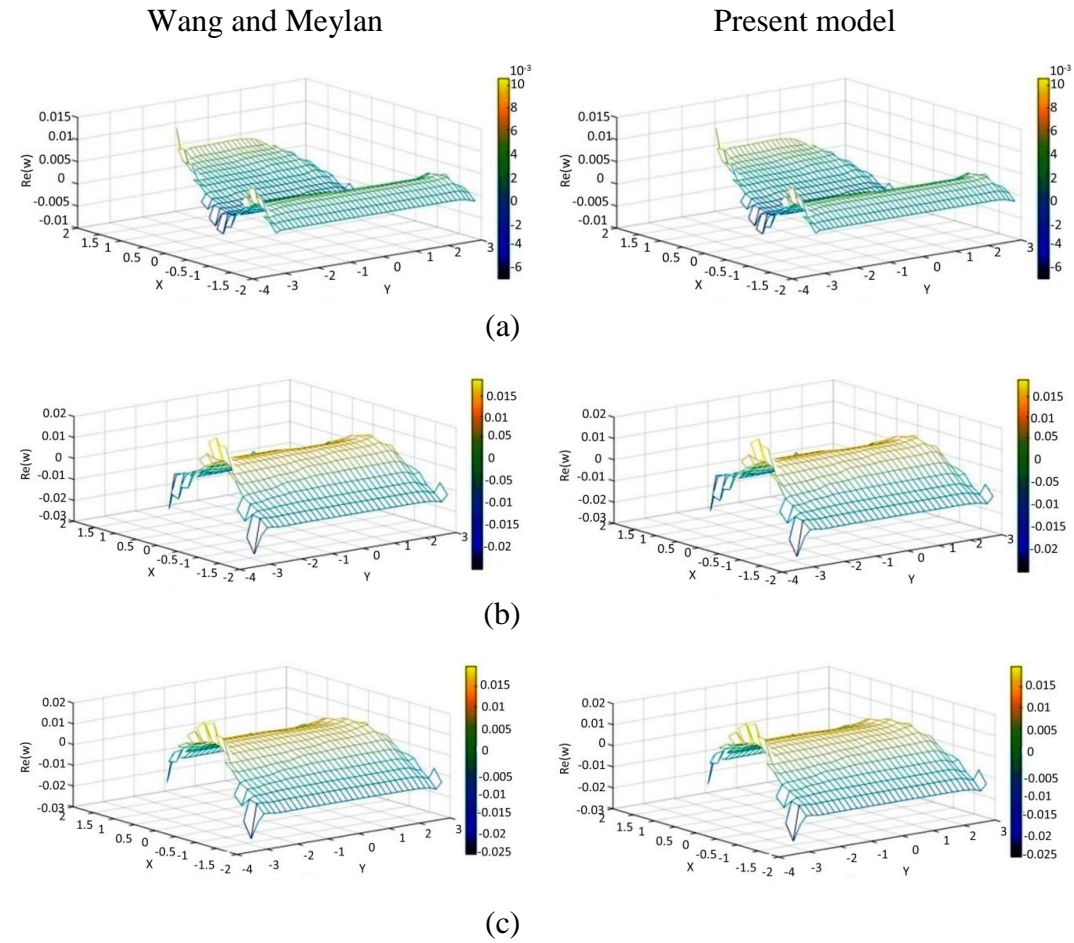


Fig 4.17: Deflection of trapezoidal plate for different wave angles of attack: (a)  $\theta = 0$ , (b)  $\theta = \pi/4$ , (c)  $\theta = \pi/6$  for  $N, M = 4$ .

Tables 4.47 – 4.49 provide comparison in the aspect of time required for simulation and error in the deflection of both models. The error in the present model is lesser than that of Wang and Meylan (2004). By considering the panel numbers as 304, the reduction in error is about 14%, 20% and 30% for wave angles of attack  $\theta = 0$ ,  $\theta = \pi/6$  and  $\theta = \pi/4$ , respectively. Further, the simulation time of Wang and Meylan (2004) is on the higher side by an average of 2% for most of the test conditions.

Table 4.47: Time and error as the function of panels for integration points  $N, M = 4$  and wave angle  $\theta = 0$ .

| <b>Present model</b>    |                |                | <b>Wang model</b> |                |
|-------------------------|----------------|----------------|-------------------|----------------|
| <b>Number of panels</b> | <b>Time(s)</b> | <b>% Error</b> | <b>Time(s)</b>    | <b>% Error</b> |
| 120                     | 19.892         | 0.3            | 20.231            | 0.369          |
| 304                     | 153.063        | 0.045          | 155.192           | 0.0512         |
| 572                     | 656.457        | 0              | 658.008           | 0              |

Table 4.48: Time and error as the function of panels for integration points  $N, M = 4$  and wave angle  $\theta = \pi/6$ .

| <b>Present model</b>    |                |                | <b>Wang model</b> |                |
|-------------------------|----------------|----------------|-------------------|----------------|
| <b>Number of panels</b> | <b>Time(s)</b> | <b>% Error</b> | <b>Time(s)</b>    | <b>% Error</b> |
| 120                     | 18.874         | 0.2089         | 19.324            | 0.295          |
| 304                     | 156.731        | 0.0267         | 157.624           | 0.0318         |
| 572                     | 644.054        | 0              | 646.005           | 0              |

Table 4.49: Time and error as the function of panels for integration points  $N$ ,  $M = 4$  and wave angle  $\theta = \pi/4$ .

| <b>Present model</b>    |                |                | <b>Wang model</b> |                |
|-------------------------|----------------|----------------|-------------------|----------------|
| <b>Number of panels</b> | <b>Time(s)</b> | <b>% Error</b> | <b>Time(s)</b>    | <b>% Error</b> |
| 120                     | 19.818         | 0.3062         | 20.145            | 0.3054         |
| 304                     | 154.070        | 0.0307         | 155.217           | 0.0399         |
| 572                     | 630.012        | 0              | 632.914           | 0              |

## CHAPTER 5

### CONCLUSION AND FUTURE WORKS

#### 5.0 GENERAL

1. The proposed model is capable of analysing the hydroelasticity for the floating plate with arbitrary shapes at finite and infinite water depths.
2. The model uses modified Green's function which differs with Wang and Meylan, (2004).
3. By using Bessels and Hankels functions, the elastic motion/vertical deflection are obtained accurately.
4. The main advantage of the proposed numerical model is that BEM and FEM accommodate the same number of basis functions.
5. Error and simulation time with respect to number of panels in the developed model has been compared with the results of Wang and Meylan, (2004).
6. The model dependency differs for different shapes of the plate. Model saturates at 900, 527 and 572 panels for rectangular, triangular and trapezoidal plates, respectively.
7. The efficacy of the model has been checked by using three different set of integration points,  $N = M = 2$ ,  $N = M = 4$  and  $N = 4$ ,  $M = 8$ .
8. Fluctuation of the error in the developed model has been observed for  $N = M = 2$  and  $N = M = 4$  subjected to oblique wave angle of attack.
9. With the use of modified Green's function, it can be concluded that the deflection profile at the corners of the triangular/trapezoidal plate can be captured very accurately and surface profile in a smooth manner.

#### 5.1 RECTANGULAR PLATE

1. It is observed that as the integration points and the number of panels increase, the time required for simulation increases and vice - versa.
2. As the number of panels increases, the error reduces gradually in the present model, whereas, the decreasing trend is not observed in Wang and Meylan (2004) as it fluctuates.

3. In finite water depth, the error is observed to be less by an average of 3% for  $N = M = 4$  when compared with  $N = M = 2$ .
4. For integration points  $N = M = 4$ , the time required for the simulation is about three times higher than that of  $N = M = 2$ .
5. For integration points  $N = M = 2$ , the percentage error is found to be high by 50%, 66%, 15% and -30% for wave angle of attack  $\theta = 0$ ,  $\theta = \pi/6$ ,  $\theta = \pi/4$  and  $\theta = \pi/2$ , respectively.
6. In infinite water, and for integration points  $N = M = 4$  the percentage decrease in error is about 30%, 80%, 74% and 19% for wave angle of attack  $\theta = 0$ ,  $\theta = \pi/6$ ,  $\theta = \pi/4$  and  $\theta = \pi/2$ , respectively.
7. The model converges as the number of panels reach 400 for integration points  $N = 4$  and  $M = 8$ , whereas, the model converges at 900 panels for  $N = M = 2$  and  $N = M = 4$ .
8. At infinite water depth, the developed numerical model lags behind the model developed by Wang and Meylan (2004) in terms of time required for the simulation, but provides good agreement with error in deflection.

## 5.2 TRIANGULAR PLATE

1. In finite water depth, and for integration points  $N = M = 4$  the present model saves the simulation time by an average of 20% when compared with Wang and Meylan (2004) model.
2. In finite water depth, the time required for the simulation using integration points  $N = M = 4$  is four times higher when compared with  $N = M = 2$ .
3. It is observed that for integration points  $N = M = 2$  the model developed by Wang and Meylan (2004) requires 1.2 times higher simulation time than that of present model.
4. In infinite water depth, and for integration points  $N = M = 2$  the error obtained by the present and Wang and Meylan (2004) models are about 1.27% & 2.7% and 1.9% & 6% for  $\theta = \pi/6$  and  $\theta = \pi/4$ , respectively.
5. The developed model in infinite water depth with  $\theta = 0$  and number of panels as 77 saves the simulation time by 50% for integration points  $N = M = 2$ .

6. In infinite water depth, the reduction in percentage of error is observed to be about about 40% for all the angles of wave excitation.
7. The error decreases at proper interval for the developed model. Further, the model is in good agreement with the model developed by Wang and Meylan (2004).

### 5.3 TRAPEZOIDAL PLATE

1. The simulation time for  $N = M = 4$  is nearly two times greater than that of  $N = M = 2$
2. In finite water depth, it can be observed that the time required for the simulation is lesser than Wang and Meylan (2004) by an average of 130% for panels 120, 304 and 572 with angle of wave attack  $\theta = 0$ .
3. By considering integration points as  $N = M = 4$ , it is observed that there is 20% of time saving for all the angles of wave attack when compared with Wang and Meylan (2004).
4. In infinite water depth, the usage of integration point  $N = M = 2$  saves simulation time by an average of 3% and 7% for  $\theta = 0$  and  $\theta = \pi/6$ , respectively. The percentage of error is lesser by an amount of 8% for  $\theta = 0$ .
5. By considering the panel numbers as 304, the reduction in error is about 14%, 20% and 30% for wave angles of attack  $\theta = 0$ ,  $\theta = \pi/6$  and  $\theta = \pi/4$ , respectively. Further, the simulation time of Wang and Meylan (2004) is on the higher side by an average of 2% for most of the test conditions in infinite water depth with integration points as  $N = M = 4$ .

### 5.4 LIMITATIONS OF THE STUDY

- The developed numerical model is best suited for the analysis of structure in Cartesian coordinate system, whereas, the model requires modification to analyze the structure in polar coordinate system.
- The plate is assumed to be thin and thin plate theory has been incorporated to develop the numerical model, hence, thick plates cannot be analyzed.

- The developed numerical model is suited for analyzing the structure at finite and infinite water depths.
- The plate is assumed to be continuous without any connections in-between.
- Accuracy of the vertical deflection can be further improved by adopting eight noded finite element basis function and higher integration points.

### **5.5 SCOPE FOR FUTURE WORK**

- The developed numerical model can be further extended to study the structure in polar coordinates.
- The singularity in the model can be reduced to study the behavior of structure in shallow water.
- Amount of time required to construct the VLFS is less.
- Connection designs for multiple structures can be studied further.
- By incorporating shell theory, the model can be utilized to analyze both thin and thick plates.
- The effect of airplane landing and takeoff, can be adopted to analyze the floating structure.
- How and up to what extent the VLFSs are environment friendly.

## REFERENCES

---

- Andrianov, A. I., and Hermans, A. J. (2003). “The influence of water depth on the hydroelastic response of a very large floating platform.” *Marine Structures*, 16 (5), 355-371.
- Andrianov, A. I., and Hermans, A. J. (2005). “Hydroelasticity of a circular plate on water of finite or infinite depth.” *Journal of Fluids and Structures*, 20 (5), 719-733.
- Andrianov, A. I., and Hermans, A. J. (2006a). “Hydroelastic behavior of a floating ring-shaped plate.” *Journal of Engineering Mathematics*, 54 (1), 31-48.
- Andrianov, A. I., and Hermans, A. J. (2006b). “Hydroelastic analysis of a floating plate of finite draft.” *Applied Ocean Research*, 28 (5), 313-325.
- Andrianov, A., and Hermans, A. (2002). “A VLFP on infinite, finite and shallow water.” *In the proceedings of 17th International workshop on water waves and floating bodies, Cambridge, UK*.
- Athanassoulis, G. A., and Belibassakis, K. A. (1999). “A consistent coupled-mode theory for the propagation of small-amplitude water waves over variable bathymetry regions.” *Journal of Fluid Mechanics*, 389, 275-301.
- Babich, V. M., and Buldyrev, V. S. (1991). “*Short-wavelength diffraction theory: asymptotic methods*.” Springer-Verlag.
- Babich, V. M., and Kirpichnikova, N. Y. (2003). “Boundary layer approach to the theory of localized waves.” In IEEE proceedings of *International Seminar on Diffraction*, 13-21.
- Balmforth, N. J., and Craster, R. V. (1999). “Ocean waves and ice sheets.” *Journal of Fluid Mechanics*, 395, 89-124.
- Banerjee, P. K., Ahmad, S., and Wang, H. C. (1988). “A new BEM formulation for the acoustic eigenfrequency analysis.” *International Journal for Numerical Methods in Engineering*, 26 (6), 1299-1309.
- Belibassakis, K. A., and Athanassoulis, G. A. (2004). “Three-dimensional Green's function for harmonic water waves over a bottom topography with

different depths at infinity.” *Journal of Fluid Mechanics*, 510, 267-302.

- Belibassakis, K. A., and Athanassoulis, G. A. (2005). “A coupled-mode model for the hydroelastic analysis of large floating bodies over variable bathymetry regions.” *Journal of Fluid Mechanics*, 531, 221-249.
- Brebbia, C. A. (1978). “The BEM for engineers.” *Pentech Press, UK*.
- Brebbia, C. A., and Dominguez, J. (1977). “Boundary element methods for potential problems.” *Applied Mathematical Modelling*, 1(7), 372-378.
- Cheng, Y., Ji, C., Zhai, G., and Oleg, G. (2016). “Dual inclined perforated anti-motion plates for mitigating hydroelastic response of a VLFS under wave action.” *Ocean Engineering*, 121, 572-591.
- Cheung, K. F., Phadke, A. C., Smith, D. A., Lee, S. K., and Seidl, L. H. (2000). “Hydrodynamic response of a pneumatic floating platform.” *Ocean Engineering*, 27 (12), 1407-1440.
- Cho, I. H., and Kim, M. H. (2013). “Transmission of oblique incident waves by a submerged horizontal porous plate.” *Ocean Engineering*, 61, 56-65.
- Chung, H., and Linton, C. M. (2003). “Interaction between water waves and elastic plates: Using the residue calculus technique.” *18th International Workshop on the Water Waves and Floating Bodies, France*.
- Clough, R. W. (1960). “The finite element method in plane stress analysis.” *In the proceedings of 2nd ASCE Conference on Electronic Computation, Pittsburgh*.
- Costabel, M. (1986). “Principles of boundary element methods.” *Techn. Hochsch., Fachbereich Mathematik*.
- Cruse, T. A. (1969). “Numerical solutions in three dimensional elastostatics.” *International Journal of Solids and Structures*, 5 (12), 1259-1274.
- Doronin, Y. P., and Kheisin, D. E. (1977). “Sea ice.” *Arctic Science and Technology Information System*.
- Endo, H. (2000). “The behavior of a VLFS and an airplane during takeoff/landing run in wave condition.” *Marine Structures*, 13 (4-5), 477-491.

- Evans, D. V., and Davies, T. V. (1968). “wave-ice interaction.” *Stevens Inst of Tech Hoboken NJ Davidson Lab*.
- Evans, D. V., and Porter, R. (2003). “Wave scattering by narrow cracks in ice sheets floating on water of finite depth.” *Journal of Fluid Mechanics*, 484, 143-165.
- Fox, C., and Squire, V. A. (1994). “On the oblique reflection and transmission of ocean waves at shore fast sea ice.” *Philosophical transactions of the royal society London. A*, 347 (1682), 185-218.
- Gao, R. P., Tay, Z. Y., Wang, C. M., and Koh, C. G. (2011). “Hydroelastic response of very large floating structure with a flexible line connection.” *Ocean Engineering*, 38 (17-18), 1957-1966.
- Gehring, G. (1860). “Differential equations, which are defined as crystal equilibrium and motion of the plate.” *Schultzii printed*.
- Greenhill, A. G. (1887). Wave Motion in Hydrodynamics (continued). *American Journal of Mathematics*, 97-112.
- Guéret, R. A. M. (2003). “Interaction of free surface waves with elastic and air-cushion platforms.” *Doctoral thesis, Delft University Press*.
- Guiggiani, M., and Gigante, A. (1990). “A general algorithm for multidimensional Cauchy principal value integrals in the boundary element method.” *Journal of Applied Mechanics*, 57 (4), 906-915.
- Guret, R., and Hermans, A. J. (2001). “An air cushion under a floating offshore structure.” *In the Proceedings of 16th International Workshop on Water Waves and Floating Bodies, Hiroshima, Japan*, 1-4.
- Hamamoto, T., Suzuki, A., and Fujita, K. I. (1997). “Hybrid dynamic analysis of large tension leg floating structures using plate elements.” *In the Proceedings of 7th International Offshore and Polar Engineering Conference*, International Society of Offshore and Polar Engineers.
- He, J., Tofighi, N., Yildiz, M., Lei, J., and Suleman, A. (2017). “A coupled WC-TL SPH method for simulation of hydroelastic problems.” *International Journal of Computational Fluid Dynamics*, 31 (3), 174-187.
- Hermans, A. J. (2000). “A boundary element method for the interaction of

free-surface waves with a very large floating flexible platform.” *Journal of Fluids and Structures*, 14 (7), 943-956.

- Hermans, A. J. (2001). “A geometrical-optics approach for the deflection of a floating flexible platform.” *Applied Ocean Research*, 23 (5), 269-276.
- Hermans, A. J. (2003). “The ray method for the deflection of a floating flexible platform in short waves.” *Journal of Fluids and Structures*, 17 (4), 593-602.
- Hermans, A. J. (2004). “Interaction of free-surface waves with floating flexible strips.” *Journal of Engineering Mathematics*, 49 (2), 133-147.
- Hirdaris, S. E., Price, W. G., and Temarel, P. (2003). “Two- and three-dimensional hydroelastic modelling of a bulker in regular waves.” *Marine Structures*, 16 (8), 627-658.
- Hrennikoff, A. (1941). “Solution of problems of elasticity by the framework method.” *Journal of Applied Mechanics*.
- Huang, L. L., and Riggs, H. R. (2000). “The hydrostatic stiffness of flexible floating structures for linear hydroelasticity.” *Marine Structures*, 13 (2), 91-106.
- Humamoto, T., and Fujita, K. (2002). “Wet-mode superposition for evaluating the hydroelastic response of floating structures with arbitrary shape.” *In the Proceedings of 12th International Offshore and Polar Engineering Conference*, International Society of Offshore and Polar Engineers.
- Huntley, D. A. (1977). Le Méhauté, B. 1976. “An introduction to hydrodynamics and water waves.” Springer-Verlag, New York, 22 (5), 974-975.
- Isobe, E. (1999). “Research and development of Mega-Float.” *In the Proceedings of the 3rd International Workshop on Very Large Floating Structures*, 7-13.
- Jagite, G., Xu, X. D., Chen, X. B., and Malenica, Š. (2018). “Hydroelastic analysis of global and local ship response using 1D–3D hybrid structural model.” *Ships and Offshore Structures*, 1-10.

- Jaswon, M. A. (1963). "Integral equation methods in potential theory." *In the Proceedings of royal society of London A*, 275, 23-32.
- John, F. (1949). "On the motion of floating bodies. I. " *Communications on Pure and Applied Mathematics*, 2 (1), 13-57.
- John, F. (1950). "On the motion of floating bodies II. Simple harmonic motions." *Communications on Pure and Applied Mathematics*, 3 (1), 45-101.
- Karmakar, D., and Sahoo, T. (2005). "Scattering of waves by articulated floating elastic plates in water of infinite depth." *Marine Structures*, 18 (5), 451-471.
- Kashiwagi, M. (1998). "A B-spline Galerkin scheme for calculating the hydroelastic response of a very large floating structure in waves." *Journal of Marine Science and Technology*, 3 (1), 37-49.
- Kashiwagi, M. (1999). "Research On Hydroelastic Responses of VLFS" Recent Progress And Future Work. " *In the Proceedings of 9th International Offshore and Polar Engineering Conference*, International Society of Offshore and Polar Engineers.
- Kay, I., and Kline, M. (1965). "Electromagnetic theory and geometrical optics (text on mathematical relationship of classical geometrical optics to electromagnetic theory, noting use of Taylor and asymptotic series expansions)." *New York, Interscience Publishers*, 527.
- Khabakhpasheva, T. I., and Korobkin, A. A. (2002). "Exact solutions of floating elastic plate problem." *In the Proceedings of the 17th International Workshop on Water Waves and Floating Bodies*, Cambridge, UK, 81-84.
- Kim, J. G., Cho, S. P., Kim, K. T., and Lee, P. S. (2014). "Hydroelastic design contour for the preliminary design of very large floating structures." *Ocean Engineering*, 78, 112-123.
- Kim, J. W. (1998). "An eigenfunction expansion method for predicting hydroelastic behavior of a shallow-draft VLFS." *In the Proceedings of 2nd International Conference on Hydroelasticity in Marine Tech., Fukuoka*.
- Kim, K. T., Lee, P. S., and Park, K. C. (2013). "A direct coupling method for 3D hydroelastic analysis of floating structures." *International Journal for*

*Numerical Methods in Engineering*, 96 (13), 842-866.

- Kirchhoff, GR (1876). “Lectures on mathematical physics.” *Mechanics* (Vol. 1), Teubner press.
- Kochin, N. E., Il'ja, A. K., and Roze, N. V. (1964). “Theoretical hydromechanics.” *Interscience*.
- Kohout, A. L., and Meylan, M. H. (2008). “An elastic plate model for wave attenuation and ice floe breaking in the marginal ice zone.” *Journal of Geophysical Research: Oceans*, 113 (C9).
- Kohout, A. L., Meylan, M. H., Sakai, S., Hanai, K., Leman, P., and Brossard, D. (2007). “Linear water wave propagation through multiple floating elastic plates of variable properties.” *Journal of Fluids and Structures*, 23 (4), 649-663.
- Kohout, A. L., Williams, M. J. M., Dean, S. M., and Meylan, M. H. (2014). “Storm-induced sea-ice breakup and the implications for ice extent.” *Nature*, 509 (7502), 604.
- Korobkin, A. A. (2000). “Numerical and asymptotic study of the two-dimensional problem of the hydroelastic behavior of a floating plate in waves.” *Journal of Applied Mechanics and Technical Physics*, 41 (2), 286-292.
- Korobkin, A. A., and Khabakhpasheva, T. I. (2001). “Reduction of hydroelastic response of floating platform in waves.” *In the proceedings of the 16th International Workshop on Water Waves and Floating Bodies, UK*.
- Kouzov, O. P. (1963). “Diffraction of a plane hydroacoustic wave on the boundary of two elastic plates.” *Journal of Applied Mathematics and Mechanics*, 27 (3), 806-815.
- Lachat, J. C., and Watson, J. O. (1976). “Effective numerical treatment of boundary integral equations: A formulation for three-dimensional elastostatics.” *International Journal for Numerical Methods in Engineering*, 10 (5), 991-1005.
- Lamb, H. (1945). “Hydrodynamics Dover.” *New York*.
- Landau, L. D., and Lifshits, E. M. (1959). “Fluid mechanics.” *Pergamon*

*Press, UK.*

- Lewis, R. M., and Keller, J. B. (1964). “Asymptotic methods for partial differential equations: the reduced wave equation and Maxwell's equation (No. EM-194).” *Courant Institute of Mathematical Sciences - New York University.*
- Li, R., Shu, Z., and Wang, Z. (2003). “A numerical and experimental study on the hydroelastic behavior of the box-typed very large floating structure in waves.” *In the proceedings of the 13th International Offshore and Polar Engineering Conference.* International Society of Offshore and Polar Engineers.
- Lighthill, M. J. (1978). “Waves in fluids” *Cambridge University Press, Cambridge, UK*
- Linton, C. M., and Chung, H. (2003). “Reflection and transmission at the ocean/sea-ice boundary.” *Wave Motion*, 38 (1), 43-52.
- Love, A. E. H. (1906). “Mathematical theory of elasticity.” *Cambridge University Press Cambridge, UK*
- Lu, D., Fu, S., Zhang, X., Guo, F., and Gao, Y. (2016). “A method to estimate the hydroelastic behaviour of VLFS based on multi-rigid-body dynamics and beam bending.” *Ships and Offshore Structures*, 1-9.
- Luneburg, R. K., and Herzberger, M. (1964). “Mathematical theory of optics.” *University of California Press, USA.*
- Mamidipudi, P. (1994). “The motion performance of a mat-like floating airports.” *In the proceedings of International conference On Hydroelasticity in Marine Technology.*
- Mandal, S., Sahoo, T., and Chakrabarti, A. (2017). “Characteristics of eigen-system for flexural gravity wave problems.” *Geophysical & Astrophysical Fluid Dynamics*, 111 (4), 249-281.
- Mei, C. C., and Black, J. L. (1969). “Scattering of surface waves by rectangular obstacles in waters of finite depth.” *Journal of Fluid Mechanics*, 38 (3), 499-511.
- Mei, C. C., and Tuck, E. O. (1980). “Forward scattering by long thin

bodies.” *SIAM Journal on Applied Mathematics*, 39 (1), 178-191.

- Meylan, M. H. (2001). “A variational equation for the wave forcing of floating thin plates.” *Applied Ocean Research*, 23 (4), 195-206.
- Meylan, M. H. (2002). “Wave response of an ice floe of arbitrary geometry.” *Journal of Geophysical Research: Oceans*, 107 (C1).
- Meylan, M. H., and Squire, V. A. (1996). “Response of a circular ice floe to ocean waves.” *Journal of Geophysical Research: Oceans*, 101 (C4), 8869-8884.
- Michailides, C., and Angelides, D. C. (2012). “Modeling of energy extraction and behavior of a flexible floating breakwater.” *Applied Ocean Research*, 35, 77-94.
- Mindlin, RD (1951). “Influence of rotatory inertia and shear on flexural motions of isotropic, elastic plates.” *Journal of Applied Mechanics*, 18, 31.
- Morse, P. M., and Feshbach, H. (1953). “Methods of theoretical physics. International series in pure and applied physics.” *McGraw-Hill*, 1, 29.
- Murai, M., Inoue, Y., and Nakamura, T. (2002). “On the prediction method of a hydroelastic responses of a VLFS considering a seabed topography.” *Journal of the Society of Naval Architects of Japan*, 309-318.
- Nagata S., Yoshida H., Fujita T. and Isshiki H. (1998). “Reduction of the motion of an elastic floating plate in waves by breakwaters.” *In the proceedings of the 2<sup>nd</sup> International Conference on Hydroelasticity in Marine Technology, Fukuoka, Japan*, 229-238.
- Nagata, S., Niizato, H., Yoshida, H., Ohkawa, Y., and Kobayashi, K. (2003). “Effects of breakwaters on motions of an elastic floating plate in waves.” *International Journal of Offshore and Polar Engineering*, 13 (01).
- Newman, J. N. (1977). “Marine Hydrodynamics.” *Cambridge, Massachusetts and London, England*.
- Noble, B. (1958). “Methods based on the Wiener-Hopf technique for the solution of PDEs.” *Physics Today*, 12<sup>th</sup> report.
- Ohkusu, M. (1996). “Analysis of hydroelastic behavior of a large floating platform of thin plate configuration in waves.” *In the proceedings of*

*International Workshop on VLFS*, 143-148.

- Ohkusu, M., and Namba, Y. (1998). "Hydroelastic behaviour of a large floating platform of elongated form on head waves in shallow water." *In the proceedings of the 2nd Hydroelasticity in Marine Technology, Kyushu University, Fukuoka, Japan*, 1-3.
- Ohkusu, M., and Namba, Y. (2004). "Hydroelastic analysis of a large floating structure." *Journal of Fluids and Structures*, 19 (4), 543-555.
- Ohmatsu, S. (2000). "Numerical calculation method for the hydroelastic response of a pontoon-type very large floating structure close to a breakwater." *Journal of Marine Science and Technology*, 5 (4), 147-160.
- Pan, Y., Sahoo, P. K., and Lu, L. (2016). "Numerical study of hydrodynamic response of mooring lines for large floating structure in south china sea." *Ships and Offshore Structures*, 11 (7), 774-781.
- Papathanasiou, T. K., and Belibassakis, K. A. (2014). "Hydroelastic analysis of VLFS based on a consistent coupled-mode system and FEM." *The IES Journal Part A: Civil & Structural Engineering*, 7 (3), 195-206.
- Peter, M. A., and Meylan, M. H. (2004). "The eigenfunction expansion of the infinite depth free surface Green function in three dimensions." *Wave Motion*, 40 (1), 1-11.
- Peter, M. A., Lee, R. S., and Chung, H. (2003). "Wave scattering by a circular plate in water of finite depth: a closed form solution." *In the proceedings of the 13th International Offshore and Polar Engineering Conference*. International Society of Offshore and Polar Engineers.
- Phillips, O. M. (1966). "The dynamics of the upper ocean." *Cambridge university press, New York*.
- Pinkster, J. A. (1998). "The behaviour of large air cushion supported structures in waves." *In the proceedings of Hydroelasticity, Fukuoka Japan*, 497-506.
- Porter, D., and Porter, R. (2004). "Approximations to wave scattering by an ice sheet of variable thickness over undulating bed topography." *Journal of Fluid Mechanics*, 509, 145-179.

- Riyansyah, M., Wang, C. M., and Choo, Y. S. (2010). "Connection design for two-floating beam system for minimum hydroelastic response." *Marine Structures*, 23 (1), 67-87.
- Rizzo, F. J. (1967). "An integral equation approach to boundary value problems of classical elastostatics." *Quarterly of Applied Mathematics*, 25 (1), 83-95.
- Senjanović, I., Malenica, Š., and Tomas, S. (2008). "Investigation of ship hydroelasticity." *Ocean Engineering*, 35 (5-6), 523-535.
- Senjanović, I., Malenica, Š., and Tomašević, S. (2009). "Hydroelasticity of large container ships." *Marine Structures*, 22 (2), 287-314.
- Senjanović, I., Tomić, M., and Vladimir, N. (2015). "An advanced procedure for hydroelastic analysis of very large floating airport exposed to airplane load." *In the proceedings of 7th International Conference on Hydroelasticity in Marine Technology*.
- Seto, H. (1998). "A hybrid element approach to hydroelastic behavior of a very large floating structure in regular waves." *In the proceedings of the 2nd International Conference on Hydroelasticity in Marine Technology*, 185-194.
- Shuku, M., Horiba, S., Inoue, S., Kobayashi, E., and Simamune, S. (2001). "Overview of Mega-Float and its utilization." *Mitsubishi Heavy Industries Technical Review*, 38 (2), 39-46.
- Skene, D. M., Bennetts, L. G., Meylan, M. H., and Toffoli, A. (2015). "Modelling water wave overwash of a thin floating plate." *Journal of Fluid Mechanics*, 777.
- Slepyan, L. I., and Fadeev, V. M. (1988, March). "Reflection, refraction and emission of waves in a piecewise-uniform elastic system interacting with a fluid." *In the proceedings of Soviet Physics, Doklady*, 236.
- Squire, V. A., and Dixon, T. W. (2000). "An analytical model for wave propagation across a crack in an ice sheet." *In the proceedings of 10th International Offshore and Polar Engineering Conference*. International Society of Offshore and Polar Engineers.
- Squire, V. A., Robinson, W. H., Langhorne, P. J., and Haskell, T. G. (1988).

- “Vehicles and aircraft on floating ice.” *Nature*, 333 (6169), 159.
- Stoker, J. J. “Water Waves.” 1957. *Interscience, New York*.
  - Sturova, I. V. (2000). “Diffraction of shallow-water waves on a floating elastic platform.” *Journal of Applied Mathematics and Mechanics*, 64, 1004-1012.
  - Sturova, I. V. (2001). “The diffraction of surface waves by an elastic platform floating on shallow water.” *Journal of Applied Mathematics and Mechanics*, 65 (1), 109-117.
  - Sturova, I. V. (2002). “The action of periodic surface pressures on a floating elastic platform.” *Journal of Applied Mathematics and Mechanics*, 66 (1), 71-81.
  - Sturova, I. V. (2003). “Response of unsteady external load on the elastic circular plate floating on shallow water.” In the proceedings of the 18th International Workshop on Water Waves and Floating Bodies, Le Croisic, France, 177-180.
  - Sun, Y., Lu, D., Xu, J., and Zhang, X. (2017). “A study of hydroelastic behavior of hinged VLFS.” *International Journal of Naval Architecture and Ocean Engineering*.
  - Symm, G. T. (1963). “Integral equation methods in potential theory.” *In the proceedings of Royal society of London. A*, 275, 33-46.
  - Takagi, K. (1996). “Interaction between tsunami and artificial floating island.” *In the proceedings of 6th International Offshore and Polar Engineering Conference*. International Society of Offshore and Polar Engineers.
  - Takagi, K. (2001). “Parabolic approximation of the hydro-elastic behavior of a very large floating structure in oblique waves.” *In the proceedings of 16th International Workshop on Water Waves and Floating Bodies in Waves*.
  - Takagi, K. (2002). “Hydroelastic response of a very large floating structure in waves—a simple representation by the parabolic approximation.” *Applied Ocean Research*, 24 (3), 175-183.
  - Takagi, K. (2004). “Quarter-plane problem of a floating elastic

plate.” *Journal of Engineering Mathematics*, 48 (2), 105-128.

- Takagi, K., and Kohara, K. (2000). “Application of the ray theory to hydroelastic behavior of VLFS.” *In the proceedings of 10th International Offshore and Polar Engineering Conference*. International Society of Offshore and Polar Engineers.
- Takagi, K., and Nagayasu, M. (2001). “Hydroelastic behavior of a mat-type very large floating structure of arbitrary geometry.” *In the proceedings of IEEE Conference and Exhibition*, 3, 1923-1929.
- Takagi, K., and Noguchi, J. (2005). “PFFT-NASTRAN coupling for hydroelastic problem of VLMOS in waves.” *In the proceedings of 20th International Workshop on Water Waves and Floating Bodies*.
- Takagi, K., and Yano, W. (2003). “Analysis of hydroelastic behavior of a very large mobile offshore structure in waves.” *In the Proceedings of the 18th International Workshop on Water Waves and Floating Bodies*, 181-184.
- Takagi, K., Shimada, K., and Ikebuchi, T. (2000). “An anti-motion device for a very large floating structure.” *Marine Structures*, 13 (4-5), 421-436.
- Taylor, R. E., and Ohkusu, M. (2000). “Green functions for hydroelastic analysis of vibrating free-free beams and plates.” *Applied Ocean Research*, 22 (5), 295-314.
- Timoshenko, S. P., and Woinowsky-Krieger, S. (1959). “Theory of plates and shells.” *Tata McGraw-hill*.
- Tkacheva, L. A. (2001a). “Surface wave diffraction on a floating elastic plate.” *Fluid Dynamics*, 36 (5), 776-789.
- Tkacheva, L. A. (2001b). “Scattering of surface waves by the edge of a floating elastic plate.” *Journal of Applied Mechanics and Technical Physics*, 42 (4), 638-646.
- Tkacheva, L. A. (2001c). “Hydroelastic behavior of a floating plate in waves.” *Journal of Applied Mechanics and Technical Physics*, 42 (6), 991-996.
- Tkacheva, L. A. (2002). “Diffraction of surface waves at floating elastic plate.” *In the Proceedings of 17th International Workshop On Water Waves*

*and Floating Bodies* Peterhouse, Cambridge, UK.

- Tkacheva, L. A. (2003). "Plane problem of surface wave diffraction on a floating elastic plate." *Fluid Dynamics*, 38 (3), 465-481.
- Tsubogo, T. (2001). "The motion of an elastic disk floating on shallow water in waves." *In the Proceedings of 11th International Offshore and Polar Engineering Conference*. International Society of Offshore and Polar Engineers.
- Usha, R., and Gayathri, T. (2005). "Wave motion over a twin-plate breakwater." *Ocean Engineering*, 32 (8-9), 1054-1072.
- Utsunomiya, T., and Watanabe, E. (2001). "Accelerated Green's function method for wave response of very large floating structures." *In the Proceedings of the 16th Ocean Engineering Symposium, The Society of Naval Architects of Japan*, 313-320.
- Utsunomiya, T., Watanabe, E., and Taylor, R. E. (1998). "Wave response analysis of a box-like VLFS close to a breakwater." *In the Proceedings of the 17th International Conference on Offshore Mechanics and Arctic Engineering, ASME*.
- Utsunomiya, T., Watanabe, E., Wu, C., Hayashi, N., Nakai, K. and Sekita, K., (1995). "Wave response analysis of a flexible floating structure by BE-FE combination method." *In the Proceedings of 5th International Offshore and Polar Engineering Conference*. International Society of Offshore and Polar Engineers.
- Wadhams, P., Squire, V. A., Ewing, J. A., and Pascal, R. W. (1986). "The effect of the marginal ice zone on the directional wave spectrum of the ocean." *Journal of Physical Oceanography*, 16 (2), 358-376.
- Wadhams, P., Squire, V. A., Goodman, D. J., Cowan, A. M., and Moore, S. C. (1988). "The attenuation rates of ocean waves in the marginal ice zone." *Journal of Geophysical Research: Oceans*, 93 (C6), 6799-6818.
- Wang, C. D., and Meylan, M. H. (2004). "A higher-order-coupled boundary element and finite element method for the wave forcing of a floating elastic plate." *Journal of Fluids and Structures*, 19 (4), 557-572.

- Wang, C. M., Tay, Z. Y., Takagi, K., and Utsunomiya, T. (2010). "Literature review of methods for mitigating hydroelastic response of VLFS under wave action." *Applied Mechanics Reviews*, 63 (3), 030802.
- Wang, C. M., Xiang, Y., Watanabe, E., and Utsunomiya, T. (2004). "Mode shapes and stress-resultants of circular Mindlin plates with free edges." *Journal of Sound and Vibration*, 276 (3-5), 511-525.
- Watanabe, E. (2003). "Floating bridges: past and present." *Structural Engineering International*, 13 (2), 128-132.
- Watanabe, E., Maruyama, T., Tanaka, H., and Takeda, S. (2000). "Design and construction of a floating swing bridge in Osaka." *Marine Structures*, 13 (4-5), 437-458.
- Watanabe, E., Utsunomiya, T., & Wang, C. M. (2006). "Benchmark hydroelastic responses of a circular VLFS under wave action." *Engineering Structures*, 28(3), 423-430.
- Watanabe, E., Utsunomiya, T., and Wang, C. M. (2004a). "Hydroelastic analysis of pontoon-type VLFS: a literature survey." *Engineering Structures*, 26 (2), 245-256.
- Watanabe, E., Utsunomiya, T., Wang, C. M., and Xiang, Y. (2003). "Hydroelastic analysis of pontoon-type circular VLFS." *In the Proceedings of 13th International Offshore and Polar Engineering Conference*. International Society of Offshore and Polar Engineers.
- Watanabe, E., Wang, C. M., Utsunomiya, T., and Moan, T. (2004b). "Very large floating structures: applications, analysis and design." *CORE report*, 2, 104-109.
- Watson, G. N. (1944). "Bessel functions." *Cambridge University Press, Cambridge*, 19, 22.
- Weaver Jr, W., Timoshenko, S. P., and Young, D. H. (1990). "Vibration problems in engineering." *John Wiley & Sons*.
- Wehausen, J. V., and Laitone, E. V. (1960). "Surface waves." *Fluid Dynamics*, 446-778.
- Williams, T. D., and Squire, V. A. (2002). "Wave propagation across an

oblique crack in an ice sheet.” *In the Proceedings of 12th International Offshore and Polar Engineering Conference*. International Society of Offshore and Polar Engineers.

- Wu, C., Watanabe, E., and Utsunomiya, T. (1995). “An eigenfunction expansion-matching method for analyzing the wave-induced responses of an elastic floating plate.” *Applied Ocean Research*, 17 (5), 301-310.
- Yeung, R. W., and Kim, J. W. (2000). “Effects of a translating load on a floating plate—structural drag and plate deformation.” *Journal of Fluids and Structures*, 14 (7), 993-1011.
- Yiew, L. J., Bennetts, L. G., Meylan, M. H., French, B. J., and Thomas, G. A. (2016). “Hydrodynamic responses of a thin floating disk to regular waves.” *Ocean Modelling*, 97, 52-64.
- Yan, S., Ma, Q. W., Chen, C., and Lu, J. (2010). “Fully nonlinear analysis on responses of a moored FPSO to waves in shallow water.” *Twentieth International Offshore and Polar Engineering Conference*. International Society of Offshore and Polar Engineers.
- Yoneyama, H., Hiraishi, T., and Ueda, S. (2004). “Recent technological advances of ship mooring analysis and construction of floating structures in Japan.” *Bulletin-International Navigation Association*, (116), 79-90.
- Yoon, J. S., Cho, S. P., Jiwinangun, R. G., & Lee, P. S. (2014). “Hydroelastic analysis of floating plates with multiple hinge connections in regular waves.” *Marine Structures*, 36, 65-87.
- Zienkiewicz, O. C., and Cheung, Y. K. (1967). “The finite element method in structural and continuum mechanics: numerical solution of problems in structural and continuum mechanics (Vol. 1).” *McGraw-Hill*.
- Zilman, G., and Miloh, T. (2000). “Hydroelastic buoyant circular plate in shallow water: a closed form solution.” *Applied Ocean Research*, 22 (4), 191-198.

## LIST OF PUBLICATIONS

### International Journals

1. Shirkol, A. I., Nasar, T., & Karmakar, D. (2016). Wave interaction with Very Large Floating Structure (VLFS) using BEM approach– Revisited. *Perspectives in Science*, 8, 533-535.
2. Shirkol, A. I., & Thuvanismail, N. (2017). Wave interaction with Floating platform of different shapes and supports using BEM approach. *Journal of Naval Architecture and Marine Engineering*, 14 (2), 115-133.
3. Shirkol, A. I., & Nasar, T. (2018). Coupled boundary element method and finite element method for hydroelastic analysis of floating plate. *Journal of Ocean Engineering and Science*, 3 (1), 19-37
4. Shirkol, A. I., & Nasar, T. (2018). Coupled boundary element method and finite element method for hydroelastic analysis of floating plate. *Lecture Notes in Civil Engineering*, 22, ISBN - 978-981-13-3118-3.
5. Shirkol, A. I., & Nasar, T. (2019). Coupled BEM and FEM for the analysis of floating elastic plate with arbitrary shapes - *Journal of Ships and Offshore Structures*. 10.1080/17445302.2018.1564540.

### International Conferences

1. Wave interaction with Very Large Floating Structure (VLFS) using BEM approach. International Conference on Recent Trends in Engineering and Material Sciences, 17-19 March 2016, Jaipur National University, Jaipur, India
2. Coupled Boundary Element Method And Finite Element Method For Hydroelastic Analysis Of Floating Plate – 4<sup>th</sup> International Conference in Ocean Engineering, 2018 (ICOE), 18-21 Feb 2018, Indian Institute of Technology Madras, India.



## **Anoop I Shirkol**

Research Scholar, Department of Applied Mechanics and  
Hydraulics,  
National Institute of Technology Karnataka, Surathkal,  
Mangalore, India 575 025.



91-9538462532 | [anoopshirkol@gmail.com](mailto:anoopshirkol@gmail.com)

Permanent Address : Anoop I.Shirkol  
S/O Iranna T.Shirkol  
“Gangotri”  
Kamanakatti,  
Kumbar Oni  
Dharwad  
580001

### **EDUCATION**

| <b>Course</b>                   | <b>Department</b>                   | <b>Institute</b>   | <b>Percentage/<br/>CGPA</b> | <b>Year of<br/>passing</b>                    |
|---------------------------------|-------------------------------------|--|-----------------------------|---|
| <b>Ph. D</b>                    | Applied Mechanics<br>and Hydraulics | <b>National Institute<br/>of Technology<br/>Karnataka,<br/>Surathkal</b> | <b>7.4</b>                  | <b>Thesis<br/>Submitted on<br/>21/12/2018</b> |
| <b>M. Tech<br/>(Structures)</b> | Civil Engineering                   | <b>SDMCET,<br/>Dharwad</b>   | <b>78.3%</b>                | <b>2015</b>                                   |
| <b>B. Tech</b>                  | Civil Engineering                   | <b>SDMCET,<br/>Dharwad</b>   | <b>8.30</b>                 | <b>2013</b>                                   |

## **AREAS OF RESEARCH INTEREST**

---

- Structural engineering
- Structural Dynamics
- Steel structures
- Mechanical Vibrations
- RCC/ Earthquake engineering
- Wave hydrodynamic
- Offshore structures
- Computational Fluid Dynamics
- Wave structure interaction
- Fluid structure interaction

## **TEACHING ASSISTANTSHIP AT NITK**

---

- Strength of Mechanics
- Engineering Mechanics
- Fluid Mechanics
- Fluid Mechanics Laboratory
- Strength of Mechanics Laboratory

## **PROFESSIONAL EXPERIENCE**

---

| <b>Designation</b> | <b>Institute</b>                            | <b>Duration</b>      |
|--------------------|---|----------------------|
| Lecture            | K H Kabbur Institute of Technology, Dharwad | 2014-2015            |
| Guest Lecture      | University of Agricultural College, Dharwad | July 2015 – Dec 2015 |

## **COURSES HANDELED**

---

- Fluid Mechanics
- Hydraulics and Hydraulic Machines
- Surveying I&II
- Design of Steel Structures
- RCC
- Strength of Mechanics

## RESEARCH EXPERIENCE

---

|        | <b>Project Title</b>  | <b>Affiliation</b>                                    |
|--------|---|---|
|        | Hydroelastic Analysis Of Very Large Floating Structure (VLFS) Using Boundary Element Approach   |   |
|        | <i>Abstract</i>   |   |
| Ph.D   | <p>A numerical procedure has been proposed to analyze the equation of motion of the elastic plate with arbitrary geometry subjected to monochromatic gravity waves. The numerical model is capable of investigating the Very Large Floating Structure (VFLS) at finite (<math>0.05 \leq h/\lambda \leq 0.5</math>) and infinite (<math>h/\lambda \leq 0.5</math>) water depths. VLFS of rectangular, triangular and trapezoidal geometries are considered and elastic motion or vertical deflections of these shapes have been studied. A hybrid numerical model which combines Boundary Element Method (BEM) and Finite Element Method (FEM) is developed and used to solve fluid structure interaction. A Higher Order Boundary Element Method (HOBEM) has been adopted. Two equations have been derived to develop the relationship between the displacement of the plate and the velocity potential under the plate. The first equation is derived from the equation of motion for the plate and is solved by Finite Element Method (FEM) to extract the displacement of the floating structure. The second equation is from water wave theory which is based on Boundary Integral Equation (BIE) that relates the displacement of the floating plate and velocity potential using free-surface Green's function. A modified Green's function has been developed by using Bessel's, Hankel and Struve functions of order zero. Both the equations are solved simultaneously to get the displacement of floating elastic plate and velocity potential.</p> | National Institute of Technology Karnataka, Surathkal |
| M-Tech | Analysis of Laminated Composite Plate by Using Meshless method of Analysis by MATLAB  | SDMCET, Dharwad                                       |
| B-Tech | Developing a Digital Terrain Model of SDMCET Campus. March 2012. Technologies Used: GIS. (Mini-Project)   |   |
|        | Installation of Mini or Micro Hydel Power plant in Benihalla using GIS (Major-Project/B. Tech thesis)   | SDMCET, Dharwad                                       |

## ACHIEVEMENTS

---

- Awarded **Best Paper Certificate** for the paper titled “*Calculation of sediment Yield in Bennihalla using GIS*” presented at the International Conference on Water Resources and management, 2014 organized by JNTU Hyderabad.

## TECHNICAL SKILLS

---

**Analysis/ Modelling software** : ANSYS, ETABS, STAAD.Pro, AutoCAD, Solid Edge

**Languages/software products** : MATLAB, Visual basics.

**Tools** : MS Office.

## PUBLICATIONS

---

- Shirkol, A. I., & Nasar, T. (2019). “*Coupled BEM and FEM for the analysis of floating elastic plate with an arbitrary shape*”. Journal of ships and offshore structures. DOI : 10.1080/17445302.2018.1564540.  
<https://www.tandfonline.com/eprint/5WCspYbAykDnzgqXHcdy/full>
- Shirkol, A. I., & Nasar, T. (2018). “*Coupled boundary element method and finite element method for hydroelastic analysis of floating plate*”. Journal of Ocean Engineering and Science. DOI : 10.1016/j.joes.2017.11.003.  
<https://www.sciencedirect.com/science/article/pii/S2468013317301146>
- Shirkol, A. I., & Thuvanismail, N. (2017). “*Wave interaction with Floating platform of different shapes and supports using BEM approach*”. Journal of Naval Architecture and Marine Engineering, 14(2), 115-133. DOI : 10.3329/jname.v14i2.28267.  
<https://www.banglajol.info/index.php/JNAME/article/view/28267>
- *Coupled Boundary Element Method and Finite Element Method for Hydroelastic analysis of floating plate* – Lecture notes in Civil Engineering22, ISBN - 978-981-13-3118-3.  
<https://www.springer.com/la/book/9789811331183#otherversion=9789811331190>

- Shirkol, A. I., Nasar, T., & Karmakar, D. (2016). “*Wave interaction with Very Large Floating Structure (VLFS) using BEM approach–Revisited*”. Perspectives in Science, 8, 533-535. – Published (Elsevier).DOI:10.1016/j.pisc.2016.06.012.  
<https://www.sciencedirect.com/science/article/pii/S2213020916301513>
- *Coupled Boundary Element Method and Finite Element Method for Hydroelastic analysis of floating plate* – 4th International Conference in Ocean Engineering, 2018 (ICOE), 18-21 Feb 2018.
- *Wave interaction with Very Large Floating Structure (VLFS) using BEM approach*. International conference on Emerging Materials and Science, ICEMS 2016, Jaipur.
- Anoop I Shirkol, I. T. Shirkol, Sachin Wajpey. “ *Calculation of sediment Yield in Bennihalla using GIS* ”, Water Resources and management.2014
- Anoop I Shirkol, N. S. Patil, Sachin Wajpey. “*Installation of Mini or Micro Hydel Power plant in Bennihalla using GIS*, In: Proceedings of International Conference on ‘Water Resources and management ’, Hyderabad, December 2012.

## **WORKSHOPS, GIAN PROGRAMS & SHORT TERM COURSES**

---

- 6week industrial training at KWB Dharwad. Worked on Lotus Tool for laying of Pipe line for 24\*7 Water supply scheme. June – July 2012
- Participated in one day Workshop on “**Tsunami threat and its mitigation along Indian coast**” held at Department of Applied Mechanics & Hydraulics, NITK, Surathkal, India on 2<sup>nd</sup> November 2015
- Participated in the workshop on “**Coastal Hydrodynamics & Modelling**” held on 7th October 2016 Organized by Department of Applied Mechanics & Hydraulics, NITK, Surathkal.
- Participated Awareness Program on “**Intellectual Property Rights**” for MSME’S on 1<sup>st</sup> September 2016 jointly organized by National Law School of India University and NITK, Surathkal.

- Participated in the GIAN short-term course on “**Offshore Renewable Energy (Wave, Wind and Tidal Energy)**” held at Department of Applied Mechanics & Hydraulics, NITK, Surathkal, India during 7<sup>th</sup>-11<sup>th</sup> November 2016.
- Participated in the GIAN short-term course on “**Computational hydroelasticity**” held at Department of Ocean Engineering and Naval Architecture, IIT Kharagpur, India during 12<sup>th</sup> – 16<sup>th</sup> December 2016.
- Participated in the MIKE Powered by DHI training course on ‘**Training on coastal and marine modelling using MIKE 21 and LITPACK**’ during 22-26, August 2016 at Department of Applied Mechanics & Hydraulics, NITK, Surathkal.

## CONTACT REFERENCES

---

| Name and Designation                                     | Institution  | Contact  |
|--|--|--|
| • Dr. T. Nasar,<br>Assistant professor                   | Applied Mechanics and Hydraulics, NITK Surathkal, Karnataka, India | <a href="mailto:t.nasara@gmail.com">t.nasara@gmail.com</a><br>+91 9449719077                 |
| • Prof. Lakshman Nandagiri,<br>Professor                 | Applied Mechanics and Hydraulics, NITK Surathkal, Karnataka, India | <a href="mailto:lnand@rocketmail.com">lnand@rocketmail.com</a><br>+91-824-2474000 Extn. 3302 |
| • Prof. Udaykumar R Yaragatti,<br>Director and Professor | Director, MNIT Jaipur, India                                       | <a href="mailto:udaykumarry@yahoo.com">udaykumarry@yahoo.com</a><br>+91-9448147806           |
| • Dr. Raviraj H M<br>Assistant professor                 | Civil Engineering Department, NITK Surathkal, India                | <a href="mailto:ravirajmh@rediffmail.com">ravirajmh@rediffmail.com</a><br>+91 9448861733     |

## PERSONAL DETAILS

---

|                   |  |
|-------------------|--|
| Full Name         | Anoop Iranna Shirkol   |
| Father's Name     | Iranna T. Shirkol  |
| Mother's Name     | Mandakini I. Shirkol   |
| Date of Birth     | 28/09/1991   |
| Nationality       | Indian   |
| Permanent Address | Anoop I.Shirkol, S/O Iranna T.Shirkol<br>"Gangotri" Kamanakatti, Kumbar Oni<br>Dharwad<br>Pin - 580001 |
| Languages         | English, Hindi, Kannada  |

\*\*\*\*\*